2012

3D coupled thermo-mechanical FE analysis of surface defects in continuous casting slab during hot rolling

Shengnan Yang
University of Wollongong

3D Coupled Thermo-mechanical FE Analysis of Surface Defects in Continuous Casting Slab during Hot Rolling

By

SHENGNAN YANG

A thesis submitted in partial fulfillment of the
requirements for the award of the degree of

MASTER OF ENGINEERING
(Mechanical)

From

UNIVERSITY OF WOLLONGONG
FACULTY OF ENGINEERING

August 2012

DECLARATION

This is to certify that the work presented in this thesis was carried out by the author in the school of Mechanical, Materials and Mechatronic Engineering, University of Wollongong, New South Wales, Australia. It has not been submitted for a degree to any other university or institute.

Shengnan Yang

August 2012

ACKNOWLEDGEMENTS

I gratefully acknowledge my supervisor Professor Zhengyi Jiang whom I thank for his excellent guidance and tireless assistance during the course of this thesis. It has been an honour to study under such a kind teacher and great academic scholar.

Thanks must also go to my co-supervisor Dr. Dongbin Wei who helped me along the way throughout the year at this wonderful university.

In addition, I would like to thank the following people that gave me encouragement and invaluable advice:

Firstly, thanks go to my family for sacrificing so much to give me an education. Without it, I would not have had the skills to research, write and compile this thesis. The value you placed on education and learning is truly appreciated.

Thank you to Mr. Khoa Duy Vo, Mr. Ninan Mathew and Ms. Xiawei Cheng for being so amazing at pinpointing my issues and consistently helping me throughout the year. Thanks also go to Mr. Qiang Zhu and Mr. Mao Liu for their valuable insights and contributions to my work.

Finally, I express my deep thankfulness to all my friends for their much cherished loyalty and love, and to all the staff and tutors for their ongoing assistance and

support. I was very fortunate to be a Mechanical Engineering student at the University of Wollongong.

Thank you all indeed.

ABSTRACT

The behaviour of the surface defects on continuously casting slabs during hot rolling is investigated by using commercial FE-code LS-DYNA3D. The objective of this study is to find out if surface cracks will disappear or be minimised after rolling.

The material used in the simulation models is austenitic stainless steel 304, which is a commercially used material in the manufacturing industry. The coupled thermo-mechanical method for simulation was implemented in this study. The main surface defects studied are edge cracks, transverse cracks, V-shaped transverse cracks and longitudinal cracks.

The simulation results show that it is hard for edge cracks to close after hot rolling, and the situation actually deteriorates. Edge cracks near the bottom of the slab are enlarged much more than those near the top surface of the slab. For transverse and longitudinal cracks, the two surfaces will come into contact with each other, causing the defects to be healed to some extent. Due to the closure of some of the crack area, the oxidation of these areas will be minimised. However, because of the non-uniformity of the flow stress around the cracks on the top surface of the slab, it is highly possible that it will form folder layers.

The simulated models also indicate the temperature distribution for the global strip and for the crack areas. By considering contact heat transfer, convection and radiation, it is found that contact heat transfer is the dominant factor affecting the temperature difference of both the work piece and the work roll. Heat generated from the plastic deformation of the strip only accounts for a small proportion of the temperature

difference and would not compensate for the heat loss through the ambient air and through the strip/roll contact.

By analysing the temperature of the cracks and the slab, it is becoming possible to predict the formation of the chemical conditions which are likely to cause oxidation and defects.

It is recommended that the oxidation in the crack areas could be simulated to examine its effect on the crack evolution behaviour during hot rolling process. Experiments should be carried out to compare the simulation results with the experimental ones. By investigating the microstructure of the crack behaviour it becomes possible to take effective steps to avoid crack propagation and to ensure the surface quality of the final products.

LIST OF CONTENTS

DECLARATION i
ACKNOWLEDGEMENTS ii
ABSTRACT iv
LIST OF CONTENTS vi
LIST OF FIGURE CAPTIONS x
LIST OF TABLE CAPTIONS xiv
NOMENCLATURE xv
LIST OF PUBLICATIONS xviii
Chapter 1 Introduction 1
1.1 Significance of this research 2
1.2 Research objectives 3
1.3 Research methodology 3
1.4 Outline of the thesis 4
Chapter 2 Literature Review 6
2.1 Chatter and oscillation marks 6
2.1.1 Chatter mark surface 6
2.1.2 Deep oscillation mark and hook surface 7
2.1.3 Main surface crack 9
2.2 Internal crack 17
2.2.1 Central crack 17
2.2.2 Inclusions and bubbles 19
2.3 Grinding method 22
2.4 Characteristics of oxidation around defects 23
2.5 Analytical modelling 24

2.6 Surface defect recovery mechanism 25
2.7 Problems and findings from the literature review 26
2.8 Research scope in the present study 27
Chapter 3 Methodology 28
3.1 Introduction 28
3.2 Basic theory of thermo-elastic-plastic coupled FE method 29
3.2.1 The equilibrium between elastic and plastic deformation 29
3.2.2 Material model for workpiece 33
3.3 Simulation method 34
3.4 Thermal governing theory 35
3.4.1 Governing equation for the conversion of deformation energy to heat 35
3.5 Contact between the slab and the work roll 36
3.6 Finite element modeling of surface defects 36
3.6.1 Model of the edge crack on the slab 36
3.6.2 Model of the transverse crack on the slab 38
3.6.3 Model of the V-shaped transverse crack on the slab 38
3.6.4 Model of the longitudinal crack on the slab 40
3.7 Thermal boundary conditions 41
3.7.1 Heat transfer of the contact surface between the slab and the work roll 42
3.7.2 Convection boundary condition 42
3.7.3 Radiation boundary condition 43
3.7.4 Segment set for the convection and radiation 43
3.8 Mechanical boundary condition 44
3.9 Thermal and mechanical properties for the austenitic stainless steel 304 45
3.9.1 Chemical compositions of AISI 304 45
3.9.2 Thermal and mechanical properties for FEM simulation models 46

3.10 The integration method for explicit dynamic FEM 49

Chapter 4 Simulation Results and Discussion 51

4.1 Introduction 51

4.2 Edge crack behaviour during hot rolling process 52

4.2.1 Edge crack variation 52

4.2.2 Rolling force 54

4.2.3 Von Mises stress distribution 55

4.2.4 Analysis of crack tip 56

4.2.5 Analysis of rolling process 64

4.2.6 Thermal effect 68

4.2.7 Influence of rolling conditions 73

4.3 Transverse crack 76

4.3.1 Behaviour of transverse crack 76

4.3.2 Lateral deformation of crack 77

4.3.3 Rolling force 78

4.3.4 Crack width evolution 79

4.4 V-shaped transverse crack 80

4.4.1 Behaviour of V-shaped transverse crack 81

4.4.2 Rolling force 82

4.4.3 Von Mises stress distribution 85

4.4.4 Plastic strain distribution 86

4.4.5 Effect of mesh density 88

4.4.6 Pressure distribution 89

4.4.7 Distribution of maximum shear stress 90

4.4.8 Distribution of effective strains 92

4.4.9 Distribution of temperature 93

4.4.10 Influence of rolling conditions 94

4.5 Longitudinal crack behavior during hot rolling process 98

4.5.1 Behaviour of longitudinal crack 98
4.5.2 Rolling force 100
4.5.3 Effect of location on longitudinal crack behaviour 102
4.5.4 Von Mises stress distribution 104
4.5.5 Plastic strain distributions 105
4.5.6 Pressure distribution 106
4.5.7 Distributions of temperature 107
4.5.8 Effect of convection and radiation through the environment 109
4.5.9 Effect of contact heat transfer 110
4.5.10 Effect of deformation heat 111
4.5.11 Heat loss by convection and radiation 112
Chapter 5 Conclusions and Recommendations 113
5.1 Conclusions 113
5.2 Recommendations 114
References 116
Appendix A Kinetic Energy 124
Appendix B Internal Energy 130
Appendix C Comparisons of Crack Behaviours 136

LIST OF FIGURE CAPTIONS

Figure 2.1	Effects of chattering on rolled sheet and the rolling equipment [7]	7
Figure 2.2	An ultra-low-carbon steel sample showing a curved hook-type oscillation mark [8]	8
Figure 2.3	(a) Longitudinal cracks on the surface of a continuously cast slab, (b) cross-section showing a longitudinal crack [11]	10
Figure 2.4	V-shaped transverse crack at a steel block to be rolled at the experiment rolling mill [15]	10
Figure 2.5	Transversal crack in slab rolling [16]	11
Figure 2.6	A representative star crack on the surface of steel slab [19]	12
Figure 2.7	Surface defects due to inclusion entrapment resulting in (a) blisters (b) slivers in final product [21]	13
Figure 2.8	Predicted crack growth path, showing the thermal and crack-face pressure effect for $f = 0.1$ [26]	14
Figure 2.9	A photograph showing typical side cracks formed on the strip surface [32]	15
Figure 2.10	Edge crack results of experiment and FEM [38]	16
Figure 2.11	Central rectangular crack closing behaviour during rolling [41]	18
Figure 2.12	(a) Effective strain distribution for a soft inclusion and its surrounding material, T = 1200 ℃, (b) effective strain distribution for a hard inclusion and its surrounding material, T = 700 ℃ [46]	19
Figure 2.13	Six inclusion locations at start rolling (a), positions of inclusions at end of rolling (b) [21]	20

Figure 2.14	Crack propagation in the inclusion [29]	21
Figure 2.15	Bubbles attached to Al_2O_3 inclusions in slab [49]	22
Figure 2.16	Schematic illustrations of the machine process [54]	23
Figure 2.17	Schematic diagram of the mechanism of FeO and internal oxide formation [55]	24
Figure 2.18	Scheme of MPHL mechanism [71]	26
Figure 3.1	Model of edge crack on the slab	37
Figure 3.2	The model of transverse crack on the slab	38
Figure 3.3	Model of V-shaped crack in the center on the slab surface	39
Figure 3.4	Surface longitudinal crack on the slab	40
Figure 3.5	Segment set on the surface for the radiation and convection	44
Figure 3.6	Thermal properties for the material models	47
Figure 4.1	Edge crack evolution at different time	53
Figure 4.2	Edge shapes from the top and bottom surfaces of the slab	53
Figure 4.3	Rolling force for different reductions	54
Figure 4.4	Von Mises stress distribution at t = 0.008 s	55
Figure 4.5	Von Mises stress distribution after deformation (Pa)	55
Figure 4.6	Effective plastic strain of the crack tip	57
Figure 4.7	Contact pressure of the edge crack tip	59
Figure 4.8	Effective stresses at crack tip	61
Figure 4.9	Crack size effect on the maximum shear stress at crack tip	63
Figure 4.10	Crack width behaviour at tow surfaces	63
Figure 4.11	Variation of crack depth along thickness direction	64
Figure 4.12	Plastic strain distributions for edge crack	65
Figure 4.13	Pressure distributions for edge crack	66
Figure 4.14	Maximum shear stress distributions for edge crack	68
Figure 4.15	Temperature distributions for the strip	69
Figure 4.16	Temperature distributions of the work roll	71

Figure 4.17	Temperature distributions along the crack depth	72
Figure 4.18	Temperature distributions along the thickness direction	73
Figure 4.19	Initial crack width effect	73
Figure 4.20	Initial crack depth effect	74
Figure 4.21	Effect of roll diameter on crack width	75
Figure 4.22	Effect of rolling reduction on crack closure behaviour	75
Figure 4.23	Behaviour of transverse crack during hot rolling process	77
Figure 4.24	Lateral deformation of transverse crack	78
Figure 4.25	Rolling force for the transverse crack (Reduction 20%)	79
Figure 4.26	Crack width along the slab width	79
Figure 4.27	Solid 168 element	80
Figure 4.28	Solid 164 element	80
Figure 4.29	Evolution of V-shaped transverse crack	81
Figure 4.30	Comparison of V-shaped transverse crack evolution along crack length	82
Figure 4.31	Comparison of V-shaped transverse crack evolution along the direction of slab thickness	82
Figure 4.32	Rolling force for the V-shaped transverse crack	84
Figure 4.33	Distribution of von Mises stress for the V-shaped transverse crack	86
Figure 4.34	Plastic strain distribution	87
Figure 4.35	V-shaped transverse crack with element type of ten-node	88
Figure 4.36	Evolution of V-shaped transverse crack along crack depth direction	88
Figure 4.37	Evolution of V-shaped transverse crack along crack length direction	89
Figure 4.38	Pressure distributions (Pa)	90
Figure 4.39	Distributions of maximum shear stresses (Pa)	91

Figure 4.40	Distribution of effective strain	92
Figure 4.41	Temperature distributions along the symmetrical plane	93
Figure 4.42	Location of selected areas A and B	93
Figure 4.43	Crack width behaviour	95
Figure 4.44	Crack length effect	95
Figure 4.45	Crack depth effect	96
Figure 4.46	Reduction effect on crack width	97
Figure 4.47	Effect of work roll diameter on crack width	97
Figure 4.48	Longitudinal crack rolls into the work roll gap	98
Figure 4.49	The section plane in the strip showing the state of deformation zone	99
Figure 4.50	Longitudinal crack behaviour	100
Figure 4.51	Rolling forces for longitudinal crack	102
Figure 4.52	Longitudinal crack evolution (d = 10 mm)	103
Figure 4.53	Distributions of von Mises stress (Pa)	105
Figure 4.54	Distribution of plastic strains	106
Figure 4.55	Pressure distribution of the longitudinal crack (Pa)	107
Figure 4.56	Temperature distribution for longitudinal crack (℃)	108
Figure 4.57	Cross-section temperature distributions of longitudinal crack (℃)	109
Figure 4.58	Temperature distributions along the longitudinal crack shape	109
Figure 4.59	Effects of convection and radiation on strip corner	110
Figure 4.60	Effect of contact heat transfer	111
Figure 4.61	Heat generated from deformation	111
Figure 4.62	Line contours of temperature	112

LIST OF TABLE CAPTIONS

Table 3.1	The schedule of the rolling models for edge cracks (mm)	37
Table 3.2	Models proposed for V-shaped transverse cracks on the slab (mm)	39
Table 3.3	Proposed models for the longitudinal surface crack on the slab(mm)	40
Table 3.4	Chemical compositions for the austenitic stainless steel 304	46
Table 3.5	Thermo-physical properties of the work roll	48
Table 3.6	Thermo-physical properties of the slab	48
Table 4.1	Rolling conditions of longitudinal crack	101

NOMENCLATURE

SEM	Scanning Election Microscopy
EBSD	Election Backscattering Diffraction
EDXS	Energy Dispersive X-ray Spectroscopy
EPMA	Electron Probe Micro-analysis
MPHL	Micro-plasto-hydro-dynamic Lubrication
S_r	Thermal effect
e	Elasticity
p	Plasticity
$d\{\varepsilon\}_e$	Incremental elastic strain
$d\{\varepsilon\}_p$	Incremental plastic strain
$d\{\varepsilon\}_t$	Incremental thermal strain
$[D]_e$	Elastic matrix
v	Poisson's ratio
f	Plastic potential
$\bar{\sigma}$	Effective stress
$\bar{\varepsilon}$	Effective strain
$\dot{\bar{\varepsilon}}$	Effective strain rate
T	Temperature
k	Thermal conductivity
ρ	Thermal density
c	Specific heat
$\dot{Q}_v$	Volumetric generation rate
$\dot{Q}_p$	Heat transformed from plastic deformation
$\dot{Q}_f$	Heat generated at slab/roll interface due to friction

C_{ijkl}	Temperature dependent elastic constitutive matrix
α	Coefficient of thermal expansion
σ_o	Initial yield modulus
E_p	Plastic hardening modulus
η	Efficiency of conversion of deformation energy to heat
D_{roll}	Diameter of the work roll
W	Slab width
H	Slab thickness
L	Slab length
d	Crack depth
w	Crack width
t	Thickness of reduction
θ	Crack open angle
R	Rolling reduction
b	Crack length
s	Distance between slab centre and crack centre
h	Coefficient of heat generation at slab/roll interface
T_∞	Temperature of the environment
l_x, l_y, l_z	Normal direction cosines on the boundaries
h_i	Interfacial heat transfer coefficient between the slab and the work roll
T_s	Temperature of the slab
T_R	Temperature of the work roll
h_c	Convection coefficient between the slab and the ambient air
σ	The constant of Stefan-Boltzmann
ε	The blackness of the slab surface
τ_{crit}	The critical shear stress
μ	Coefficient of friction

P	Contact pressure
$\ddot{u}(t)$	Acceleration vector of the system nodes
$\dot{u}(t)$	Velocity vector of the system nodes
M	Mass matrix
C	Damping matrix
K	Stiffness matrix
$Q(t)$	Vector of nodal nodes
l	Characteristic length of the element
c	Speed of sound of the material
E	Young's modulus

LIST OF PUBLICATIONS

1. **Shengnan Yang**, Zhengyi Jiang, Dongbin Wei, 3D coupled thermo-mechanical FE analysis of surface defects in continuously casting slab, Applied Mechanics and Materials 275-277 (2013), 2214-2220.

Statement of Authorship to Jointly Authored Works Contained in the Publications

The paper is composed of my original work since the commencement of Master by Research course, and does not contain any material previously published or written by other persons except where due references have been made in the text.

Prof. Zhengyi Jiang, as my principal supervisor at University of Wollongong (UOW), has continuously guided the direction of the research and provided comments and valuable suggestions on the submission.

My co-supervisor Dr. Dongbin Wei provided me with some helpful advice and suggestions on the research method and direction.

Chapter 1

Introduction

The surface quality of continuous casting slabs is one of the key quality parameters for these slabs and much effort has been made to ensure the highest quality products. Surface defects are often found to be cracks on the strip surface and they have proved to be difficult to eliminate during the subsequent hot and cold rolling processes. There are many reasons why these surface defects occur such as the non-homogeneous cooling and solidification, tensile stresses, phase transformation, friction and some other casting process parameters.

Many experiments have been carried out to study whether it is possible to eliminate the defects or to minimise their influence during the hot rolling process. Also, simulations have also been chosen to investigate the behaviours of defects due to the high reliability of simulations and their comparatively lower cost. In thermo-mechanical applications, simulations are helpful for examining various numerical parameters such as temperatures, heat generation, crack propagation, pressure, strain and heat transfer. In comparison with other numerical methods for investigating the process, the finite element method is the most practical and accurate one [1]. For the finite element method, there are different conditions hypothesised for the behaviour of materials.

Although the finite element method is a powerful approach for simulation of surface defects, nonlinear problems usually consume much more computational time. For achieving good results within a reasonable time, it is important to choose the proper types of formulations, solution techniques, discretisations and analysis methods.

1.1 Significance of this research

In order to meet customer demands without incurring prohibitive costs, the defects on slab surfaces should be reduced or eliminated. The reality is that the continuous casting process, not unlike most materials processes, is complex and must be understood in the context of industry production [2]. The study of surface defects behaviour during hot rolling is significant for understanding the deformation mechanism of cracks and for guiding productivity.

The materials used have various applications due to their different physical, chemical and mechanical properties [3]. The finite element method could predict the possible mechanical behaviour of the defects as well as data on the coupled thermo-mechanical behaviour, which is hard to obtain using an experimental approach. Finite element modelling could be especially successful with regard to revealing the stress, strain, pressure and temperature distribution around the defect area. The closure and growth of cracks on the slab surface could be predicted and analysed by taking into account the influence of the friction coefficient, the crack size, the work roll radius and rolling reduction.

The behaviour of defects can result in significant morphological changes of the cracks during hot rolling and afford valuable contributions to a deep understanding of the underlying processes in detail. By using systematic variations of geometric variables, the topology of surface defects on slabs could be identified and detected after hot rolling.

This study leads to concepts of crack closure and crack propagation in terms of the position, shape, orientation and dimensions of cracks. As outlined in the next section,

special emphasis is put on the quantitative correlation between the initial condition of the defects and the resulting deformation dimension and shape, as well as its influential parameters. This study also makes significant findings on the thermal effects that have not been studied during hot rolling process.

1.2 Research objectives

As mentioned above, researchers have encountered difficulties in studying the crack behaviour during hot rolling process with the experimental method. The finite element simulation approach was introduced to identify and classify defects and their relevant process variables. The objective of this research is to examine the possibility of crack self-healing or crack propagation. By studying rolling conditions and process data, the reliability of the models is examined and the corrective changes are optimised to achieve accurate results. The objectives of this study are listed as follows:

1. To examine the effect of process parameters on crack behaviour;
2. To find out possible approaches for minimising or eliminating surface cracks;
3. To determine the process data that affects crack size;
4. To improve the accuracy of solution techniques which are based on crack type and location;
5. To classify the defects in terms of increased risk, helping steel manufacturers to focus on the most critical crack problems;
6. To predict the occurrence of possible areas of folded layers and oxidation based on flow stresses and temperature changes.

1.3 Research methodology

The research methodology used in this study is finite element modelling based on explicit dynamic analysis. This is a recent innovation that relies on ANSYS/LS-DYNA software to provide a framework for building up the models and obtaining a keyword file to make calculations on higher performance computer clusters.

There is a fundamental feature of three-dimensional modelling used which makes it possible to fully understand the mechanical behaviour occurring in the process of hot rolling, especially in the deformation region. As most simulations described in the literature are two-dimensional models, the models in this thesis are designed in a three-dimensional format for steady state calculations. Metal flow is affected by the temperature distribution in the slab, because the properties of stress are strongly dependent on temperature. The introduction of coupled thermo-mechanical analysis is helpful for determining heat generation and strip/roll interface friction effects.

In order to develop a basic understanding of the metallurgical behaviour of surface defects, it is also necessary to predict the temperature, strain and strain rate that influence the recrystallisation of the materials. This also results in better prediction of the rolling force and softening of the materials. The oxide scale is formed on the strip surface when it is exposed to the ambient air under a high rolling temperature of about 1000 ℃. This also indicates the need for prediction of the variation of temperature distribution during different phases of the process.

In the hot rolling process, the contact condition is of crucial importance for obtaining reasonable results as it influences the final shape and profile of the workpiece and the defects it contains. The boundary conditions are vital to achieving optimum processing because the convection and radiation could be an influential factors in determining the change of thermal effects.

1.4 Outline of the thesis

The thesis comprises five chapters, and the appendices and reference materials. The content in each chapter is as follows.

Chapter one is the introduction. It provides background information about surface defects in continuous casting slabs. The thermo-dynamic method and the objectives of

this thesis are discussed, as well as its significance in the quest to ensure surface quality. The effects of processing parameters on surface profile products and defect behaviours are addressed in the proposed research.

Chapter two reviews the previous work done using both experiments and simulations. It includes the commonly found types of defects in the continuous casting slabs. The mechanisms of crack propagation and related theories are also discussed. The microstructures obtained by experiments are introduced as well as FE application results.

Chapter three outlines the basic theory of the finite element method and its constitutive equations. It includes the material models, proposed finite element models, the thermal and mechanical properties of materials, mesh density, and the initial types of surface cracks investigated under different rolling conditions with varying crack sizes. The thermal and mechanical boundary conditions are also described in order to obtain a thermo-mechanical coupled result.

Chapter four consists of the analysis of the three types of cracks and the influential parameters of the evolution of the cracks. The rolling force, pressure, stress, strain, and temperature are discussed and analysed for the proposed models. The predictions of crack behaviours are depicted and investigated for drawing conclusions in terms of parameters affecting the process.

Chapter five presents the research conclusions and recommendations for future work. This chapter includes the experiments on oxidation, lubrication, and varying material database. Finite element methods examine different material types, element types and mesh approaches. In order to examine the reliability of the available data, the results from experiments and simulations are compared to optimise the methods used to eliminate the slab defects.

Chapter 2

Literature Review

In this chapter the process parameters in the casting process will be analysed in order to investigate surface defects in continuous casting slabs such as surface cracks, inclusions, deep oscillation marks and corner cracks. This chapter begins with a brief description of theories relating to surface defects. The second part describes evolution of defects during hot rolling. Following this, an analysis of grinding methods and their effects on hot rolling is carried out. This chapter concludes with a discussion of problems and findings from the literature review and an outline of the scope of the present study.

2.1 Categories for surface defects analysis

2.1.1 Chatter marks

In the advent of chatter, the strip surface is covered with traverse bright strips called chatter marks (Figure 2.1). By optimisation of the hot rolling process, it is possible to minimise chattering. This will greatly reduce the possibility of chatter marks and roll wear, which influence product quality. Investigation of the process parameters will reduce plant down time and production waste.

As chatter diminishes, the distance between the strip chatter marks becomes larger until they vanish. In practical terms this means that if the distance between chatter marks is

larger than the circumference of the work roll, the level of vibration is considered safe. Designers and manufacturing engineers have investigated tool design as a means of controlling vibration during the rolling process. Ubici [4] developed finite element models to analyse the clearances of the mobile assemblies of the rolling mill stand and found that the clearances should be decreased. Some researchers investigated the frequency bands and made the rolling conditions stable by changing rolling speeds to limit these bands. Sun et al. [5] and Yang et al. [6] have proposed methods to statistically analyse the correlation between the variations and vibrations which is seen as a crucial piece of information.

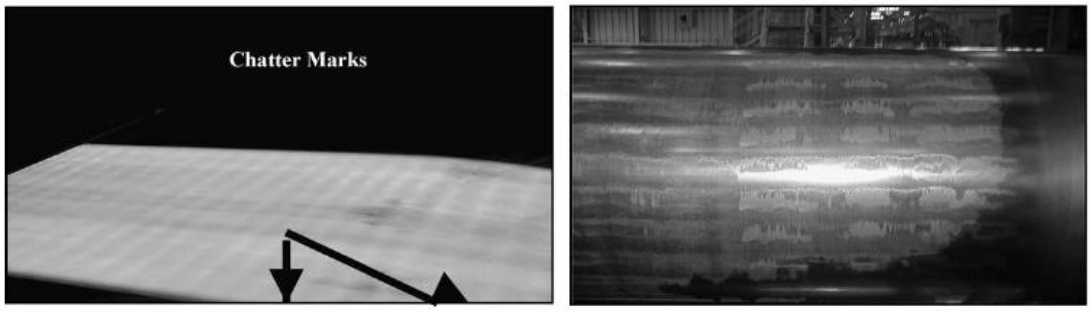

(a) Strip surface with chatter marks (b) Chatter marks along roll surface

Figure 2.1 Effects of chattering on rolled sheets and the rolling equipment [7]

Through optimisation of the critical process parameters such as the slab temperature, reduction ratio and rolling speed, it is practicable to keep the rolling force below a certain level and thereby reduce the incidence of chatter marks. Consequently, the flatness and profile of the slab could be improved, and the stability of the equipment performance could be strengthened.

2.1.2 Deep oscillation marks and hook surfaces

Deep oscillation marks and subsurface hooks in continuous casting slabs can cause many slab quality problems. The argon bubbles and inclusions may easily entrap hooks and lead to slivers, blisters and transverse cracks. Researchers have proposed many methods

to select different parameters to optimise the mould oscillation system in the continuous casting process of steel manufacturing. Lubrication has been considered to be a practicable method to reduce the intensity of oscillation marks. The amplitude, frequency and waveform of the oscillations involved have been introduced by an updated algorithm [8]. This objective functions aim at maximising the lubrication and minimising the depth of oscillation marks and the cycle peak friction.

Continuous casting is a critical step in the steel manufacturing process where molten metal is solidified in the form of slabs of rectangular cross-sections [9]. The products can be impacted by minor variations in this process and as a result the production chain could be broken down. Two interlinked sub-processes, namely, mould oscillation and lubrication addition could improve the continuous casting process. The mould is made to oscillate along its longitudinal direction to help in detach the solidified slab from the mould wall. The lubrication is added to fill the small gap between the shell and the mould to facilitate this process. During this procedure, there will be an overflow of liquid steel that gives a rise to oscillation marks at the corners in the casting direction, as shown in Figure 2.2.

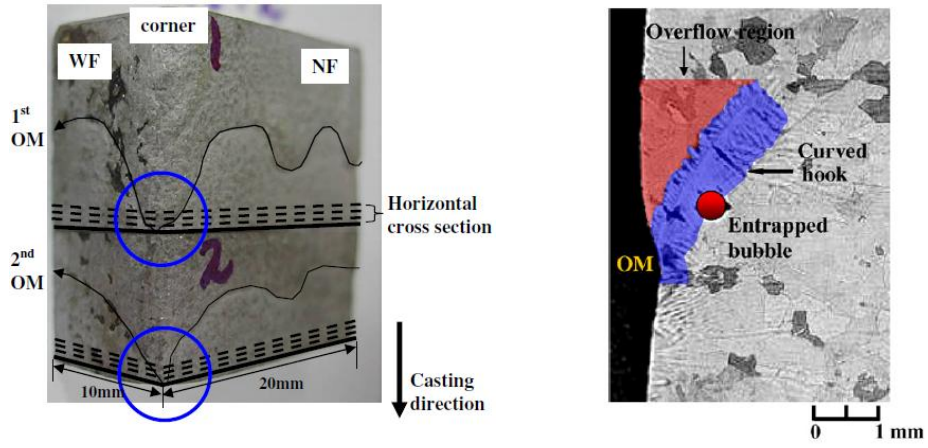

(a) Oscillation mark located on the slab (b) Optical micrograph of curved hook

Figure 2.2 An ultra-low-carbon steel sample showing a curved hook-type oscillation mark [8]

The mechanism of the microstructure is supported by using optical microscopy, scanning election microscopy (SEM), election backscattering diffraction (EBSD), energy dispersive X-ray spectroscopy (EDXS) and electron probe micro-analysis (EPMA) techniques [10].

2.1.3 Main surface cracks

Surface cracks are often found on continuous casting slabs and hot spots are also often found on the skin of the slab during casting [11]. These surface defects in continuous casting slabs can be elongated or kept down, depending on the type, size and distribution of primary defects as well as on rolling parameters [12]. The possible source of surface defects could come from some phases in the manufacturing processes such as the production and casting of steel, the heating and cooling of material, hot slab rolling and cold slab rolling.

Surface defects could come from the steel casting process which leads to inclusions, blowholes, scars, layers of oxidation, holes, longitudinal cracks, transverse cracks and edge cracks [13].

2.1.3.1 Longitudinal cracks

Longitudinal cracks, as shown in Figure 2.3, are usually deeper than other kinds of surface defects. They are often formed near the central line of the slab surface due to non-homogeneous cooling conditions during the solidification and the increase of transverse tensile stresses.

The behaviour of the cracks has been studied using the finite element method [14]. The behaviour of the cracks as influenced by rolling schedules, friction, roll radius and rolling reduction is analysed by using the commercial finite element code. Much research has been carried out to identify the sensitive steel grades which are characterised by

approximately 0.12% C and a higher content of sulphur compared with manganese. However, no theoretical work has been found which deals with crack behaviour by taking into account thermal effects and the location influences.

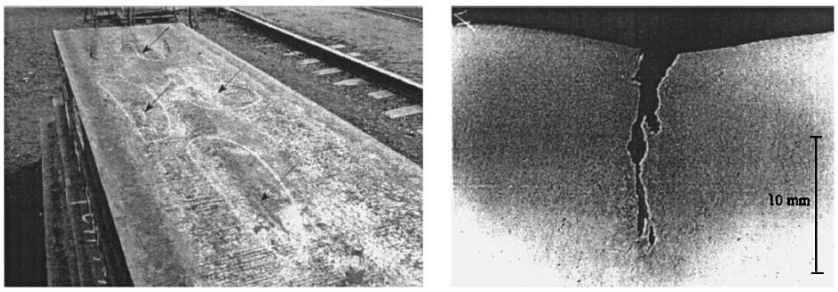

(a) (b)

Figure 2.3 (a) Longitudinal cracks on the surface of a continuously cast slab. (b) cross-section showing a longitudinal crack [11]

2.1.3.2 Transverse cracks

Transverse cracks are often found (Figure 2.4) on the surface in continuous casting slabs. If the cracks cannot be healed after the hot rolling process, they might be made worse in subsequent processes such as cold rolling, and this can give rise to the problem of slab surface quality. Due to the temperature gradients, these cracks are formed due to the thermal effects and chemical composition of the materials.

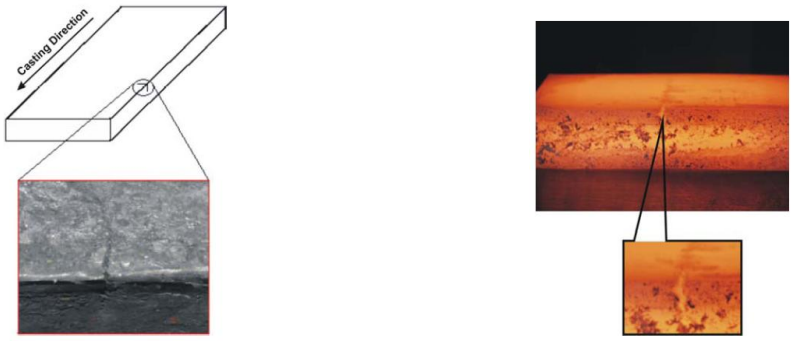

(a) V-shaped transverse crack on the slab (b) A detailed sample before hot rolling

Figure 2.4 V-shaped transverse crack on a steel block to be rolled at the experimental rolling mill [15]

Similar to longitudinal cracks, transverse cracks are also dependent upon steel grades containing aluminium, niobium, vanadium and manganese which are regarded as very sensitive [16]. Figure 2.5 shows a transverse surface crack on a continuous casting slab. Many researchers have studied the mechanism of crack formation [17]. The generation of these defects is promoted by severe cooling conditions during solidification in the continuous casting mould, and thermal and mechanical stresses generated during secondary cooling and slab bending operations.

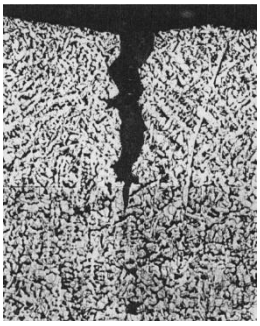

Figure 2.5 Transversal crack in slab rolling [16]

2.1.3.3 Star cracks

One type of surface defect found in slabs (Figure 2.6) is the so-called star crack. This defect is discovered after the oxidation layer of the slab surface has been disposed of. This procedure could cause changes in thermal and mechanical properties on the surface and the formation mechanism could be affected due to the loss of evidence.

During the manufacturing process, slab surfaces containing anomalies comprising certain kinds of chemicals are examined after the scarfing of the entire surface. The aim of this study is to ensure that small pieces of steel containing these anomalies are cut off by convectional grinding and polishing methods. A scanning electron microscope (SEM) is used to check for crack propagation and metallographical information.

Some experiments were carried out to study the characteristics of star cracks found in industrially produced steel slabs. Through investigating the solidification of molten steel when introducing Cu in the moulds, the propagation and formation of star cracks has been shown to occur during cooling conditions [18].

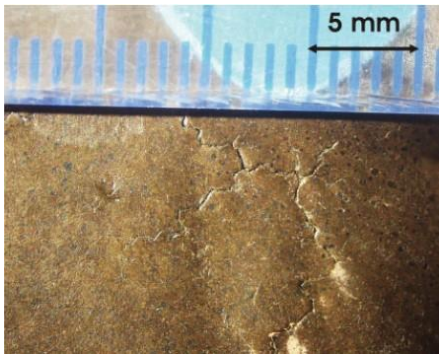

Figure 2.6 A representative star crack on the surface of steel slab [19]

When the content of Cu in the slab exceeds its solubility in austenite, liquid Cu will precipitate at the slab surface during oxidation when the temperature is high, and this could lead to the penetration of Cu into the grain boundaries [20].

2.1.3.4 Blisters and slivers

The blisters and slivers on the slab surface could affect the performance, durability and integrity of the processing. It is very important to understand the morphological behaviour after hot and cold rolling. Through a step machining method, the initial defects could be located and this could provide guidance for tracing their movement by using numerical methods [21, 22].

Argon is introduced, along with liquid steel during slab casting, and this helps in flushing out non-metallic inclusions such as the mould powder. However, entrapment of the argon or the mould powder will cause blisters or slivers, and these defects will deteriorate after

the rolling processes which follow. Figure 2.7 shows typical photographs of blisters and slivers on a continuous casting slab surface.

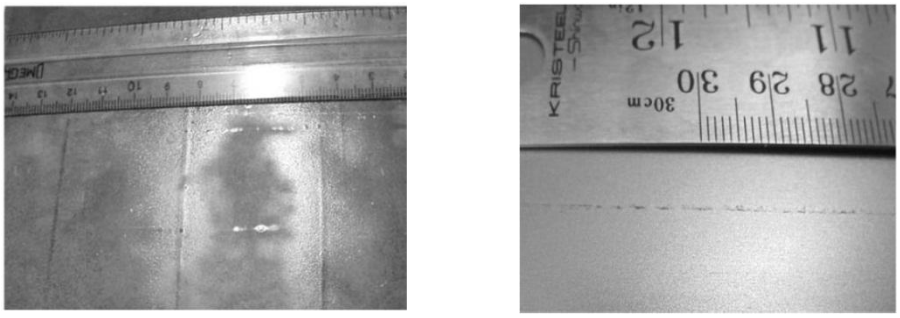

(a) (b)

Figure 2.7 Surface defects due to inclusion entrapment resulting in (a) blisters and (b) slivers in final product [21]

In order to reduce the downgrading of surface defects during the rolling process, some measures such as scarfing or machining need to be undertaken before further rolling processes. It has also been reported that the size and number of defects are inversely correlated with depth from the slab surface [22]. They reduce exponentially with the initial depth during the casting process.

2.1.3.5 Contact fatigue cracks

Surfaces in rolling contact are influenced by interaction between contact elements which are exposed to material contact fatigue. Contact fatigue can be defined as a kind of damage resulting from changes to the material microstructures which lead, initially to crack initiation, and then to crack propagation, under the influence of time-dependent rolling and sliding contact loads [23, 24].

The fluid film between the contact surfaces has been considered in the contact fatigue process by Ogura and Miyoshi [25], and they found that non-propagation cracks occur when the value of the effective stress intensity factor decreases and reaches its threshold value. The growth and arrest behaviours are found to be closely correlated with

mechanical parameters. The stress intensity factor is evaluated by using the following formulas:

$$K = 1.1215\sigma\sqrt{\pi a} \quad \text{for } a < \rho \tag{2-1}$$

$$\sigma = K_t\sigma_n\sqrt{1/(1 + 4.5\,a/\rho)} \tag{2-2}$$

$$K = F(\xi)\sigma_n\sqrt{\pi(a + d)} \quad \text{for } a > \rho \tag{2-3}$$

$$F(\xi) = \sqrt{(\tan\xi/\xi)}(0.923 + 0.199(1 - \sin\xi)^4)/\cos\xi \quad \xi = \pi a/2B \tag{2-4}$$

where a is a crack length, ρ is a notch root radius, d is a notch depth, $2B$ is a specimen width and σ_n is the nominal stress based on the net section. ΔK is defined as $K_{max} - K_{min} = K_{max} \times (1 - R)$, R is the roll radius, ΔK_{eff} is calculated as $\Delta K_{eff} = U \times \Delta K$ by using the effective stress range ratio, $U(= (\sigma_{max} - \sigma_{op})/(\sigma_{max} - \sigma_{min}))$.

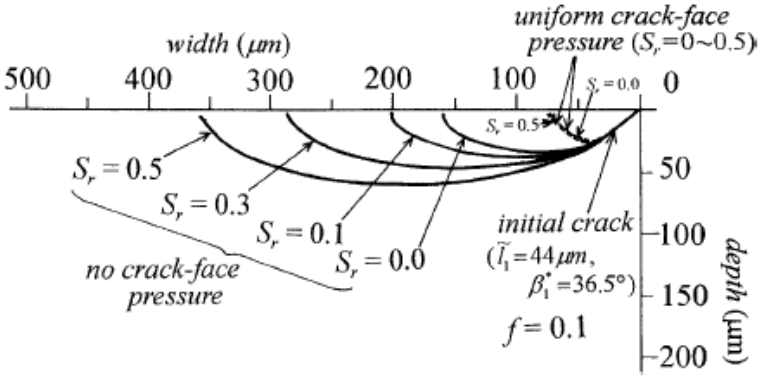

Figure 2.8 Predicted crack growth path, showing the thermal and crack-face pressure effect for $f = 0.1$ [26]

Numerical results based on stress intensity factors can be obtained to explain using these formulae to explain crack propagation. According to Figure 2.8, the initial cracks are abruptly curved toward the contact surface due to the influence of tensile stress under

uniform crack-face pressure. It is clearly shown that the predicted crack growth path will be enlarged by the thermal effect (S_r). The thermal effect, which is caused by friction heat, will cause an increase in surface growth and reduce the fatigue life. Researchers have found that the crack morphology is also affected by the rolling direction reversal [27]. The degree of this effect depends on the reversal factor.

Through an updated dimensionless size model, contact fatigue cracks were developed and tested by Bogdanski and Trajer [28], and the results are in close agreement with previous work. This method is less laborious and less time consuming. The model, based on energy release rate is analysed, which could find the direction of the crack propagation [29].

2.1.3.6 Side and edge cracks

The side cracking that is often found on the surface of the side parts along the rolling direction decreases the productivity of slabs, especially after hot rolling. When cracking occurs on the strip surfaces, side trimming and cutting are usually applied on the production line. The causes of side cracking are generally rolling conditions and the materials themselves. With respect to materials, cracks can occur when microvoids are generated along grain boundaries due to volume change during the rolling process when the phase transformation happens from austenite to ferrite [30, 31].

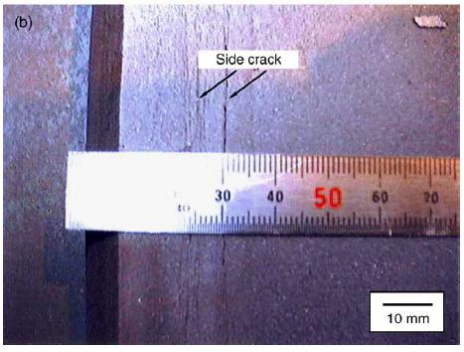

Figure 2.9 A photograph showing typical side cracks formed on the strip surface [32]

Side cracks are often found on both of the slab sides and the top and bottom of the plate surfaces, and all these side cracks are parallel to the rolling direction. Figure 2.9 shows typical side cracks on the strip surface. Most of the side cracks are fine and thread-shaped and some are large cracks several millimetres in depth, which are observed using an optical microscope and a scanning electron microscope. The austenitic grain boundary is a favourable place for cracks to originate and propagate in the temperature range of 800 to 1200 ℃ [33].

Some researchers have studied the effects of edge cracks on microstructure by considering certain temperatures and strain rates, while the effects of temperature changes were ignored [34-37]. All of the influential factors should be considered to obtain the more accurate results. The hot rolling process is complicated due to interacting processing parameters such as thermal changes, mechanical changes and ductile damage. Therefore, a coupled thermo-mechanical analysis is necessary to predict the behaviour of edge cracks in rolling slabs.

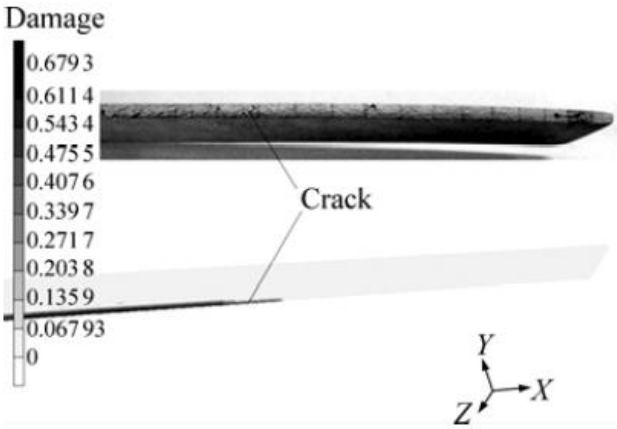

Figure 2.10 Edge crack results of experiment and FEM [38]

The Crockroft-Latham theory was used to investigate the behaviour of edge cracks. This theory assumes that the damage is caused by the maximum tensile principal stress, and

that when the energy caused by the maximum tensile principal stress and strain reaches a certain value, the damage takes place. The constitutive equation of this theory is:

$$\int_0^{\varepsilon_f} \sigma_{max} d\bar{\varepsilon} = C \tag{2-5}$$

The critical value to crack is normally set to 0.45. Figure 2.10 shows the FEM damage result and a photo of a rolled specimen of an alloy sheet. The cracks at the edge arise because of the maximum tensile principal stress and the increased principal plastic strain at the rolled edge. Cracks will be generated when the deformation is beyond the stress or strain limit, and the stress-strain energy is beyond the critical value.

2.2 Internal cracks

Internal cracks are one of the key reasons for defects in steel plate products, and they are found to be caused by inclusion, pore, gravity segregation, shrinkage and so on. It is reported that these cracks could be closed with sufficient reduction and compressive stress, but they will propagate in condition of insufficient reduction and tensile stress during rolling [39]. Geometrical and mechanical conditions are the main factors influencing the closure of cracks during the rolling processing of slabs.

2.2.1 Central cracks

The possible occurrence of central bursts has been studied and it is found that they will happen due to large friction, low reduction, large initial thickness of the workpiece and small roll radius for a given material. Wei et al. [40] and some other researchers have studied the critical conditions of crack closure during rolling processes and the relationships between the critical closing conditions and process parameters have been reported by applying ANSYS/LS-DYNA.

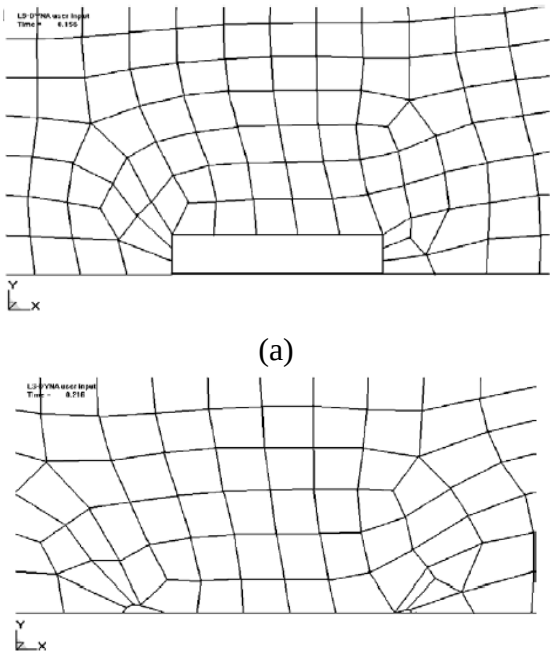

(a)

(b)

Figure 2.11 Central rectangular crack closing behaviour during rolling [41]

Researchers have analysed the critical conditions influencing the behaviour of central rectangular cracks. The shape evolution of these cracks is displayed in Figures 2.11 (a) and (b) where the initial conditions and the final conditions can be clearly seen. The critical conditions of an internal rectangular crack closing for slabs during hot rolling by applying an upper-bound triangular velocity field is given as follows [42]:

$$\frac{l}{\bar{t}} \leq \left(\frac{l}{\bar{t}}\right)_{critical} \tag{2-6}$$

where l is the contact arc length, and $\bar{t} = \left(t_0 + t_f\right)/2$ is mean plate thickness. It is found that a large gap between the pass reduction of the workpiece and the critical reduction is needed for crack closure. So the rolling pass reduction of the workpiece should be increased up to a certain degree, according to Equation (2-6), to avoid internal defects.

2.2.2 Inclusions and bubbles

Inclusions in steels can be indigenous inclusions or exogenous inclusions. The former are deoxidation products or inclusions precipitated during cooling and solidification processes. The latter arise primarily from the incidental chemical and mechanical interactions of liquid steel with its surroundings. The sources of most fatigue problems in steels are hard and brittle oxides, especially large alumina particles over 30 μm [43-45].

The final properties of the steel slabs are influenced by the deformability of inclusions during the hot rolling process. Some experimental work has been proposed to investigate the behaviour of inclusions during hot rolling.

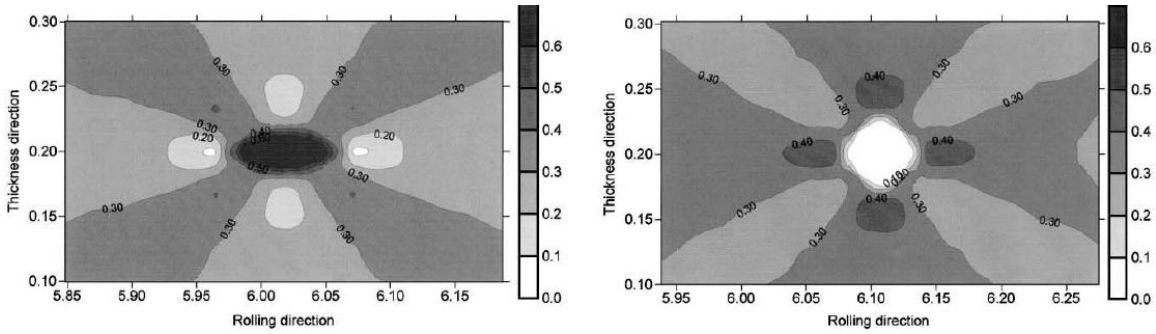

(a) (b)

Figure 2.12 (a) Effective strain distribution for a soft inclusion and its surrounding material, T = 1200 ℃, (b) effective strain distribution for a hard inclusion and its surrounding material, T = 700 ℃ [46]

The deformation characteristics of a hard inclusion and a soft inclusion within a cell element are shown in Figure 2.12. The soft inclusion is elongated along the rolling direction at high rolling temperature. The hard inclusion, on the other hand, remains almost undeformed or rigid. It is also concluded that the strain distribution in the steel matrix near the inclusion acts in an opposite way [46]. The rolling temperature is the most active parameter that affects the deformation of silicate inclusions during the hot rolling of low carbon steels. The inclusion remains rigid before the transition temperature region, but it becomes deformable after this region. Near the hard particle, it is more

likely for the voids to be formed [47]. The use of larger rolls would decrease the risk of the formation of voids. Furthermore, the threat of void formation turned out to be lower for high reductions and in the vicinity of the slab surface.

As the embedded defects are hard to find, Tripathy [21] has proposed a point tracing method to locate the defects after the rolling process. This saves material and is less expensive than the step machining experimental method. Figure 2.13(a) displays the initial location of six inclusions at varying depths. Figure 2.13(b) shows how inclusion 1 remains on the surface, but inclusion 2 moves towards the surface. This means that the inclusions closer to the surface at a certain level will rise up to the surface by fracturing of the material around the inclusion, and other inclusions will remain embedded in the slab.

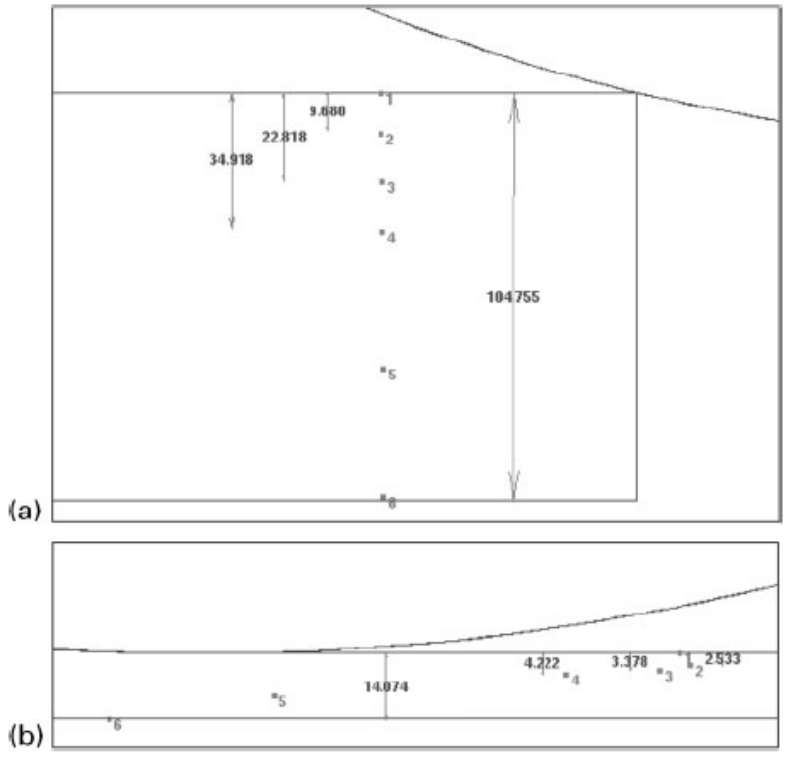

Figure 2.13 Six inclusion locations at start rolling (a), positions of inclusions at end of rolling (b) [21]

As stated before, inclusions and voids can propagate cracks during the hot rolling process. In Figure 2.14, in the inclusion there is a crack propagation that is parallel to the contact surface where the maximum shear stress occurs. It has been found that the tensile stress appears near porous areas of the slab after the rolling process [29].

Plastic strain during the rolling process is, therefore, introduced in these particular zones. The tensile residual stresses and tensile hydrostatic pressures will occur due to these plastic strains as well as the elastic recovery of the materials.

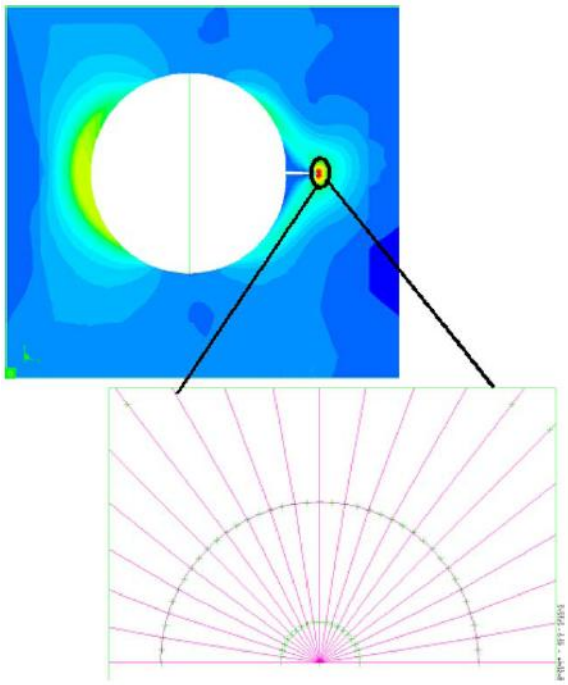

Figure 2.14 Crack propagation in the inclusion [29]

Bubbles entrapped on the solidifying shell are normally less than 3 mm in diameter, and are called pinholes or blowholes. Figure 2.15 shows the bubbles attached to inclusions and this will give rise to some line defects such as blisters and slivers which have been discussed in the previous section. It is found that more pinholes are near the centre of the width with a peak size of 0.3-0.4 mm [48]. This may explain the serious white band found on the centre of the surface of the rolled plate.

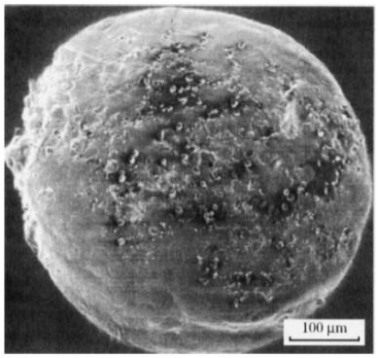

Figure 2.15 Bubbles attached to Al_2O_3 inclusions in slab [49]

2.3 Grinding method

There is a certain kind of study that will be introduced into the production line between casting and rolling. Stainless steel slabs need to be prepared before they experience the next rolling process, and the method that is normally used to remove surface imperfections is called grinding. Slab grinding removes surface irregularities that form and harden as the steel cools [50]. Typically, slabs will be cooled before grinding, and then they need reheating for rolling. The grinding machine is placed in the region between the caster and the hot mill, and this will ensure a continuous product flow.

A coarse cut will be involved in the slab grinding, which is followed by treatment using a fine grinding mill for optimising the surface roughness. The grinding pressure is adjusted according to the time used to keep metal removal to a minimum. This grinding process is designed to avoid possible defects which may be elongated during rolling.

The relationship between the machining conditions and the surface damage caused by the process was studied by researchers [51-53]. They tried to find a balance between the most economical grinding procedure and the most self-crack-healing grinding procedure. Figure 2.16 schematically shows a typical grinding procedure for the rolling process. The

smooth specimen may have some minute surface defects from a precious polishing process. By crack healing under optimised conditions, the specimen can be kept from further generation of defects and imperfections.

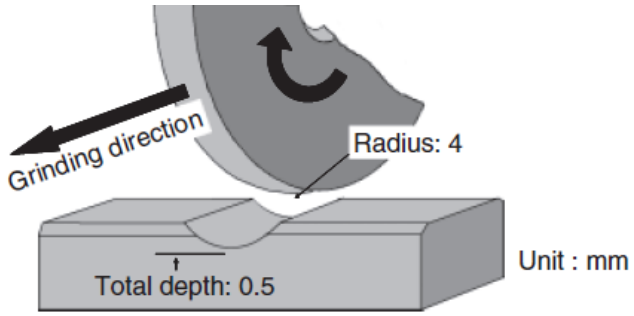

Figure 2.16 Schematic illustrations of the machined process [54]

2.4 Characteristics of oxidation around defects

Figure 2.17 shows a proposed mechanism for the formation of slab defects filled with iron oxide and internal oxides [55]. The defect contains fine oxides and other metallic oxides at a certain depth below the slab surface. The formation of these oxides is usually caused by iron oxide which is entrapped in slabs and subjected to high temperatures, and researchers have found that possible sources of oxidation exist throughout the whole process, including slab cracks, argon bubbles and pinholes, mechanical damage, scarfing, inhomogeneous reheating and roughing.

The ferrite-pearlite band structure in the slab is considerably slanted to the surface with the iron layer formed by inhomogeneous oxidisation along the slanted ferrite-pearlite band. Based on these findings, the correlation between the microstructural factors and hot rolling conditions is investigated to minimise the possible number of ways that oxidation around defects can occur. The iron oxides often form either agglomerates or pores in the interior and the brittle oxides will be smashed during the hot rolling process, and this will leave grooves on the slab surface.

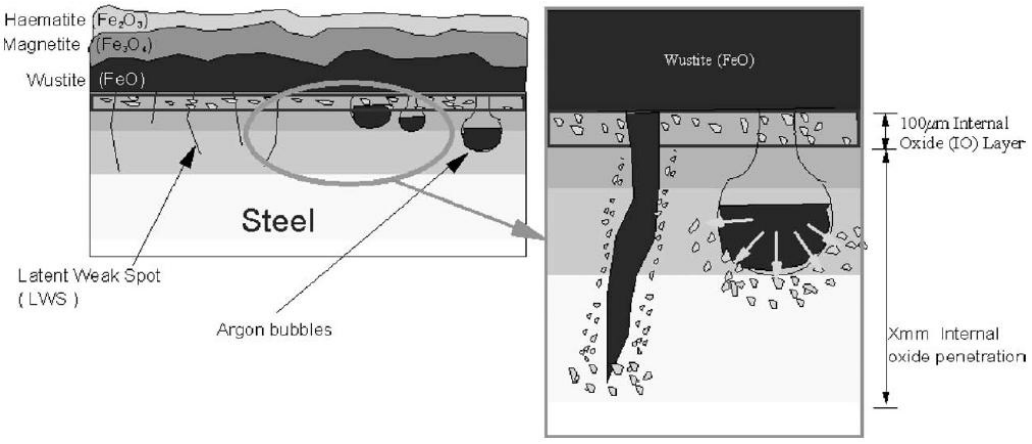

Figure 2.17 Schematic diagram of the mechanism of FeO and internal oxide formation [55]

The effect of crystallisation behaviour has been studied and it was found that crystals play an important role in a mould to facilitate uniform solidification. The internal oxide only forms at high temperatures, under higher oxygen concentrations and over relatively long time periods [56, 57].

2.5 Analytical modelling

The behaviour of surface defects has been investigated experimentally by many researchers. Numerical simulations for a three-dimensional analysis of surface defects during hot rolling have not often been reported. Rigid-plastic and elastic-plastic formulations and some simplified assumptions were taken into account by some researchers when analysing the hot rolling process [58-64]. Some simulation work has been done by using the viscoplastic, elastic-viscoplastic or thermo-elastic-viscoplastic models [65-70], which are determined by the rolling materials and the rolling conditions.

The problem can be analysed using one-, two- or three-dimensional fields when the computer computational time is considered. The reliability and accuracy of outputs is

influenced by the interaction of volume properties such as the strain-hardening function, strain-rate and temperature effects, and surface properties like friction, thermal transfer, lubricant films and transformed layers.

Models are often built which incorporate visco-plastic or rigid-plastic behaviour, and this will help to keep the flow formulations from encountering problems of enforcement of incompressibility. Also, elastic-plastic and elastic-visco-plastic constitutive equations are assumed in some models which examine these issues. The latter are models which are much more complicated and pay attention to the stress rate and the integrated time in each element. Thermal effects are the most influential factors in hot slab rolling processes through thermo-mechanical coupling as well as through their effect on microstructure. Thermal effects should also be considered even in cold slab rolling. For example, the excessive heat transformed from deformation and friction would give rise to recrystallisation at the region where the deformation and friction occur, which would largely affect the slab's mechanical properties. The friction is modelled by Coulomb's coefficient, with a limitation by a friction factor. This theory normally uses a constitutive equation and is applied in models of this thesis.

2.6 Surface defect recovery mechanism

It is known that lubrication is applied in the rolling condition to ensure the final product surface quality. In some conditions, the lubricant can be entrapped in defects where hydrostatic pressure tends to prevent its elimination. However, the lubricant could be drawn out by hydrodynamic effect and the defects could be recovered when some conditions are satisfied.

The micro-plasto-hydro-dynamic lubrication (MPHL) model is defined by using the hydrodynamic lubrication theory. This model indicates that defect elimination depends on defect geometry and hydrodynamic actions. Also, this model can be used to calculate the

microfilm thickness of the lubricant at the asperity's edge. The mechanism of the MPHL is shown in Figure 2.18.

When the thin lubricant film is drawn into the contact area between the strip and the work roll, the lubricant acquires hydrodynamic lift. This will deform the top of the asperity and generate a hydrodynamic microfilm. When the lubricant leaves a microcavity, the pressure in the valley decreases below the mean value and the defect will be stretched.

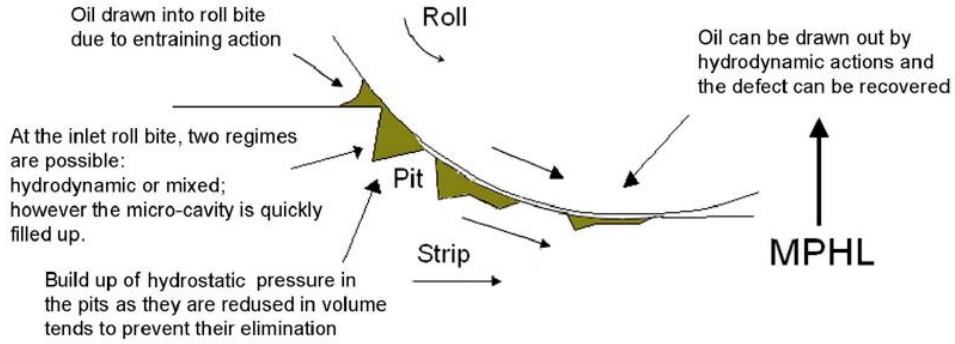

Figure 2.18 Scheme of MPHL mechanism [71]

2.7 Problems and findings from the literature review

The quality of continuous casting slabs has a significant effect on the surface quality of hot rolled slabs. Due to the fluctuation of process parameters in the casting process, it is unavoidable that surface defects exist in continuous casting slabs. These defects include surface cracks, inclusions, deep oscillation marks and corner cracks. Conditioning has to be conducted before the slabs go to the next step of the process. Conditioning of slabs plays a decisive role in quality assurance because a small surface defect can become elongated during the rolling process and can become an extensive product defect, resulting a considerable expense for conditioning and making quality assurance in all the product lines difficult. However, when some favourable conditions are satisfied, the lubricant can be drawn out by hydrodynamic action and defects can be recovered.

Grinding is adopted on many stainless steel production lines to remove surface defects. It is normally performed along the rolling direction. In some cases, the angle between the grinding and rolling directions is around 45 °. The effect of the hot rolling process on the evolution of surface defects will be the main focus, and this has a huge influence on the final surface status. Little research has been done to evaluate surface defects in hot rolling processes under three dimensional fields, and convection and radiation effects have not been introduced in such research. In addition, no research has determined the defects' influence on the rolling force during the process. Most of the analysis reported here about crack behaviour is based on experimental methods, which could not efficiently show how thermal effects interact with other processing parameters.

2.8 Research scope in the present study

In this study, a coupled thermo-mechanical method will be implemented for surface defects simulation. The material used for the proposed models is the austenitic stainless steel AISI 304. In order to investigate the behaviour of defects after the hot rolling process, some surface cracks on the stainless steel are modelled and analysed. The accuracy of the results of defects behaviour modelling is examined and compared by using different mesh densities and element types. Also, the effects of rolling conditions and processing parameters, such as the contact heat transfer, heat conductivity, initial temperature, heat generated from deformation, diameter of the work roll, thickness reduction and crack sizes, will be analysed.

The objective of this research is to investigate possible ways of eliminating or reducing surface defects by applying finite element simulations. Three types of surface defect models, considering edge cracks, transverse cracks and longitudinal cracks, are developed. Through studying process parameters, the mechanisms of crack behaviour are obtained. They could be used to identify the possible factors that cause crack propagation and stretch. It will also focus on analysing the thermal effects around the crack area, because the temperature change will cause phase transformation, and that has a dramatic influence on the surface condition and correlative mechanical properties of products.

Chapter 3

3D Finite Element Method Theory and Simulation Conditions

3.1 Introduction

The finite element method is used to study crack behaviour during the hot slab rolling process. In most research, simulations are developed using two-dimensional models. The initial conditions are symmetrical and can therefore be modelled in two dimensions, but deformation along the third dimension is not always uniform. Therefore, it is preferable to analyse these problems with three dimensional models.

Due to the largely distorted and rotated hot rolling process, nonlinearity is introduced into the deformation, material behaviour, and boundary conditions. In this study, the up-dated Lagrangian finite element method has been implemented in the simulation of crack behaviour.

The aim of this study is to view the crack deformation process from the viewpoint of three-dimensional deformation. A coupled model of thermo-elastic-plastic material under large deformation by the hot rolling process is developed. In addition, flow stress is taken as a function of strain, strain rate and temperature.

3.2 Basic theory of the thermo-elastic-plastic coupled finite element method

Crack evolution is one of the most serious problems in continuous casting slabs, and the behaviour of cracks has a large influence on the final product surface quality. The nonlinearity which is present during the rolling process has an effect on geometrical behaviour, material behaviour and boundary conditions. In LS-DYNA3D, the commonly used formulation method is the updated Lagrangian finite element method, which is applied to simulate the behaviour of defects in this study.

According to the theory of large stain deformation and updated Lagrangian formulation, the simulation of flow stress and effective stress with their incremental values can be achieved by applying the Prandtl-Reuss flow rule.

3.2.1 The equilibrium between elastic and plastic deformation

There are different kinds of expressions for stress and strain. Based on the Prandtl-Reuss hypothesis and the Mises yield criterion when the stress is less than the elastic limit, elastic deformation takes place. When the stress is beyond the elastic limit, plastic deformation occurs. When the stress is greater than the elastic limit, the material has been introduced into a plastic state, and the deformation includes two parts: elastic and plastic deformation. This is expressed as follows:

$$\mathrm{d}\{\varepsilon\} = d\{\varepsilon\}_e + d\{\varepsilon\}_p + d\{\varepsilon\}_t \tag{3-1}$$

where *e* and *p* represent elasticity and plasticity, respectively, $d\{\varepsilon\}_e$ is the incremental elastic strain, $d\{\varepsilon\}_p$ is the incremental plastic strain and $d\{\varepsilon\}_t$ is the incremental thermal strain. Within the elastic range, the stress and strain relationship satisfies

Hooke's law. When entering the plastic range, it satisfies the Prandtl-Reuss hypothesis.

3.2.1.1 Elastic range

Within the elastic range, the relationship between the stress and strain is linearised, and the stress is determined by the last stress state with its correspondence to each other, which nothing to do with the deformation process, which is written as:

$$\{\sigma\} = [D]_e\{\varepsilon\} \tag{3-2}$$

where $[D]_e$ is the elastic matrix. For isotropic materials, it could be derived based on Hooke's law as:

$$[D]_e = \frac{E}{1+\nu}\begin{bmatrix} \frac{1-\nu}{1-2\nu} & \frac{\nu}{1-2\nu} & \frac{\nu}{1-2\nu} & 0 & 0 & 0 \\ \frac{\nu}{1-2\nu} & \frac{1-\nu}{1-2\nu} & \frac{\nu}{1-2\nu} & 0 & 0 & 0 \\ \frac{\nu}{1-2\nu} & \frac{\nu}{1-2\nu} & \frac{1-\nu}{1-2\nu} & 0 & 0 & 0 \\ 0 & 0 & 0 & \frac{1}{2} & 0 & 0 \\ 0 & 0 & 0 & 0 & \frac{1}{2} & 0 \\ 0 & 0 & 0 & 0 & 0 & \frac{1}{2} \end{bmatrix} \tag{3-3}$$

where ν is Poisson's ratio.

3.2.1.2 Elasto-plastic range

For the material when the external force reaches a certain value, the equivalent stress reaches the yield limit. When the stress is beyond the elastic limit, plastic deformation occurs. A thermo-elastic-plastic constitutive equation is derived under the theory of the updated Lagrangian formulation and the Prandtl-Reuss flow rule. Plastic

deformation and the friction between the workpiece and the work roll interface will generate heat that contributes to the temperature increase of the workpiece. Then thermal strain is induced by the rise of temperature during the following process. The total incremental strain $\mathrm{d}\{\varepsilon\}$ is expressed as Equation (3-1). Therefore, the incremental stress can be expressed as follows:

$$\mathrm{d}\{\sigma\} = [D]_e\left(d\{\varepsilon\}_e - d\{\varepsilon\}_p - d\{\varepsilon\}_t\right) \tag{3-4}$$

where $[D]_e$ is the stress-strain matrix for an elastically deformable body. The incremental plastic strain $d\{\varepsilon\}_p$ is treated as a derivative of the plastic potential f:

$$d\{\varepsilon\}_p = \lambda\left\{\frac{\partial f}{\partial \sigma}\right\} \tag{3-5}$$

where λ is a non-negative constant of proportionality which may vary with the stain. As the Mises yield criterion is used in the model, the flow stress, therefore, becomes a function of temperature, effective strain, and effective strain rate. The equation for flow stress for the material is shown as:

$$\bar{\sigma} = f(\bar{\varepsilon}, \dot{\bar{\varepsilon}}, T) \tag{3-6}$$

where $\bar{\sigma}$ is the effective stress, $\bar{\varepsilon}$ the effective strain, $\dot{\bar{\varepsilon}}$ the effective strain rate, and T the temperature. It is assumed that the material hardens isotropically and the strain-hardening rate is defined as:

$$H' = \frac{d\bar{\sigma}}{d\varepsilon^p} \tag{3-7}$$

The the stress-strain relationship of Equation (3-4) becomes:

$$d\{\sigma\} = [D]_{ep}(d\{\varepsilon\} - d\{\varepsilon\}_t) + \frac{\left\{\frac{\partial f}{\partial \sigma}\right\}\left\{\frac{\partial f}{\partial \sigma}\right\}^T [D]_e d\{\varepsilon\}}{H' + \left\{\frac{\partial f}{\partial \sigma}\right\}^T [D]_e \left\{\frac{\partial f}{\partial \sigma}\right\}} \tag{3-8}$$

where

$$[D]_{ep} = [D]_e - \frac{[D]_e\left\{\frac{\partial f}{\partial \sigma}\right\}\left\{\frac{\partial f}{\partial \sigma}\right\}^T [D]_e}{H' + \left\{\frac{\partial f}{\partial \sigma}\right\}^T [D]_e \left\{\frac{\partial f}{\partial \sigma}\right\}} \tag{3-9}$$

Equation (3-8) is the thermo-elastic-plastic constitutive equation that takes account of the strain rate and temperature. It is clear that when the processing is in the elastic range, $[D]_e$ may be put into the constitutive equation instead of $[D]_{ep}$.

3.2.1.3 Thermal governing equation

There are two things causing the generation of heat during the rolling process: the plastic deformation of the workpiece and friction. Therefore, a thermal conduction equation is developed. Based on Fourier's law, the heat-conduction equation of the three-dimensional element is determined by

$$k\left[\frac{\partial^2 T}{\partial x^2} + \frac{\partial^2 T}{\partial y^2} + \frac{\partial^2 T}{\partial z^2}\right] - \rho c\left[u\frac{\partial T}{\partial x} + v\frac{\partial T}{\partial x} + w\frac{\partial T}{\partial z}\right] + \dot{Q}_v = 0 \tag{3-10}$$

where k is the thermal conductivity, ρ the thermal density, c the specific heat, and $\dot{Q}_v$ the volumetric generation rate. The heat generated from plastic deformation and the workpiece/work roll interface can be calculated as:

$$\dot{Q}_v = \dot{Q}_p + \dot{Q}_f \tag{3-11}$$

where $\dot{Q}_p$ is the heat transformed from plastic deformation, and $\dot{Q}_f$ is the heat generated at the slab/roll interface due to friction.

3.2.2 Material model for the workpiece

The basic theory for the coupled finite element constitutive equation has been discussed above. The formulation used in LS-DYNA for the material model of thermo-elastic-plastic will now be represented. Letting T represent the temperature, we compute the elastic co-rotational stress rate as

$$\sigma_{ij}^{\nabla} = C_{ijkl}(\dot{\varepsilon}_{kl} - \dot{\varepsilon}_{kl}^{T}) + \dot{\theta}_{ij}dT \tag{3-12}$$

where

$$\dot{\theta}_{ij} = \frac{dC_{ijkl}}{dT} C_{klmn}^{-1} \dot{\sigma}_{mn} \tag{3-13}$$

and C_{ijkl} is the temperature dependent elastic constitutive matrix:

$$C_{ijkl} = \frac{E}{(1+v)(1-2v)} \begin{bmatrix} 1-v & v & v & 0 & 0 & 0 \\ v & 1-v & v & 0 & 0 & 0 \\ v & v & 1-v & 0 & 0 & 0 \\ 0 & 0 & 0 & \frac{1-2v}{2} & 0 & 0 \\ 0 & 0 & 0 & 0 & \frac{1-2v}{2} & 0 \\ 0 & 0 & 0 & 0 & 0 & \frac{1-2v}{2} \end{bmatrix} \tag{3-14}$$

where v is Poisson's ratio. The thermal strain rate can be written in terms of the coefficient of thermal expansion α as:

$$\dot{\varepsilon}_{ij}^{T} = \alpha \dot{T} \delta_{ij} \tag{3-15}$$

When dealing with plasticity, we use a procedure analogous to that for material with elastic plastic characteristics with Kinematic hardening. The stresses are elastically

updated and are checked to see if the isotropic yield function is violated

$$\emptyset = \frac{1}{2} s_{ij} s_{ij} - \frac{\sigma_y T^2}{3} \tag{3-16}$$

where

$$\sigma_y(T) = \sigma_o(T) + E_p(T)\varepsilon_{eff}^p \tag{3-17}$$

The initial yield, σ_o, and plastic hardening modulus, E_p, are temperature dependent. If the behaviour is elastic, there is no need to do anything; otherwise, we scale back the stress deviators by the factor f_s:

$$s_{ij}^{n+1} = f_s s_{ij}^* \tag{3-18}$$

where

$$f_s = \frac{\sigma_y}{\left(\frac{3}{2} s_{ij}^* s_{ij}^*\right)^{1/2}} \tag{3-19}$$

and update the plastic strain by the increment

$$\Delta\varepsilon_{eff}^p = \frac{(1-f_s)\left(\frac{3}{2} s_{ij}^* s_{ij}^*\right)^{1/2}}{G+3E_p} \tag{3-20}$$

3.3 Simulation method

A three-dimensional finite element method has been used to simulate the behaviour of surface defects during a single pass of hot rolling for stainless steel 304 with the commercial element software package, ANSYS/LS-DYNA, 13.0. The formulation technique employed in modelling is the Lagrangian method as described in the above

section.

Generally, there are two ways to simulate a situation for coupled thermo-mechanical finite element analysis. One is the indirect approach, which calculates mechanical behaviour and thermal behaviour separately in sequence. These two are then correlated together by applying the thermal results to the mechanical model. The other method is the direct coupled finite element approach, and this method has been chosen for the simulations in this study.

3.4 Thermal governing theory

3.4.1 Governing equation for the conversion of deformation energy to heat

During the hot rolling process, the temperature distribution in the strip and the work roll can be calculated using the constitutive Equation (3-10) for the isotropic thermal property type.

Due to plastic deformation, heat will be generated internally in the slab. In order to take this effect into consideration the following equation is induced to control for this condition.

$$\dot{Q}_p = \eta \int_0^{\dot{\varepsilon}} \bar{\sigma}\, d\dot{\varepsilon} \tag{3-21}$$

where $\dot{Q}_p$ ($W \cdot m^{-3}$) is the heat generation term representing the heat released due to plastic work, η is the efficiency of conversion of deformation energy to heat, $\dot{\varepsilon}(s^{-1})$ is the effective strain rate and $\bar{\sigma}$ (Pa) is the effective flow stress.

3.5 Contact between the slab and the work roll

The contact at the slab/roll interface has been modelled by applying three-dimensional finite elements. In the dynamic explicit process, contact occurs when the contact surface penetrates the target surface by passing beyond the external circumference of the work roll. Then the contact stiffness matrix, the coefficient of friction at the roll/slab interface and the thermal conductance are introduced to this problem. The contact stiffness matrix works in the normal direction on the target surface and enforces the displacement compatibility by restricting the penetration of the target body. By calculating the thermal conductance between the workpiece and the workroll, it is possible to obtain the temperature distribution across the contact interface. During this contact simulation, the augmented Lagrangian method was used as the dominant algorithm, and this allowed the contact tractions, pressure and friction to increase within the equilibrium iterations and, therefore, prevent the final penetration from exceeding the allowable tolerance. Compared to most of the research that has implemented the penalty function, this method contributes to simulation results which are much more accurate.

3.6 Finite element modelling of surface defects

There are many kinds of surface defects in continuous casting slabs in manufacturing and the crack models used in this research are for edge cracks, transverse cracks, transverse V-shaped cracks and longitudinal cracks, which are all commonly detected types of cracks on these slabs.

3.6.1 Model for edge cracks

The work roll geometry is simulated with a diameter of 300 mm. Eight-node 3D solid 164 elements were employed in the coupled thermo-mechanical analysis. The geometry of the strip and work roll is shown in Figure 3.1. Work roll is assumed to be

a rigid material in the analysis. The thermal material is applied to both the slab and the work roll.

The rolling schedules are shown in Table 3.1. D_{roll}, W, H, L, d, w and t represent the diameter of the work roll, slab width, slab thickness, slab height, crack depth, crack width and thickness of reduction, respectively. θ is the crack open angle and R is the rolling reduction. In the models, the crack angle varies from 10.6 °to 18 °. The rolling reduction ranges from 30 to 35%, and can be calculated using Equation (3-22).

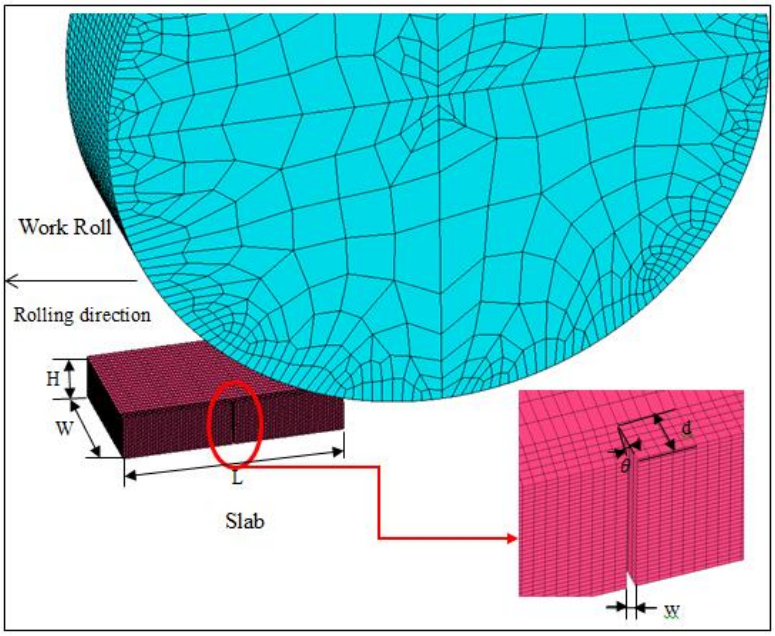

Figure 3.1 Model of edge crack on the slab

Table 3.1 The schedule of the rolling models for edge cracks (mm)

Model No.	D_{roll}	W	H	L	d	w	t
1	300	60	20	100	5	1	6
2	300	60	20	100	5	2	6
3	300	60	20	100	3	1	6
4	400	60	20	100	5	1	6
5	300	60	20	100	5	1	7

$$R = \frac{H-t}{H} \times 100\% \quad (3\text{-}22)$$

3.6.2 Model for transverse cracks

Figure 3.2 shows a transverse surface crack on the slab. It has a crack width of 1 mm and depth of 1 mm. The rest of the dimensions are the same as the parameters shown in Table 1. The symmetrical planes for this model are the back and bottom surfaces of the slab.

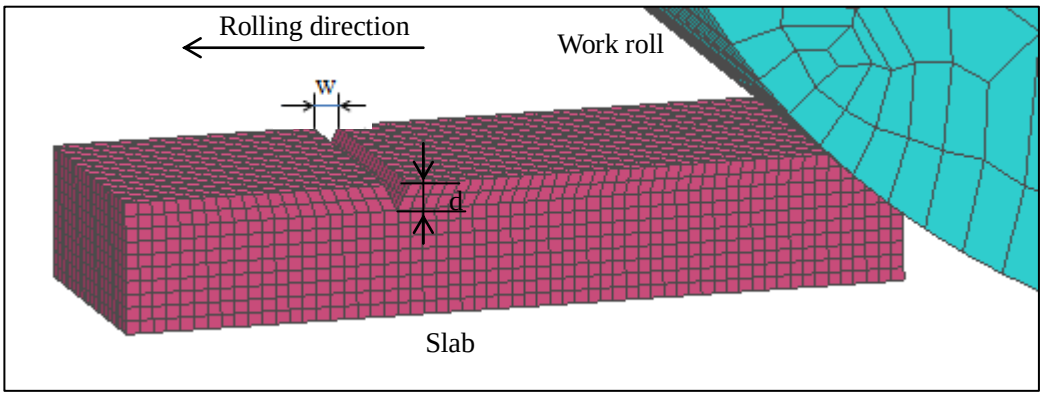

Figure 3.2 The model of transverse crack on the slab

3.6.3 Model for V-shaped transverse cracks

Figure 3.3 shows a V-shaped surface crack on the surface. The crack is located in the centre of the symmetry plane. In order to research the effect of mesh density on the accuracy of the simulation results, two different mesh densities have been chosen as the target subjects. The symmetry planes for this model are the front and the bottom surfaces of the slab, and they are indicated in the figure above. Figure 3.3(a) has a greater mesh density near the crack area than that in Figure 3.3(b). The modelling results will be discussed in the next chapter.

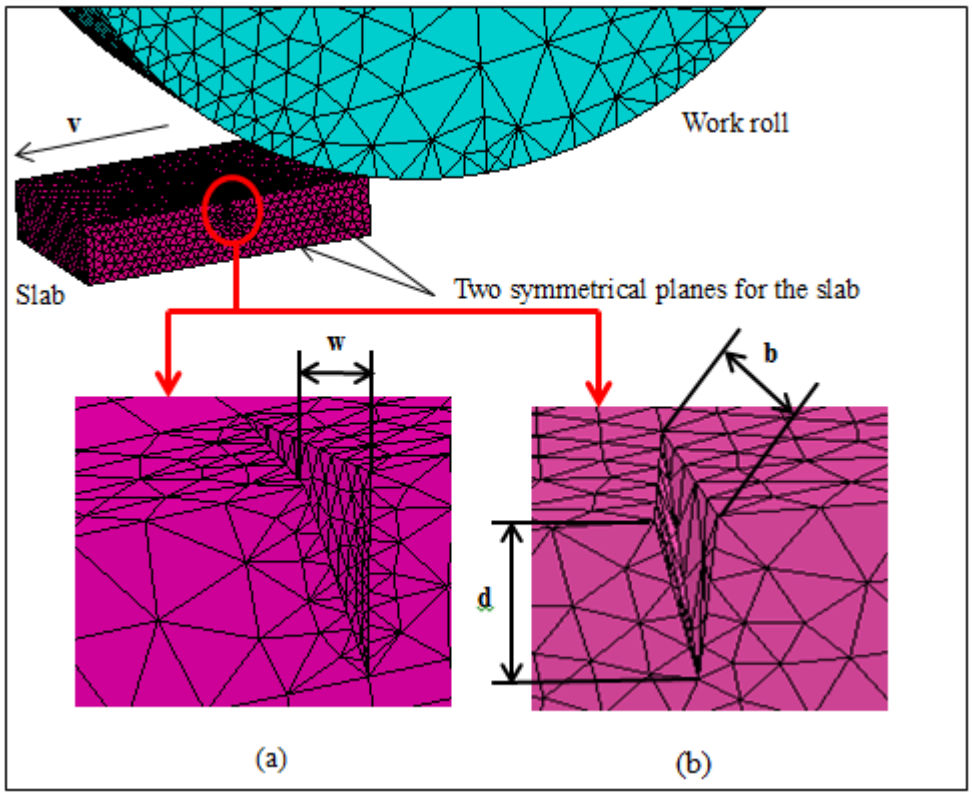

Figure 3.3 Model of V-shaped crack in the centre of the slab surface

Table 3.2 Models proposed for V-shaped transverse crack on the slab (mm)

Model No.	D_{roll}	W	H	L	w	d	b	t
1	300	60	20	100	2	6	10	6
2	300	60	20	100	1	6	10	6
3	300	60	20	100	2	6	14	6
4	300	60	20	100	2	4	10	6
5	300	60	20	100	2	6	10	4
6	400	60	20	100	2	6	10	6

It can be seen from Table 3.2 that in total there are six different shapes for the proposed simulations of V-shaped transverse cracks on the slab. The variations of the crack have different depths, widths, and lengths. These parameters will be represented by w, d and b. The thickness of reduction, it ranges from 4 to 6 mm.

3.6.4 Model of longitudinal cracks

The longitudinal surface crack model is shown in Figure 3.4 and the number of mesh elements for the work roll and the slab are about 20,000 and 90,000, respectively.

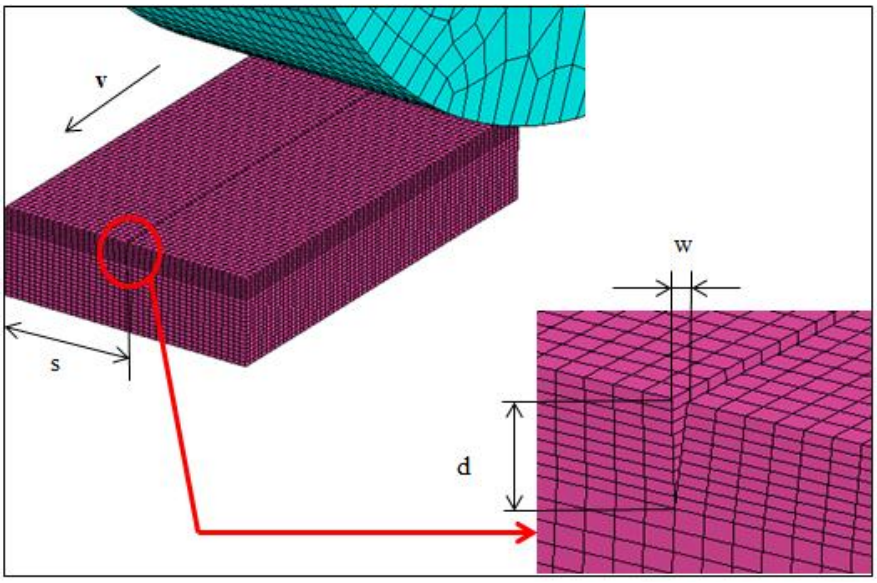

Figure 3.4 Surface longitudinal crack on the slab

Table 3.3 Proposed models for longitudinal surface cracks on the slab (mm)

Model No.	D_{roll}	W	H	L	w	d	s	t
1	300	60	20	100	0.8	5	30	5
2	300	60	20	100	0.8	5	10	5
3	400	60	20	100	0.8	5	30	5
4	300	60	20	100	1	5	30	5
5	300	60	20	100	0.8	5	30	7
6	300	60	20	100	0.8	6	30	5

As shown in Table 3.3, there are six finite element models for longitudinal cracks appearing during rolling process. None of the reports found in the literature studied

the influence of the distance between the symmetrical centre of the slab and the centre of the longitudinal crack on the evolution of the crack. Therefore, variation s has been introduced here to investigate the effect of this distance on the behaviour of the crack under hot rolling conditions.

3.7 Thermal boundary conditions

Thermal boundary conditions are very important. They are used to describe the heat transfer conditions in the slab symmetrical areas, at the slab/roll interface and the convection and radiation between the work slab and the ambient air. For the symmetrical areas of the simulation models, there is no heat transfer or heat loss through the surfaces. Hence, the main focus below is on the free surfaces and the contact surfaces. Based on Equation (3-10), these boundary conditions can be derived as:

$$-k\left[\frac{\partial T}{\partial x}l_x + \frac{\partial T}{\partial y}l_y + \frac{\partial T}{\partial z}l_z\right] = h(T - T_\infty) \tag{3-23}$$

where h is the coefficient of heat conduction at the slab/roll interface, T_∞ the temperature of the environment, l_x, l_y and l_z are the normal direction cosines on the boundaries.

Generally, heat transfer during hot rolling consists of three parts. The first one is the heat loss of the material by radiation and convection between the work roll and the environment. The second one is the heat generated due to the plastic deformation and friction at the contact interface between the slab and the work roll, which happens when the slab is rolled in the region of the deformation. The last part is the heat loss caused by the instant drop of the temperature when the contact between the slab and the work roll happens.

3.7.1 Heat transfer of the contact surface between the slab and the work roll

The heat transfer at the interface between the slab and the work roll in the models is defined as:

$$Q = h_i(T_S - T_R) \tag{3-24}$$

where h_i is the interfacial heat transfer coefficient between the slab and the work roll, T_S is the temperature of the slab, and T_R is the temperature of the work roll.

3.7.2 Convection boundary conditions

When the slab is not in the deformation zone, the two important ways in which the slab loses heat are heat convection and heat radiation. The heat is emitted to the ambient environment. The governing equation for the heat convection is described as:

$$Q = h_c(T_s - T_\infty) \tag{3-25}$$

where h_c is the convective coefficient between the strip and the ambient air, T_s is the temperature of the slab and T_∞ is the temperature of the ambient air. They will be discussed in the next section.

3.7.3 Radiation boundary conditions

On parts of the slab that are not in the deformation region, the heat radiation is much more significant than the heat convection. The heat emitted through radiation can be obtained based on the Stefan-Boltzmann equation,

$$Q = \sigma\varepsilon(T_S^4 - T_\infty^4) \tag{3-26}$$

where σ is the Stefan-Boltzmann constant, which equals to 5.67×10^{-8} W/m^2·K^4, ε is the blackness of the strip surface, T_s is the temperature of the slab, and T_∞ is the temperature of the ambient air. According to the radiation constitutive equilibrium, the convective coefficient for radiation is expressed as:

$$H_r = \sigma\varepsilon(T_s^2 + T_\infty^2)(T_s + T_\infty) \tag{3-27}$$

The blackness of the strip varies with different materials under various conditions and in this study the value of 0.8 is chosen for the austenitic stainless steel 304.

3.7.4 Segment set for convection and radiation

In the dynamic explicit software ANSYS/LS-DYNA, the segment set in the simulation process is a very important issue. However, it cannot be set directly through the GUI of the ANSYS when the heat convection and heat radiation are imposed on the surfaces of the simulation models. It is therefore necessary to find a method to generate these segments. According to the LS-DYNA user's manual, the segment for a three-dimensional element such as solid 164 is at the surface.

With the introduction of LS-PrePost software, it becomes possible to generate the segment set for the radiation and convection. It can be seen from Figure 3.5 that the segment is set at the slab surface except for the symmetrical slab surfaces, which are at the bottom and back of the slab, as well as the two surfaces of the crack for the model of edge crack. It should be noted that the segment set varies in different simulation models. The same procedure can be implemented for the work roll if the convection and radiation heat are taken into consideration. In this study, only the slab has been considered in these heat transfers, as the temperature of the work roll is much lower and, therefore, these effects are not significant.

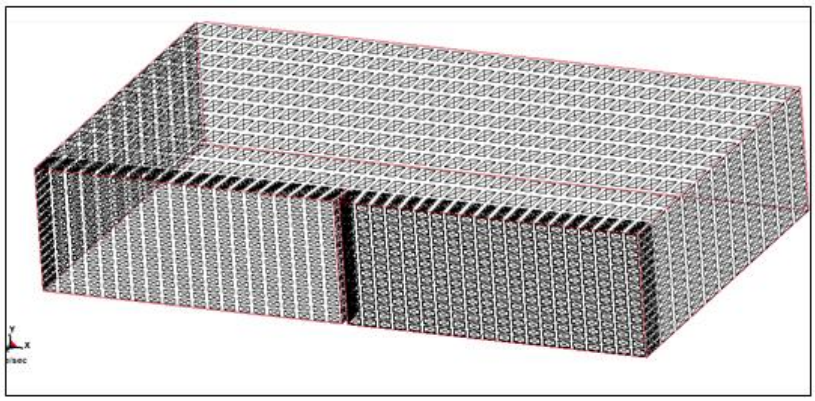

Figure 3.5 Segment set on the surface for the radiation and convection

3.8 Mechanical boundary conditions

The mechanical boundary conditions that describe the mechanical interaction of the contact areas between the slab and the work roll were imposed on their interface. The interfacial friction for the contact regions is proportional to the normal force, which is displayed in the following equation:

$$\tau_{crit} = \mu P \tag{3-28}$$

where τ_{crit}(Pa) is the critical shear stress, and μ is the coefficient of friction and P is the contact pressure. A coefficient of friction of 0.3 is used in the simulation models shown in Tables 3.1 to 3.3. However, different friction coefficients will be employed in the next section to investigate the effect of friction on the behaviour of crack changes.

Before the contact interface of the slab and the work roll begin sliding relative to each other, both of these two surfaces can sustain shear stresses below a critical magnitude. When the equivalent shear stress goes beyond the critical value, it will make the contact and target surfaces start to slide relative to each other. The calculation of

sticking and sliding states is a key factor for determining the moment when a point transfers from sticking to sliding or vice versa.

There are two symmetrical surfaces in the slab and restricting the displacement to zero will keep them from deformation. Through this simulation technique, geometric complexity will be minimised to a certain extent and this will reduce the computational time required. The rolling speed is introduced by employing a linear velocity on the work roll during the simulation.

3.9 Thermal and mechanical properties for the austenitic stainless steel 304

The slab used in the study is made of austenitic stainless steel 304 and the chemical composition of the steel is listed in the following section. The simulation is based on the slab's thermal and mechanical properties which are shown as well. For the hot rolling process, the temperature is high and therefore it is necessary to use the properties that occur at different temperatures.

3.9.1 Chemical compositions of AISI 304

The chemical composition of stainless steel 304 is shown in Table 3.4. It determines oxidation flakes during the rolling conditions, and thus it is necessary to find out the relative constitution of the slab.

Table 3.4 Chemical compositions of the austenitic stainless steel 304.

Steel grade	Austenitic stainless 304		
C	0.0480	Cu	0.1900

Si	0.3600	Ni	8.1500
Mn	1.0900	Cr	18.1400
P	0.0260	As	0.0040
S	0.0040	Sn	0.0100
Nb	0.0110	W	0.0200
Al	0.0040	O	0.0155
Ti	0.0040	N	0.0430
Mo	0.1500	Co	0.1430
B	0.0010	Fe	71.5845

3.9.2 Thermal and mechanical properties for FEM simulation models

The slab is assumed to be a thermo-elastic-plastic material with temperature dependent elastic modulus and Poisson's ratio. The ranges of temperatures, strains and strain rates experienced by the material during the hot rolling process are large, and hence it is necessary to obtain the thermal properties of the material when finite element simulations are implemented.

During the finite element simulations, the elastic state properties are represented by Young's modulus and Poisson's ratio. Also, some other factors such as the coefficient of thermal conductivity and the heat capacity of the material are important considerations throughout the process. The accuracy of the simulation can be influenced by these parameters. The thermal properties of austenitic stainless steel 304 are shown in Figure 3.6. Young's modulus, heat capacity and thermal conductivity are represented in Figures 3.6(a), (b) and (c), respectively.

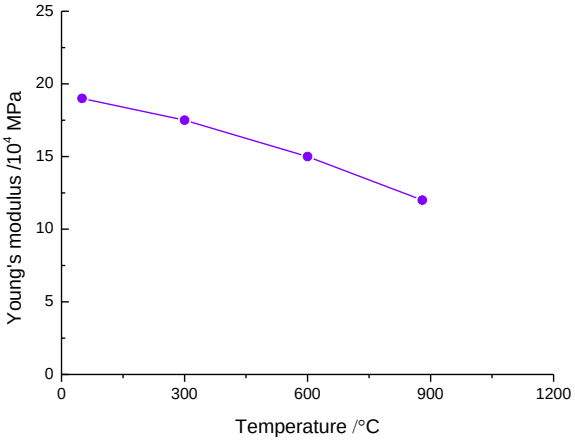

(a) Young's modulus

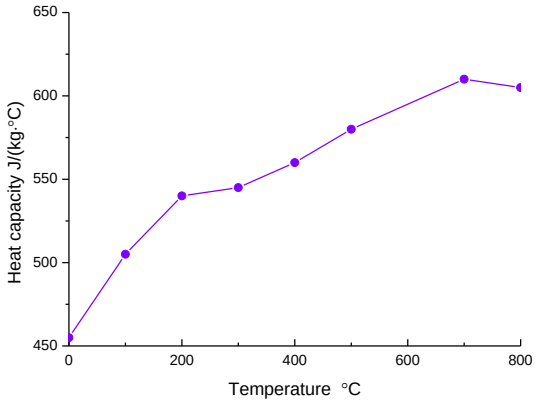

(b) Heat capacity

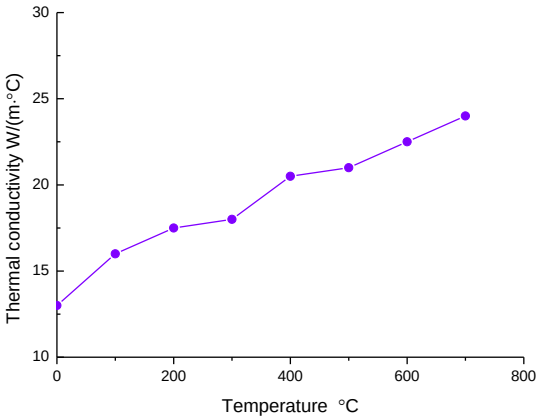

(c) Thermal conductivity

Figure 3.6 Thermal properties for the material models

The constants of the work roll are summarised in Table 3.5. The thermo-physical properties of the slab are shown in Table 3.6. The density of the slab was assumed to be at 7850 kg m^{-3}. The thermal properties which changed with temperature for the slab are listed in Figure 3.6.

Table 3.5 Thermo-physical properties of the work roll

Rigid material model	
Density	7850 Kg/m^3
Initial temperature	20 ℃
Young's modulus	210 GPa
Poisson's ration	0.3
Heat capacity	483 J/(kg·K)
Thermal conductivity	55 W/(m^2·K)

Table 3.6 Thermo-physical properties of the slab

Steel 304	
Density	7850 Kg/m^3
Blackness	0.8
Poisson's ration	0.36
Coefficient of thermal expansion	12×10^{-6}
Yield stress	124 MPa
Plastic hardening modulus	13MPa
Initial temperature of the work strip	1150 ℃
Environment temperature	20 ℃
Contact heat conductivity	20 KW/(m^2·℃)
Convection coefficient	30 W/(m^2·℃)
Stefan-Boltzmann constant	5.67×10^{-8} W/(m^2·$℃^4$)
Fraction of mechanical work converted into heat	0.9

3.10 The integration method for explicit dynamic FEM

The fundamental equation for the explicit dynamic element method is

$$M\ddot{u}(t) + C\dot{u}(t) + Ku(t) = Q(t) \tag{3-29}$$

where $\ddot{u}(t)$ is the accelaeration vector of the system node and $\dot{u}(t)$ is the velocity vector. M, C, K and $Q(t)$ represent mass matrix, damping matrix, stiffness matrix and vector of nodal nodes, respectively.

The integration method of central difference interpolation has been employed by LS-DYNA. The discrete velocity and acceleration at t_n can be expressed as follows:

$$\dot{u}_n(t_n) = \frac{1}{2\Delta t}[u(t_{n+1}) - u(t_{n-1})] \tag{3-30}$$

$$\ddot{u}(t_n) = \frac{1}{\Delta t^2}[u(t_{n+1}) - 2u(t_n) + u(t_{n-1})] \tag{3-31}$$

By substituting Equations (3-30) and (3-31) into Equation (3-29), the discrete-time recurrence equation is obtained as follows:

$$u(t_{n+1}) =$$

$$(M + \frac{\Delta t}{2}C)^{-1}\left\{\Delta t^2[Q(t_n) - Ku(t_n)] + 2Mu(t_n) - (M - \frac{\Delta t}{2}C)u(t_{n-1})\right\} \tag{3-32}$$

The displacement value at each discrete time can be obtained after the initial conditions and steps are introduced. It is necessary that the conditions are stable for the central difference method and thus its time step should be lower than the critical time step. The stable condition for the central difference method based on

Courant-Friedrichs-Levy stability is:

$$\Delta t \leq \Delta t_{min} = \frac{2}{w_{max}} = \frac{l}{c} \tag{3-33}$$

where l is the characteristic length of the element, c is the speed of sound of the material. For the three-dimensional element, the speed of sound in the material is shown as:

$$c = \sqrt{\frac{(1-v)E}{(1+v)(1-2v)\rho}} \tag{3-34}$$

where E is Young's modulus, v is the Poisson's ratio and ρ is the specific mass density.

Chapter 4

Simulation Results and Discussion

4.1 Introduction

Based on the finite element models which use the employed finite element calculation method, the analysis of surface defects behaviour during hot rolling processes has been conducted. The effects of defect size and the rolling conditions on the results are analysed in terms of the crack depth, crack width, rolling speed, friction coefficient, thickness reduction and size of the work roll. In order to investigate their influences on crack evolution, different initial thermal conditions such as the initial temperature of the workpiece are also investigated.

The stresses and strains of the crack area are also taken into consideration to detect the risk of final surface defects. The temperature distributions and their uniformity, as well as rolling force influences have been investigated through comprehensive numerical simulations. Depending on the number of elements and the size of the models, the general computational time for each model ranged from 50 to 100 hours on a Pentium 3 GHz computer with 521 MB RAM.

The main focus of the study will be on the edge cracks, transverse cracks, and

transverse V-shaped cracks and longitudinal surface cracks. Different mesh densities are also used to compare simulation results.

4.2 Edge crack behaviour during the hot rolling process

Edge crack defects on slab surfaces are undesirable and therefore it is necessary to take measures to control them to minimise their effect on final product quality. As indicated in Chapter 2, most studied in this field used experimental methods, and limited research into this problem has been done using in simulation methods, and most of the research was done under cold rolling conditions without the introduction of thermal effects.

4.2.1 Edge crack variations

Figure 4.1 shows the evolution of edge crack at different times during the hot rolling process. An edge crack is shown in Figure 4.1(a) with the initial edge width of 1 mm and an initial depth of 5 mm. The rolling speed is 2.7 m/s and the rolling reduction is 30 %.

The simulation shows that the crack width gradually increases during the rolling process. However, the changes on the top and bottom slab surfaces were different. This is because the top area experienced much more stress than the bottom part when the slab was gradually rolled into the deformation zone, and after the slab gradually left the work roll, the slab suffers more tension along the rolling direction.

As this tension distributed from the slab top and bottom along the thickness of the strip increases, therefore, the final shape of the edge cracks of the slab have different evolution behaviour.

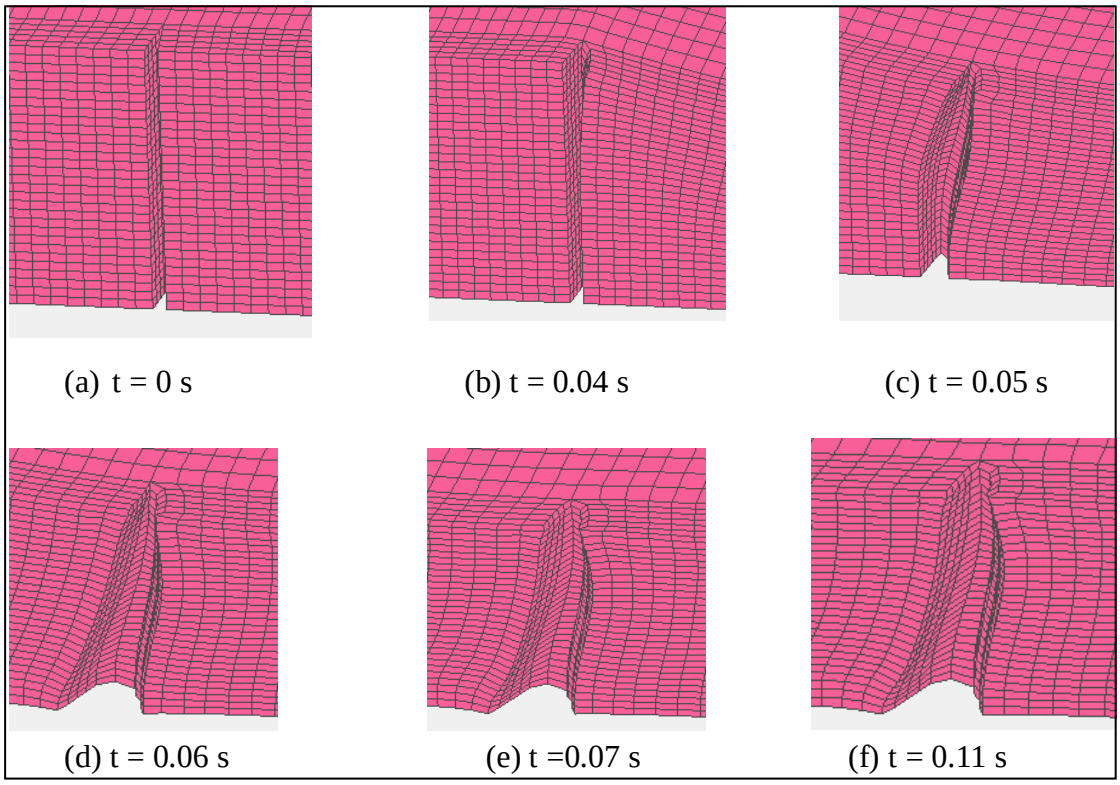

Figure 4.1 Edge crack evolution at different times

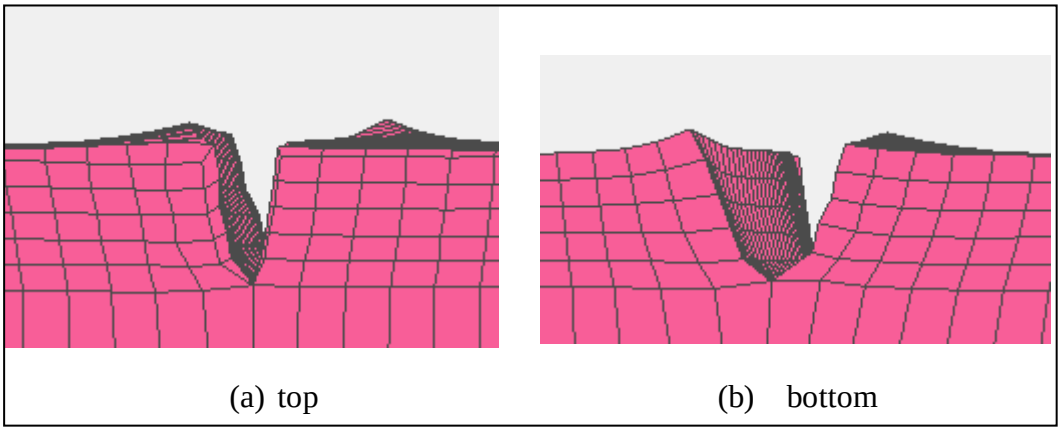

Figure 4.2 Edge shapes from the top and bottom surfaces of the slab

Figure 4.2 shows the crack shapes from the top and the bottom of the slab. It is clear that there is a large difference between the two parts and the edge crack on the top of the slab is much larger than the edge crack in the bottom of the slab.

4.2.2 Rolling force

As described in Chapter 2, only a limited number of reports have been found which consider the effect of rolling forces on slabs with cracks. The predicted rolling force obtained from finite element modelling will be discussed in this section. Accurate information about rolling force is essential when designing rolling schedules. The dimensional precision of rolled products is directly influenced by the rolling force. The rolling force is also the basis for computing the rolling torque. In order to avoid the breakdown of the rolling mill and also to ensure maximum productivity, it is imperative to fulfill the requirements of the geometry and properties of the slab. For the modeling in this study, the friction coefficient was set at a constant value of 0.3.

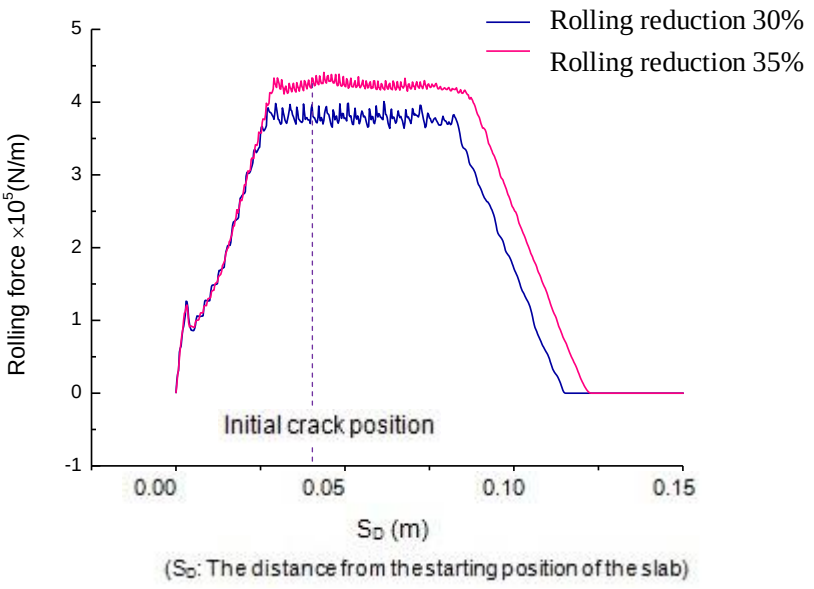

Figure 4.3 Rolling force for different reductions

Figure 4.3 shows the rolling force predicted by the FE method for cases in which the initial temperature of the strip is 1050 ℃. It can be seen that the rolling force increases gradually when the slab feeds into the roll gap, and then reaches a relatively steady level when the deformation reaches a steady regime. Through the whole rolling process, the slab takes a certain time for the process to attain a steady state and a similar period of time is taken for leaving the roll gap.

4.2.3 Von Mises stress distribution

The Von Mises stress distributions at the initial period of the rolling process and at the final rolling state are shown in Figures 4.4 and 4.5 respectively. Understanding the stresses can help us to predict where the defects will deteriorate most and how the deformation will behave during the process.

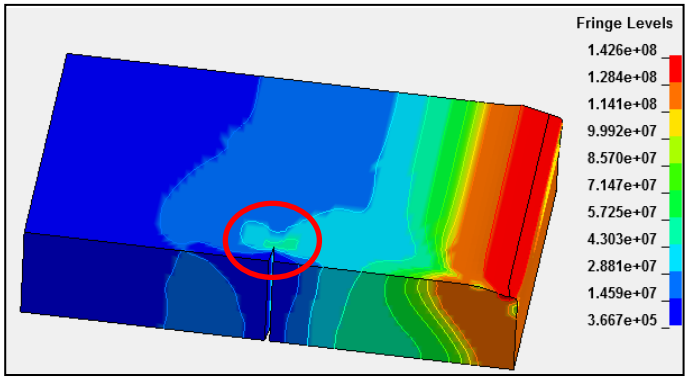

Figure 4.4 Von Mises stress distribution at S_D = 10 mm

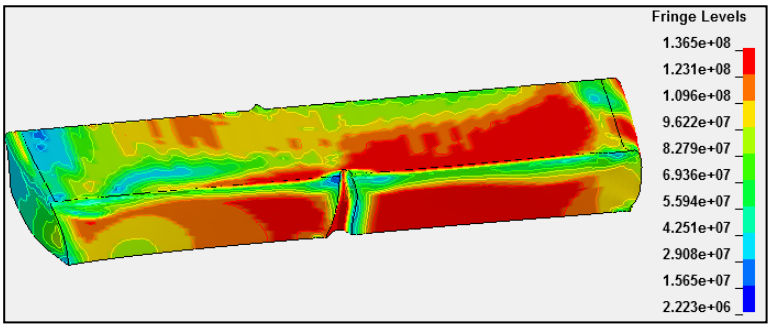

Figure 4.5 Von Mises stress distribution after deformation (Pa)

According to the description in Chapter 3, the heat in the area of the deformation will increase due to the large deformation of the material. In Figure 4.4 there is a circled area on the tip of the crack. It can be seen that the stress in this region is larger than that in the surrounding area. This may imply that the crack tip at the risk of propagating and extending. When the strip has been rolled out of the deformation

region, the stress for the region located around the bottom of the slab is greater than that at the top area. This explains why the shape of the edge crack varies considerably during the rolling process, as shown in Figure 4.2. The stress through the thickness of the slab is a compressive one and this is a typical phenomenon of rolling operations.

4.2.4 Analysis of crack tips

As discussed above, the crack tip is a special area that needs to be investigated in detail in order to understand the mechanism and its influential factors at work during the hot rolling process. Therefore, the following will discuss the effects of effective plastic strain, pressure, effective stress and maximum shear stress on crack tip states under different rolling schedules and crack sizes.

4.2.4.1 Effective plastic strain

Figure 4.6 shows the effective plastic strain of the crack tip under different conditions. The effects of the crack width, depth, work roll diameter and the reduction of thickness are represented in Figures 4.6(a), (b), (c) and (d), respectively.

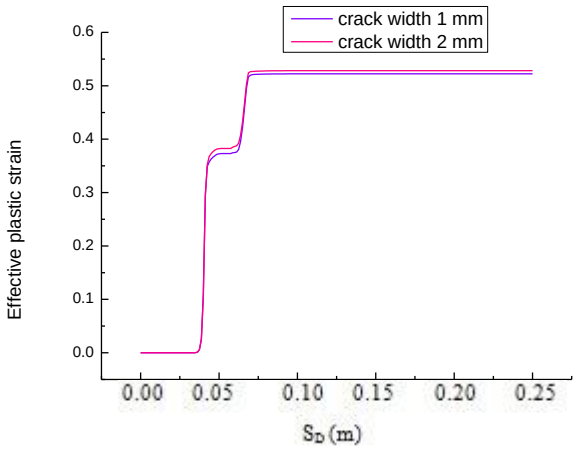

(a) Crack width effect

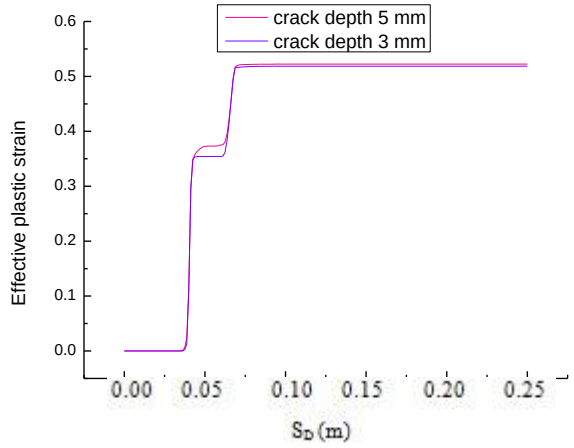

(b) Crack depth effect

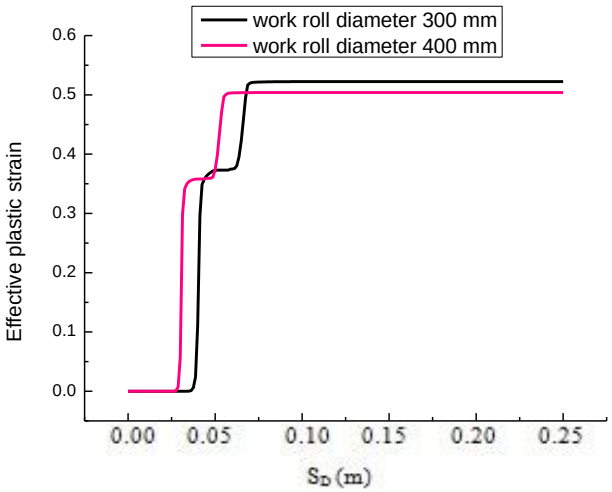

(c) Work roll diameter effect

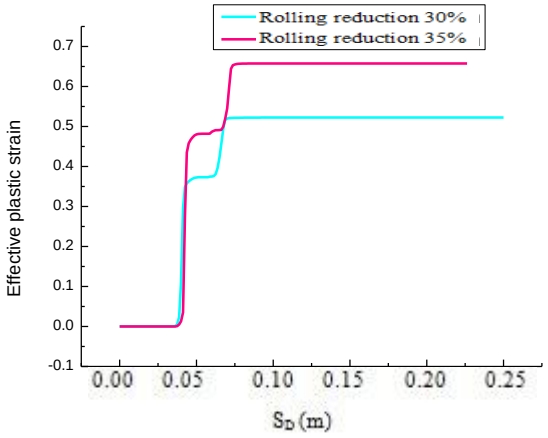

(d) Reduction effect

Figure 4.6 Effective plastic strain of the crack tip

It can be seen that the crack width and depth have an insignificant effect on the effective plastic strain of the edge crack tip. Compared with these parameters, the work roll diameter and reduction of thickness affect the strain significantly. With an increase of the work roll diameter, the strain will decrease to some extent. When increasing the reduction of thickness, the effective plastic strain increases. From Figures 4.6(a) and (b), it can be concluded that a larger effective plastic strain on the edge crack tip will cause larger crack sizes as indicated by such as characteristics as crack open angle and crack depth.

4.2.4.2 Contact pressure

Figure 4.7 shows the contact pressure of the edge crack tip under different rolling conditions, for different crack sizes. It can be seen from Figure 4.7(a) that there will be a dramatic rise for the pressure when the crack enters the work roll gap, and then the tension will act on the tip, causing it to drop to a negative value. During the rolling process, the tip experiences the pressure again. This pressure then increases to about 60 MPa and stays at that level as time increases. The influence of crack width on crack tip pressure is quite small by comparing the two conditions.

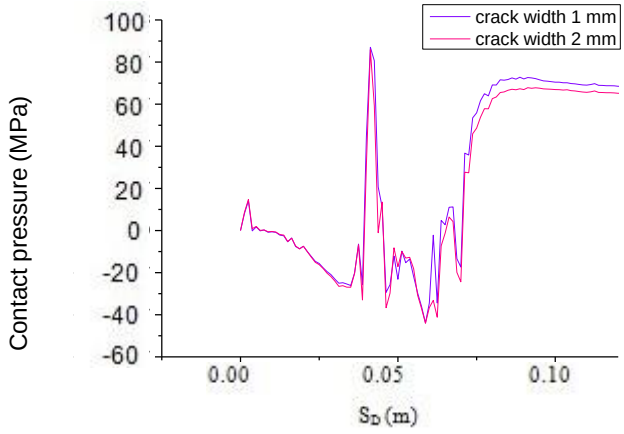

(a) Crack width effect

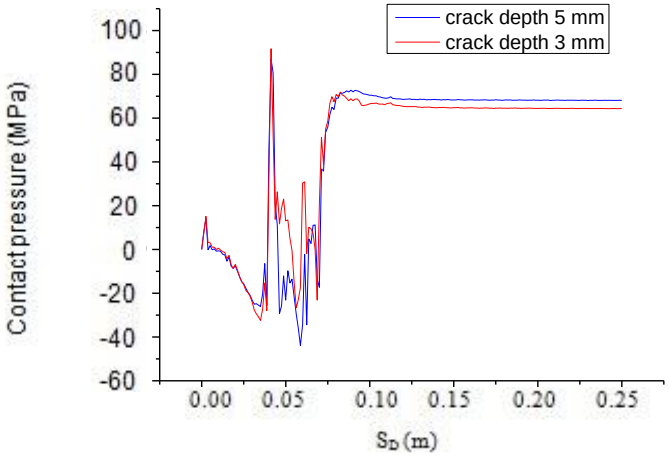

(b) Crack depth effect

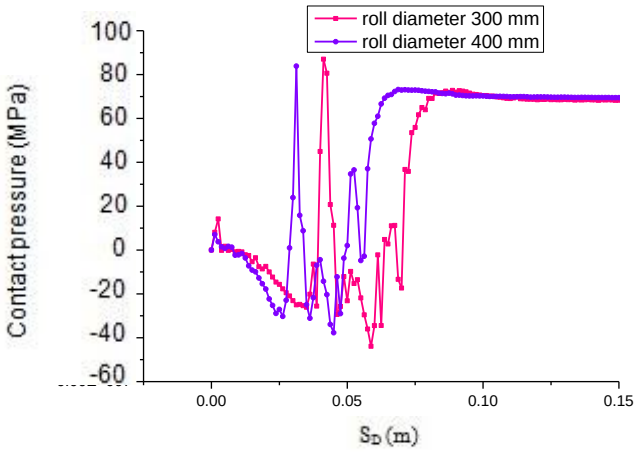

(c) Rolling diameter effect

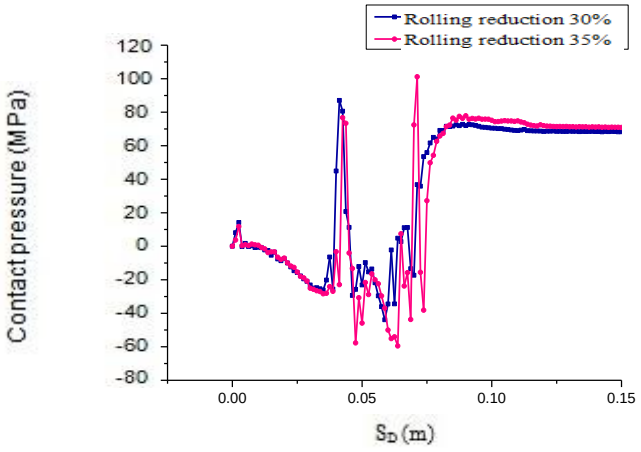

(d) Reduction effect

Figure 4.7 Contact pressure of the edge crack tip

The situation of pressure at different crack depths is shown in Figure 4.7(b). As crack depth increase, the pressure increases at the final stage, but the large fluctuations occur at the lower crack depths. Figure 4.7(c) reflects the effect of the work roll diameter on pressure. It is clear that the conditions when using different roll diameters are similar to each other, and there is only a time delay for the smaller roll to enter into this state. There is a difference compared with the effective plastic strain that the thickness reduction does not have a major effect on the pressure, as can be seen from Figure 4.7(d).

4.2.4.3 Effective stress

Figure 4.8 shows the effective stress of the crack tip under different rolling conditions and different crack open angles and crack depths. It can be seen that all of the simulation models obtained the same value for effective stress of around 130 MPa. All of the rolling parameters investigated in this part had an insignificant effect on the effective stress of the crack tip. During the rolling process it is concluded that the stress with larger value of the crack size and thickness reduction will fluctuate at a small level when it is at the unstable state in the initial rolling period.

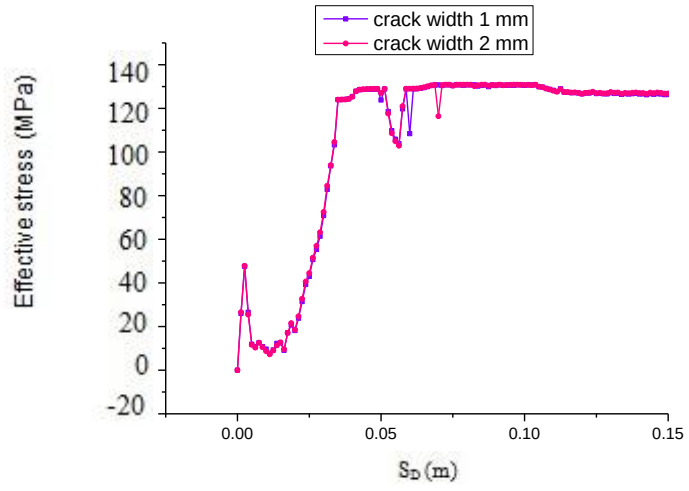

(a) Crack width effect

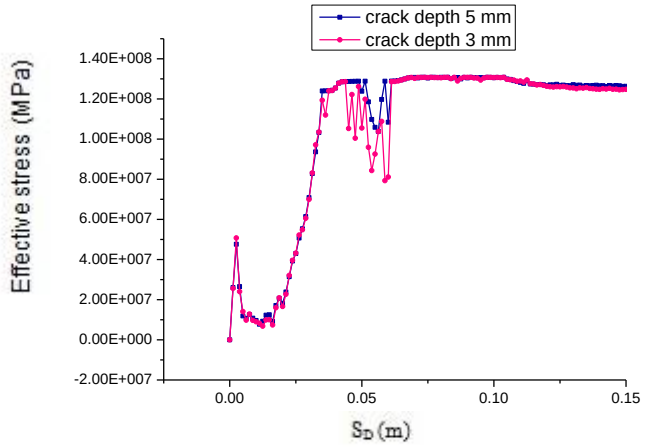

(b) Crack depth effect

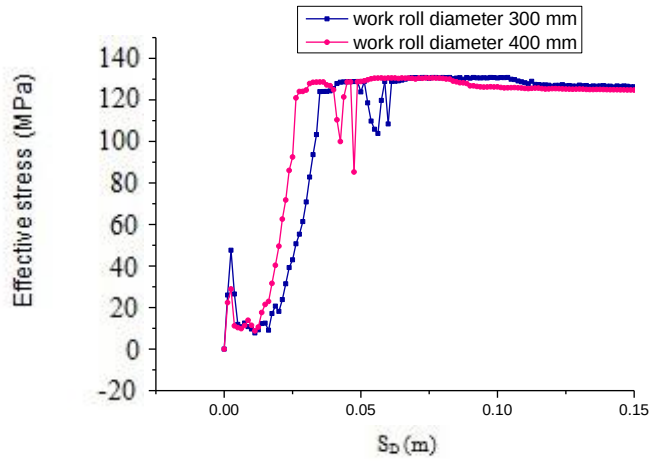

(c) Work roll diameter effect

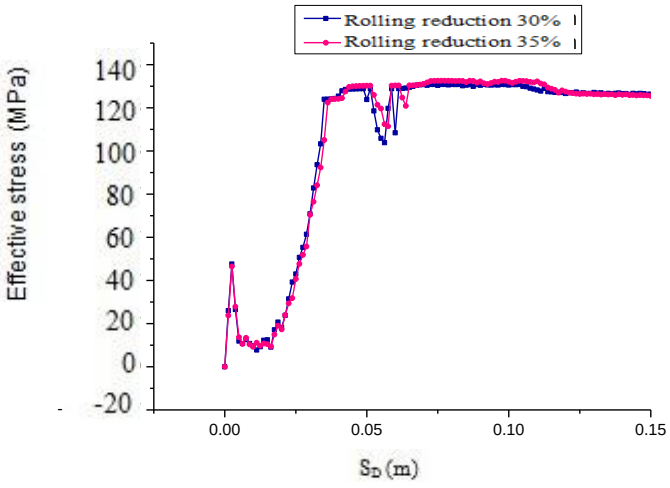

(d) Reduction effect

Figure 4.8 Effective stresses at crack tip

4.2.4.4 Maximum shear stress

It can be seen from Figure 4.9(a) that the maximum shear stress for different sizes of cracks is around a value of 75 MPa when the strip has been rolled into a steady state. By comparing the maximum shear stresses for each of the two crack sizes, it can be seen that variations in the crack depth have a larger influence on shear stress than the crack width does. An increase of 2 mm in the crack depth is associated with an increase in shear stress of approximately 5 MPa, whereas when the rolling conditions are in a stable state, crack width makes virtually no difference to the maximum shear value.

This may be attributed to the uneven deformation which occurs in the rolling process, as the slab will experience more deformation due to changes in depth than it will experience due to changes in longitudinal direction. Therefore, the influence of crack width and crack depth on the crack tip region will be different.

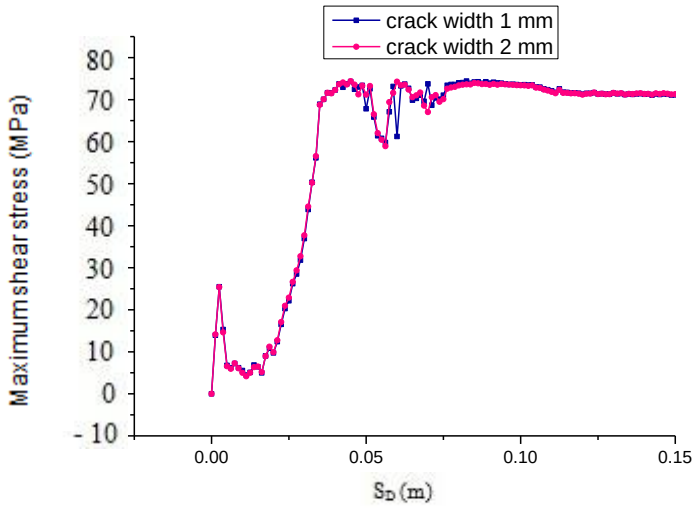

(a) Crack width effect

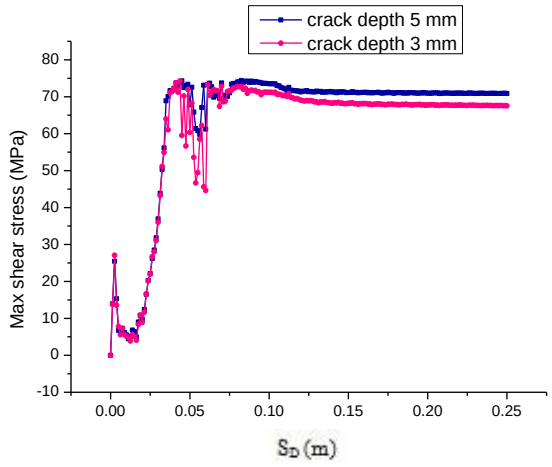

(b) Crack depth effect

Figure 4.9 Crack size effect on the max shear stress at crack tip

The behaviour of crack width on the top and bottom surfaces varies, which is shown in Figure 4.10. It can be seen that the crack width increases as the time passes, however, the bottom surface experiences more deformation than the top surface. This may result in more risk of crack propagation on the bottom surface of the slab, and this will significantly influence the final surface quality of the product.

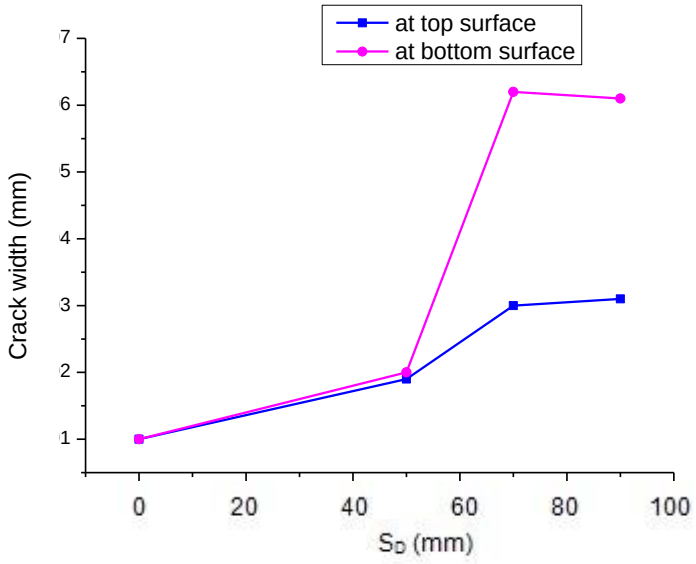

Figure 4.10 Crack widths at two surfaces

4.2.5 Analysis of the rolling process

4.2.5.1 Expansion of the crack depth

The expansion of crack depth along the thickness of the slab is shown in Figure 4.11. It can be seen that the crack depth gradually increases along thickness direction. The difference from the top surface to the bottom surface is about 0.6×10^{-3} m with a slab thickness of 20 mm.

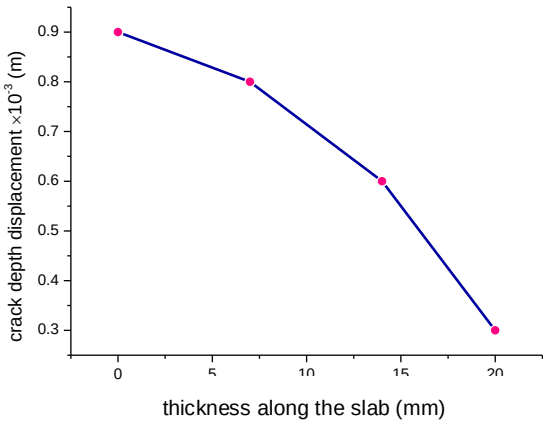

Figure 4.11 Variation of crack depth along thickness direction

4.2.5.2 Plastic strain distribution

The plastic strain for the work strip is displayed in Figure 4.12. It can be seen that when the slab is initially rolled into the roll gap, the front area on the tip of the surface has the most significant strain. When the slab is being rolled the central region of the crack always experienced larger plastic strain than its surrounding areas which can be seen from Figures 4.12(c) and (d). Also, the edge of the top surface of the work roll has a larger strain than the inner region. As explained in Chapter 3, the constitutive equilibrium shows that the plastic strain will influence the deformation to a large extent and cause the generation of heat. Therefore, it can be concluded that the central region of the edge crack has large plastic strain and thus increases the crack open angle.

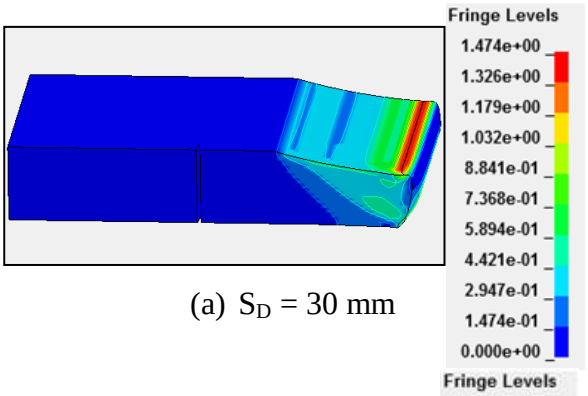

(a) S_D = 30 mm

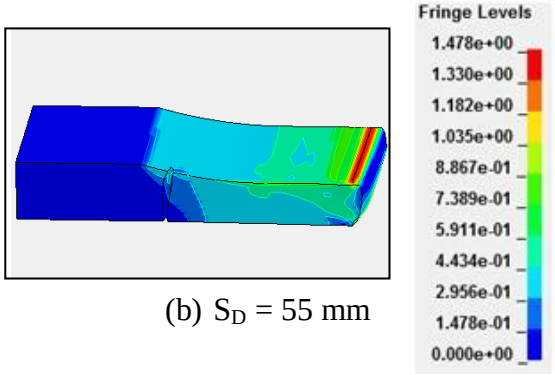

(b) S_D = 55 mm

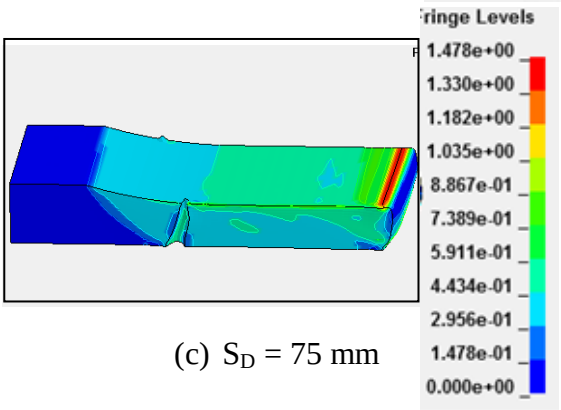

(c) S_D = 75 mm

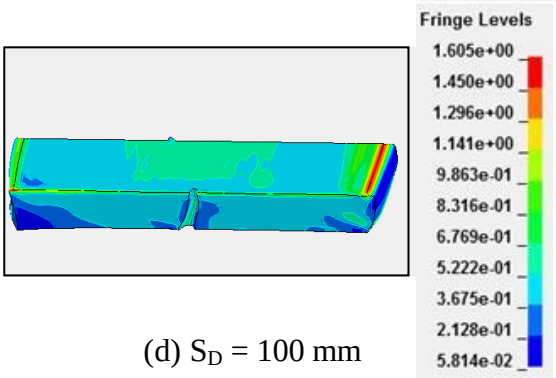

(d) S_D = 100 mm

Figure 4.12 Plastic strain distributions for edge crack

4.2.5.3 Pressure distribution

At present, little finite element research has been done on the distribution of the

pressure levels in different areas of cracks in the hot rolling process using either simulation or experimental approaches. From Figures 4.13(b) and (c), it can be seen that the maximum pressure occurs close to the region of entry, after which the pressure drops gradually. Figure 4.13(d) shows the crack tip area is much more sensitive to changes of pressure, which ranges around 110 MPa. For the rest of the areas the pressure is around 50 MPa.

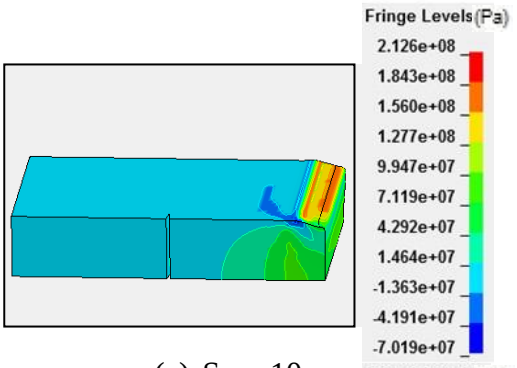

(a) S_D = 10 mm

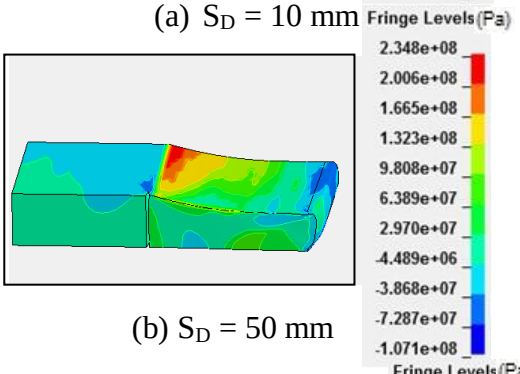

(b) S_D = 50 mm

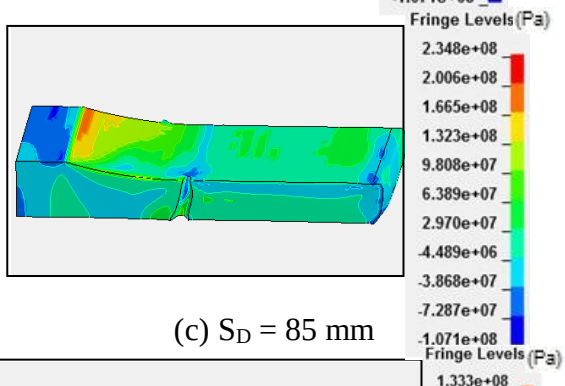

(c) S_D = 85 mm

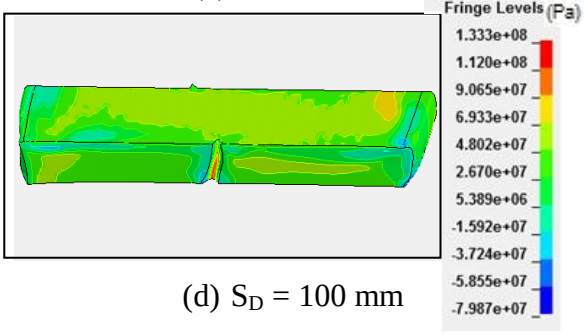

(d) S_D = 100 mm

Figure 4.13 Pressure distributions for edge crack

Comparing the pressure distributions with the plastic distributions makes it clear that the pressure distributions are less homogeneous along the width of the slab. Why some regions experience large pressure can be explained by the way that the sliding of the slab in the deformation zone increases, and consequently the increased accumulation of material at the inlet of this region increases the contact pressure.

4.2.5.4 Max shear stress distribution

In the manufacturing industry, the shear stress at the interface of the work roll and interface varies due to many variables such as the friction coefficient. Due to the difficulty of analysing this parameter using experimental methods, the shear stress distribution for the strip is expressed in Figure 4.14 using the simulation method. It can be seen that a large shear stress takes place at the deformation zone when the strip begins to enter the rolling gap region. Contact conditions for both the work roll and slab at the interface are important in determining the results.

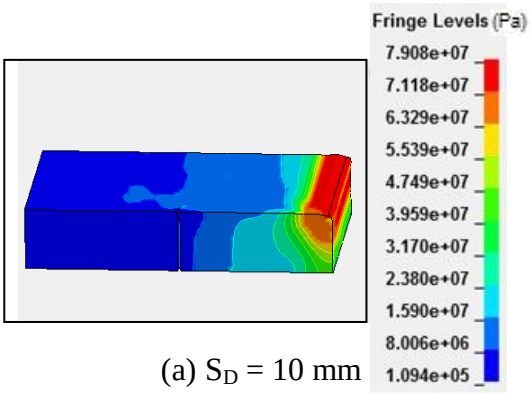

(a) S_D = 10 mm

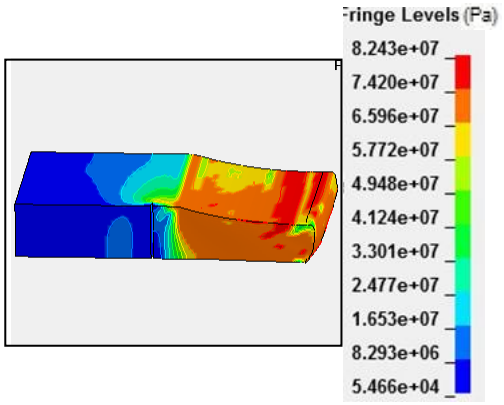

(b) S_D = 50 mm

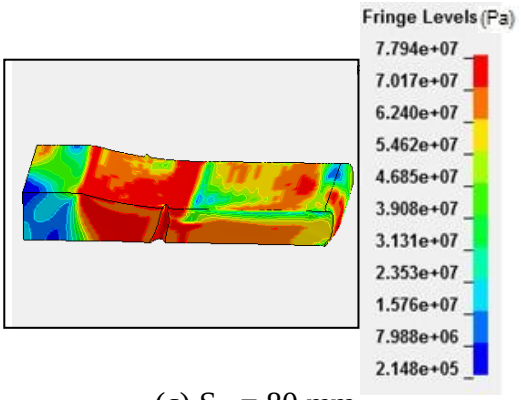

(c) S_D = 80 mm

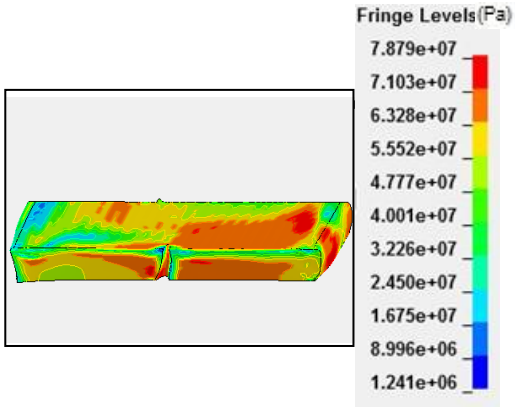

(d) S_D = 100 mm

Figure 4.14 Maximum shear stress distributions for edge crack

4.2.6 Thermal effect

4.2.6.1 Temperature distribution of the strip

The global temperature for the strip is shown in Figure 4.15. Due to the contact heat transfer at the interface between the slab and the roll, the temperature drops instantly when contact takes place between these two surfaces. It can be seen that the surface temperature drops at first when the slab goes into the contact zone, and when it leaves the contact zone its temperature will increase to some extent.

This is because the inner higher temperature will gradually compensate the heat loss of the strip surface. Another reason is that when the strip is deformed, heat will be

generated from the plastic deformation. Although heat is also generated from friction, compared with other influential factors this is not significant.

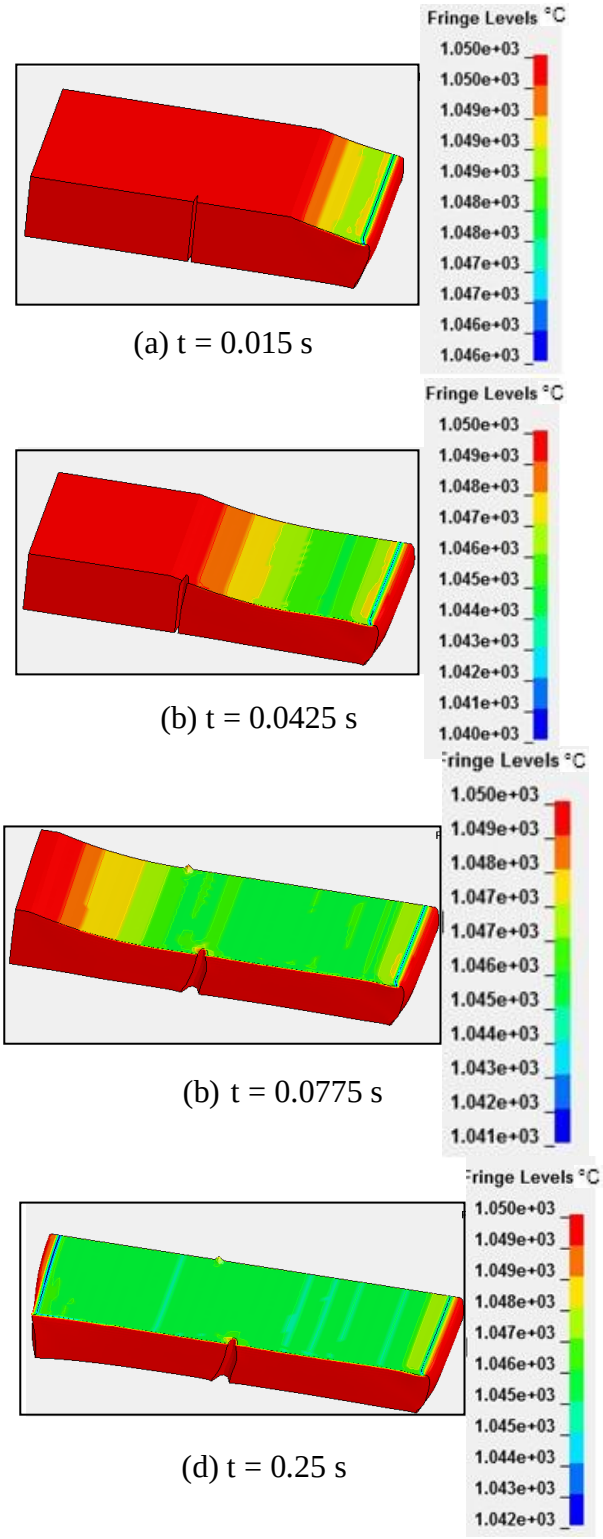

Figure 4.15 Temperature distributions of the slab

The minimum temperature of the strip occurs at the exit of the deformation zone,

because this region is in contact with the work roll for more time. It can also be seen that the temperature distribution along the direction of the strip width is comparatively uniform. For the case proposed here with an initial strip temperature of 1050 ℃, when the time reaches 0.25 s the temperature drops to around 1042 ℃.

4.2.6.2 Temperature distribution on the work roll

As described in Chapter Two, there are not many studies that discuss the temperature distribution on the work roll. In this section, the work roll temperature will be analysed with the initial work roll temperature of 20 ℃. The work roll is assumed to be rigid which means there will be no heat generation from plastic deformation. However, the contact heat transfer for the work roll cannot be neglected due to its significant influence on both the slab and the work roll.

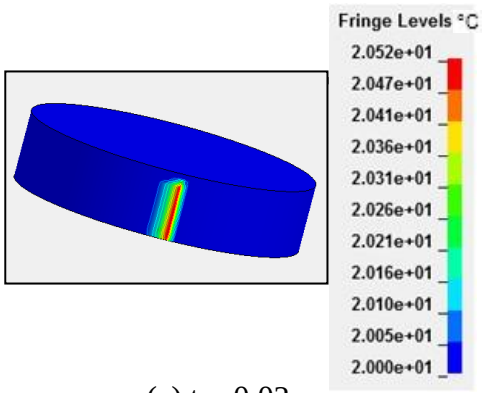

(a) t = 0.02 s

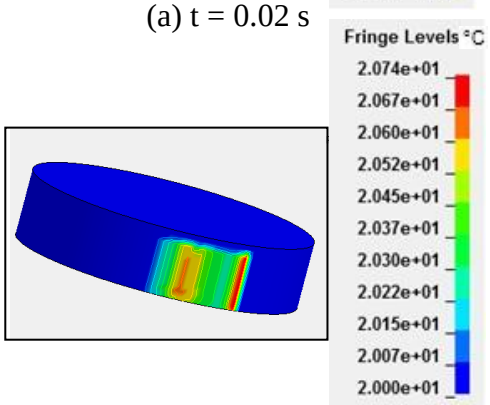

(b) t = 0.07 s

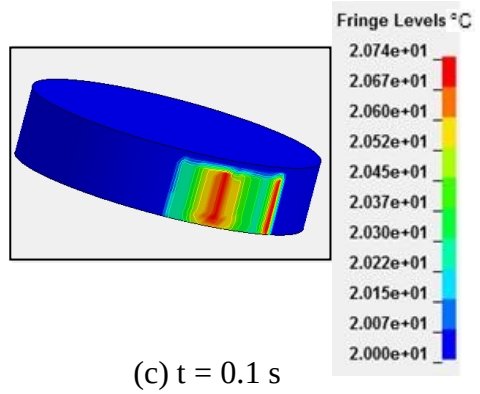

(c) t = 0.1 s

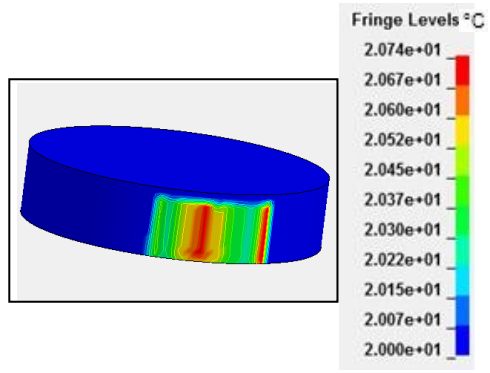

(d) t = 0.116 s

Figure 4.16 Temperature distributions of the work roll

When designing the thermal parameters for the slab and the work roll it makes little difference whether they are for the slab or the work roll. As described in Chapter Three, heat can be transferred from the material to the ambient air through the heat radiation and heat convection. These two factors are influenced significantly by temperature. In order to minimise the computer calculation time, convection and radiation have not been considered in the proposed models due to their low temperatures compared to that of the workpiece.

It can be seen from Figure 4.16 that with a gradual increase of the contact area the heat will transfer from the strip to the work roll through the contact heat transfer mechanism. High temperatures occur in the work roll when the contact time is greatest. This is scrutinised with the use the software of LS-DYNA. Through the whole time range of 0.1 s, the temperature increases from an initial value of 20.00 ℃ to a maximum of 20.74 ℃ for the work roll.

4.2.6.3 Temperature around the crack area

The temperature distributions along the crack depth are shown in Figure 4.17. The lines denoted by the characters A and B represent crack depths of 2 mm and 3 mm, respectively. It can be seen that the temperature along the deep crack is larger than along the shallow crack. This can because the deep crack gains more heat transferred from the workpiece center, but at shalower depths it will release more heat to the environment.

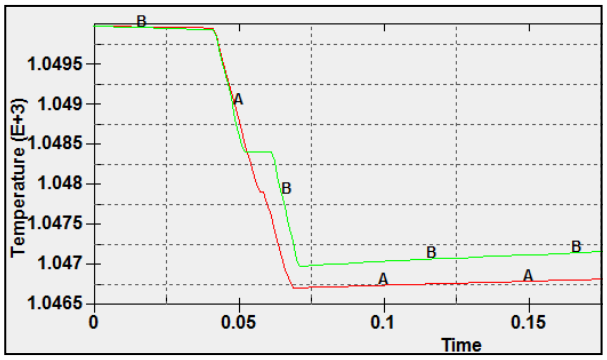

Figure 4.17 Temperature distributions along the crack depth

The temperature distribution along the thickness direction is shown in Figure 4.18 with lines denoted by A, B and C representing various slab thickness of 1, 5 and 10 mm, respectively. It is clear that the temperature near the strip and work roll interface decreases more as it is influenced significantly by contact heat transfer. However, for regions which are far from the interface, the heat loss could be compensated by the internal heat from the slab's central region.

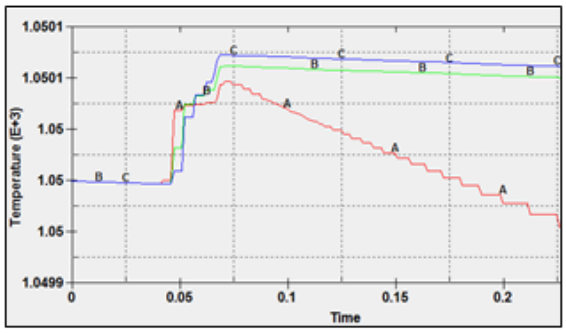

Figure 4.18 Temperature distributions along the thickness direction

4.2.7 The influence of rolling conditions

Figure 4.19 shows the crack width behaviours of two cracks with different initial conditions. The cracks become enlarged in both cases. It can be seen that the crack at bottom surface propagate more significantly than those on the top surface. It increases to a peak value at S_D = 0.05 m, and then the crack width will drop slightly. This is because when the strip is rolled out of the work roll gap, the crack area experience compression, and this leads to the closure of crack to some extent.

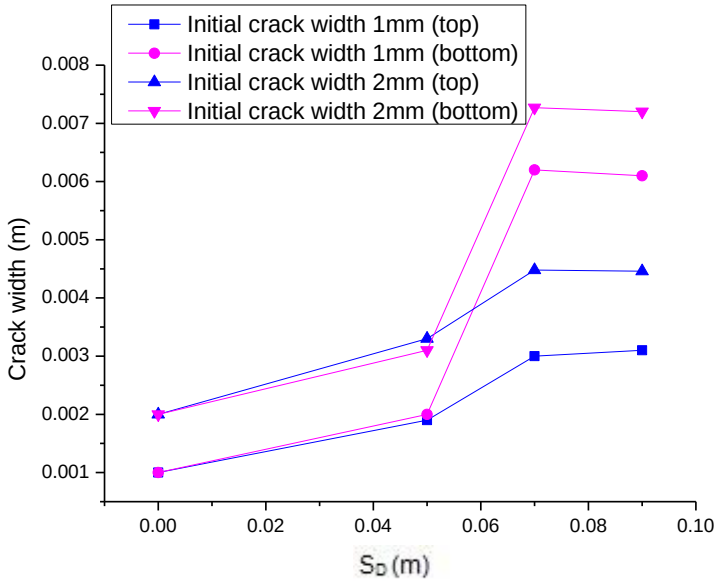

Figure 4.19 Initial crack width effect

Figure 4.20 shows the effect of different initial crack depths on crack width behaviour. It can be seen that the crack width is enlarged when the crack depth increases at the slab top surface. Also, crack depth on the bottom surface is propagated when the crack depth increase from 3 to 5 mm. This means that it is hard for the crack to be healed after hot rolling when the edge crack has a large crack depth.

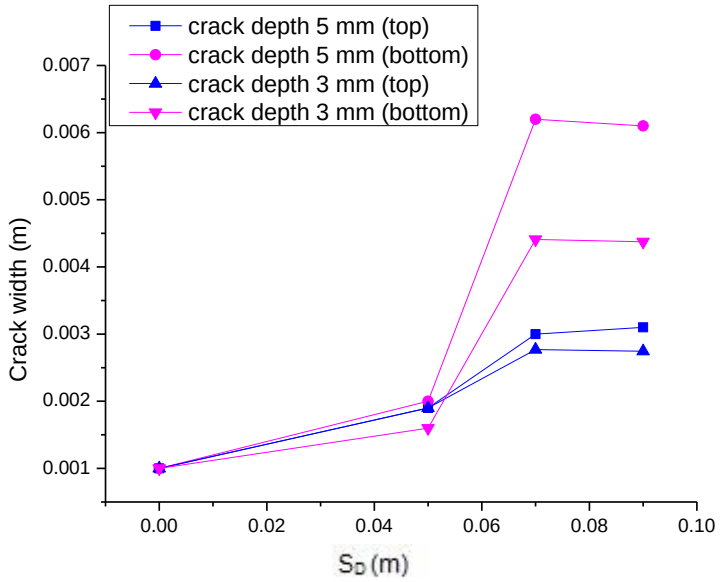

Figure 4.20 Initial crack depth effect

Figure 4.21 shows the influence of work roll diameter on the crack width at the top and bottom surfaces. It can be seen that the work roll diameter does not influence the crack width on the bottom surface. However, the crack width on the top surface is enlarged when the work roll diameter is increased.

When the work roll diameter increases from 300 to 400 mm the crack width increases from 3.1 to 3.2 mm. This phenomenon indicates that implementing large work roll diameter may give rise to the further propagation of edge cracks. Therefore, it is recommended to use the comparatively small work roll to eliminate or minimise the defects during the hot rolling process.

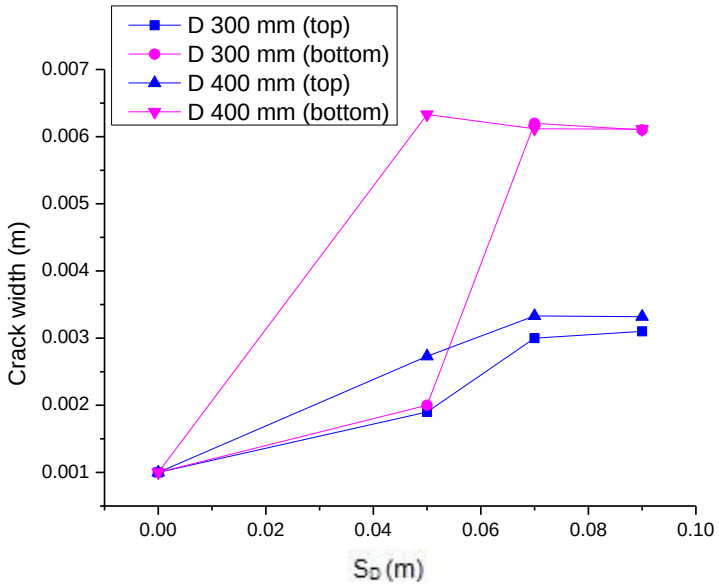

Figure 4.21 Effect of roll diameter on crack width

Figure 4.22 shows the effect of rolling reduction on crack closure behaviour. It can be seen that the rolling reduction has a significant influence on crack width changes. When reduction rises from 30 to 35%, the crack width at the top surface increases from 3.1 to 4.2 mm. Also, the crack width at the bottom surface enlarges with the implementation of a high reduction ratio.

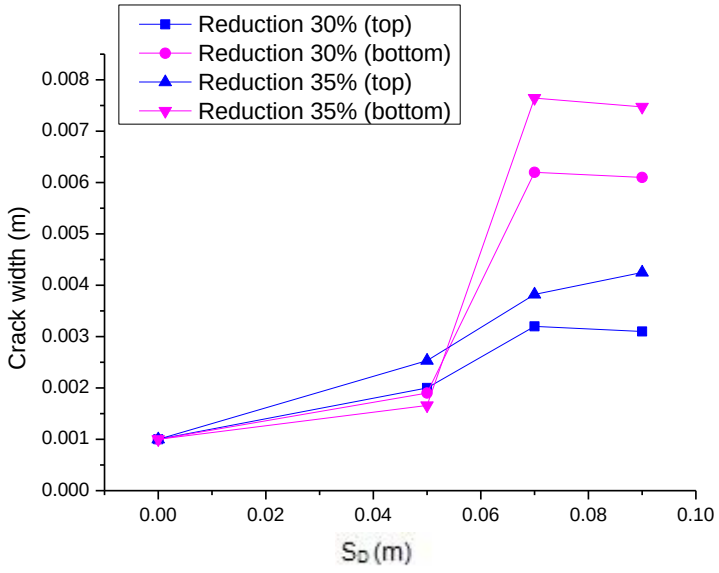

Figure 4.22 Effect of rolling reduction on crack closure behaviour

The differences of crack width in the top and bottom surfaces are 1.1 and 1.3 mm, respectively. This indicates that the rolling reduction has a comparatively greater influence on crack width on the bottom surface than on the top surface. In order to minimise the propagation of crack on the bottom surface, the reduction ratio should be lowered.

4.3 Transverse cracks

Presently, there would appear to be few reports using the finite element method to investigate the transverse behaviour in hot rolling processes for stainless steel. Since many defects such as edge cracks deteriorate during hot rolling process, it is essential to find a reliable method to examine the other crack behaviors during the development.

4.3.1 Behaviour of transverse cracks

Figure 4.23 shows the evolution of transverse cracks on the surface of the strip. The symmetrical planes for this model are the bottom and back surfaces of the strip. Five states (a), (b), (c), (d) and (e) show that the crack closes at the symmetrical plane, however, it is gradually opened at the outer surface of the slab. The final crack shape is shown in Figure 4.23 (e).

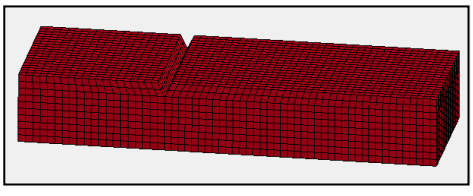

(a) S_D = 0 mm

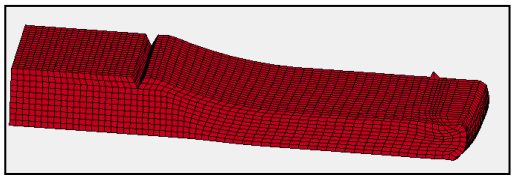

(b) S_D = 60 mm

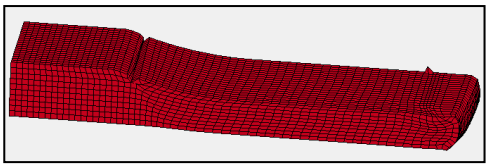

(c) S_D = 70 mm

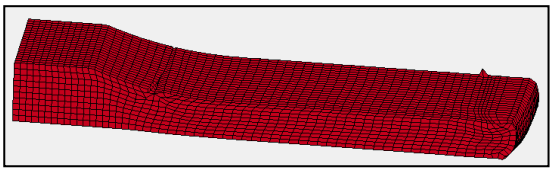

（d）S_D = 80 mm

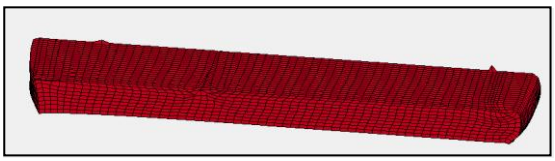

(e) S_D = 100 mm

Figure 4.23 The behaviour of transverse crack during the hot rolling process

4.3.2 Lateral deformation of cracks

Figure 4.24 shows that the lateral shape of transverse crack on top of the slab

surface is non-uniform. The crack width at the outer slab surface experiences a large expansion, and the crack width becomes small towards the slab's symmetrical centre. The lateral deformation is due to the non-homogenous boundary conditions set by the modelling procedures. It is clear that the elongation of slab at the edge regions is larger than that in the slab centre. This phenomenon is always the case in the manufacturing industry. The reason is that there is less constraint near the edge region and more constraint in the central region.

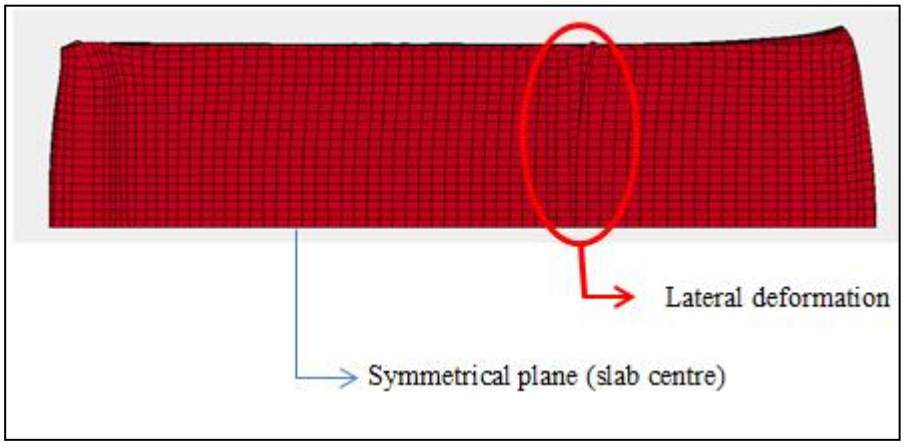

Figure 4.24 Lateral deformation of transverse crack

4.3.3 Rolling force

Figure 4.25 shows the rolling force for a slab with a transverse crack. It can be seen that the rolling force increases gradually to a statble state in which the value is about 17.5 $\times 10^3$ (N/m). When the crack goes into the deformation region, it is clear that the rolling force has a small drop, and after the crack region leaves the rolling gap its value increases to the value of the stable state again. After the whole work piece has rolled out of the work roll, the rolling force then goes down gradually to zero.

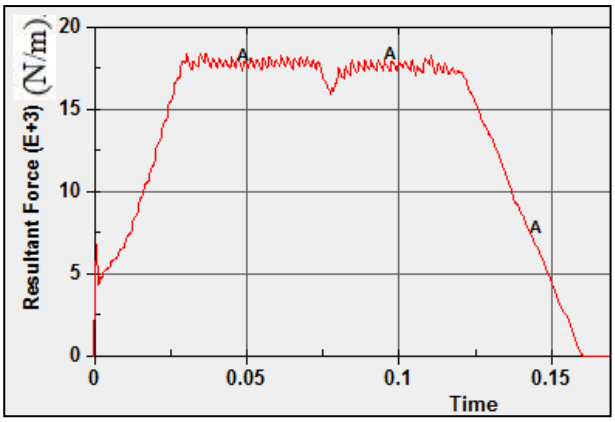

Figure 4.25 Rolling force for the transverse crack
(Reduction 20%)

4.3.4 Crack width evolution

As discussed before, the crack width varies according to the distance from the symmetrical plane to the slab centre. Figure 4.26 is an enlarged area of Figure 4.24 showing the crack region. This clearly shows the profile change along a line from slab centre to slab edge. The maximum crack width is almost double the minimum crack width value.

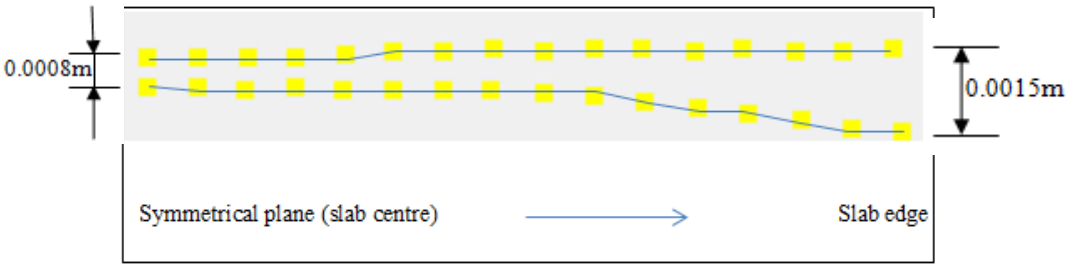

Figure 4.26 Crack width along the slab width

4.4 V-shaped transverse cracks

V-shaped transverse cracks can appear in the central area of the slab as well as the corner areas. In order to investigate the mechanism of the crack closure the FE models proposed in Chapter Three are simulated. It should be noted that the element used for simulation of V-shaped transverse cracks is different from that used for the simulation of edge and longitudinal cracks. The element used here is three-dimensional ten-node tetrahedral structural solid 168 (Figure 4.27). Due to the irregular shape of the V-shaped crack, this element is much more suited than solid 164 (Figure 4.28). The element is defined by ten nodes having three degrees of freedom at each node, with translation in the nodal x, y, and z directions.

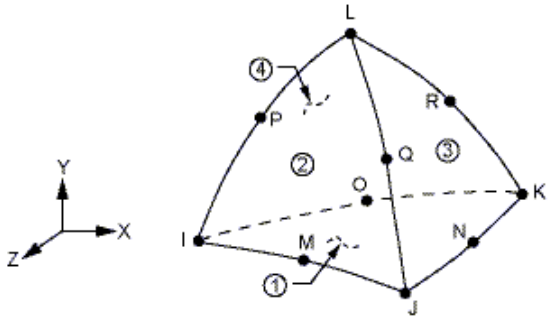

Figure 4.27 Solid 168 element

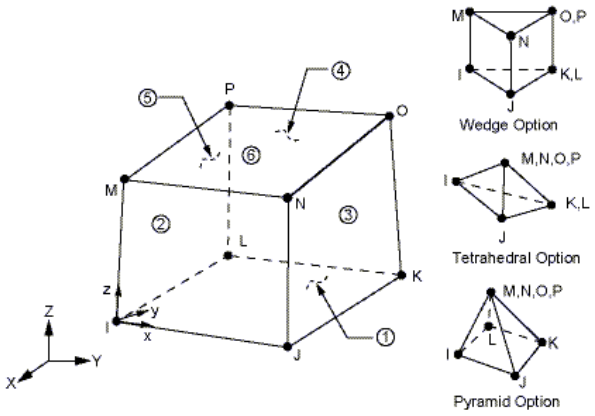

Figure 4.28 Solid 164 element

When comparison these two element types it is clear that the solid 168 with ten nodes has an appropriate shape for modelling V-shaped transverse cracks. However it also dramatically increases the computer calculation time for obtaining the FE results.

4.4.1 Behaviour of V-shaped transverse cracks

The crack evolution of model one in the proposed schedules in Chapter 3 is displayed in Figure 4.29. Through the process from (a) to (h), it can be seen that the crack width along the thickness direction will gradually close. The deep crack will close from the initial period, but the crack length will be enlarged. Finally, the crack width will gradually extend which can be seen from Figure 4.29. This is because in the bite zone, the compressive stress appears around the deformation region, and the crack gradually closes. However, when the crack is moved out of the work roll, it will experience the tensile stress with the top slab surface having more strain, therefore, the crack width toward the top surface of the slab is gradually enlarged. It is obvious that the larger compressive stress can lead to the crack closure, and the larger tensile stress can result in crack propagation.

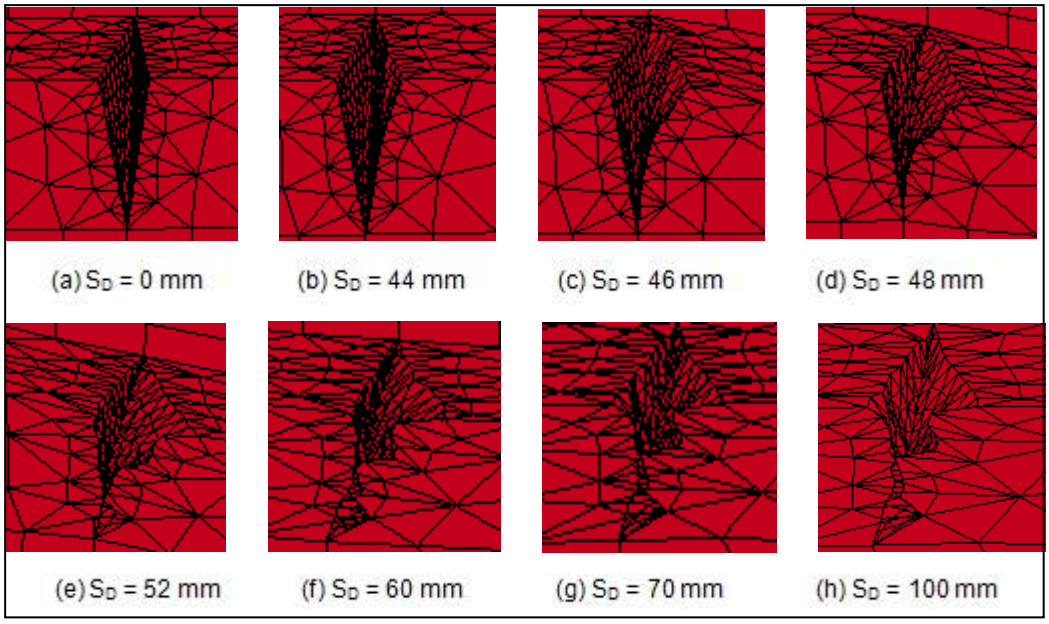

Figure 4.29 Evolution of V-shaped transverse cracks

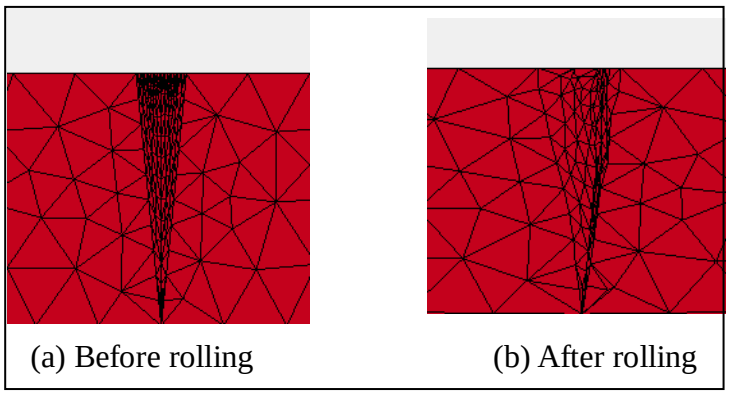

Figure 4.30 Comparison of V-shaped transverse crack evolution along crack length

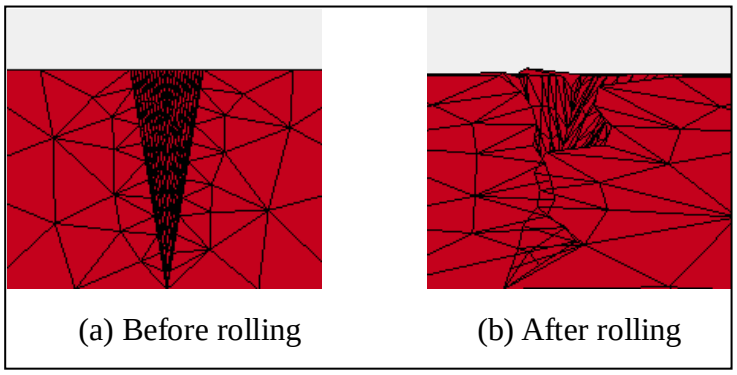

Figure 4.31 Comparison of V-shaped transverse crack evolution along the direction of slab thickness

By comparing the V-shaped transverse crack along the two coordinate directions (Figures 4.30 and 4.31), the elongations of crack width from both of two view coordinate directions are clearly indicated.

4.4.2 Rolling force

From the literature review, it is found that there is no research discussing the effect of the V-shaped transverse crack size on the rolling force. Therefore, in this section the problem will be discussed and also together with a consideration of the effects of thickness reduction and work roll diameter on rolling forces.

It can be seen from Figures 4.32(a), (b) and (c) that the crack size does not influence the rolling force as much as that of the thickness reduction and work roll diameter. When the crack size increases in terms of crack width, crack length and crack depth, the rolling force decreases to a small extent.

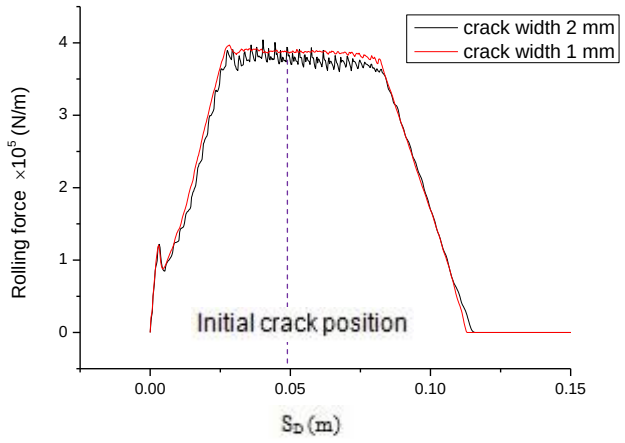

(a) Crack width effect

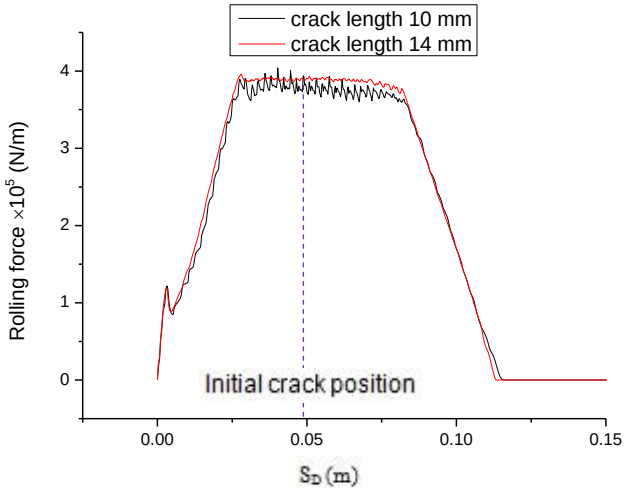

(b) Crack length effect

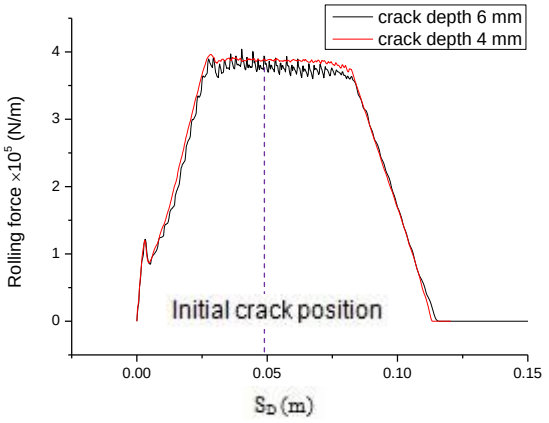

(c) Crack depth effect

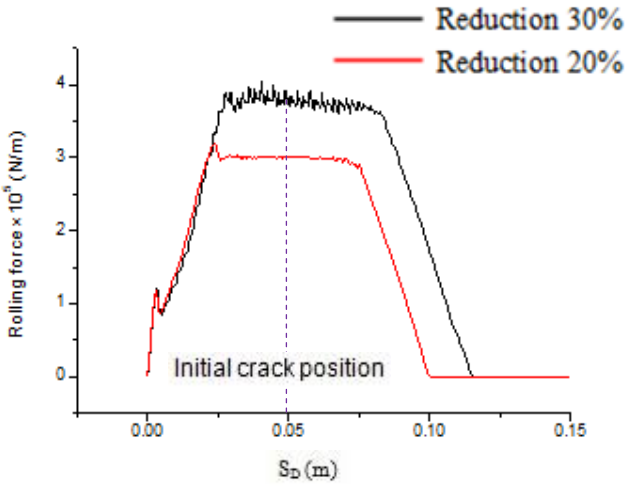

(d) Reduction effect

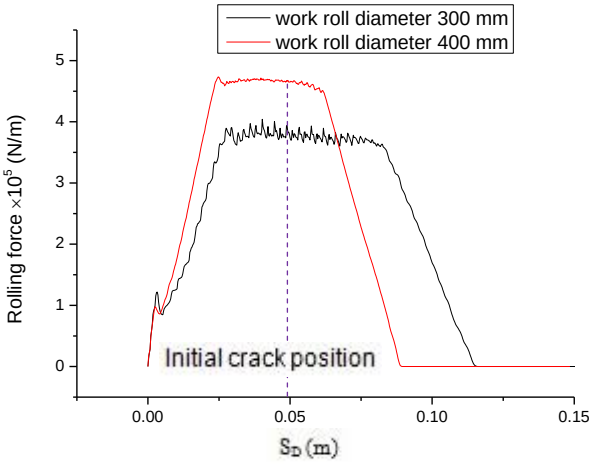

(e) Work roll diameter effect

Figure 4.32 Rolling force for the V-shaped transverse crack

From Figure 4.32(d) and (e), it can be seen that the rolling force is sensitive to the thickness reduction and the work roll diameter. When the reduction increases from 20 to 30%, the rolling force increases from 3×10^5 to 4×10^5 N/m, which can be seen from Figure 4.32(d).

The effect of the work roll diameter on the rolling force is shown in Figure 4.32(e). With an increase of work roll diameter from 300 to 400 mm, the rolling force will experience a rise from about 3.8×10^5 to 4.7×10^5 N/s. It can also be seen that the steady state with larger roll diameter has a relatively short steady state period, and it will decrease to zero a little earlier than that with the small work roll.

4.4.3 Von Mises stress distribution

It can be seen from Figure 4.33 that the deformation zone has maximum von Mises stress by observation the relative behaviour through Figure 4.33(a), (b) and (c). This indicates that the work roll has the large the von Mises stress when it starts to enter the roll gap. It will increase to a maximum level and then the value gradually decreases when the workpiece is rolled out of the contact region. The general range for the maximum and minimum of von Mises stresses is between 130 MPa and 13 MPa.

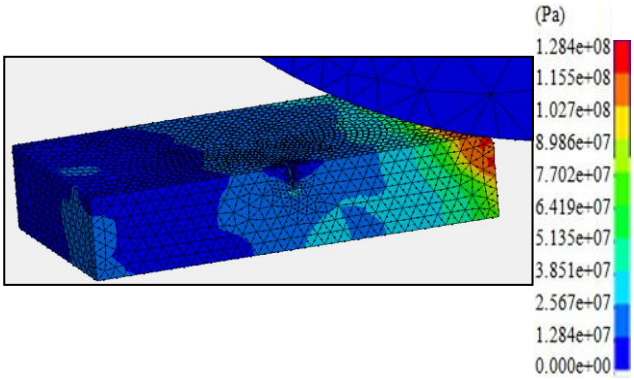

(a) S_D = 10 mm

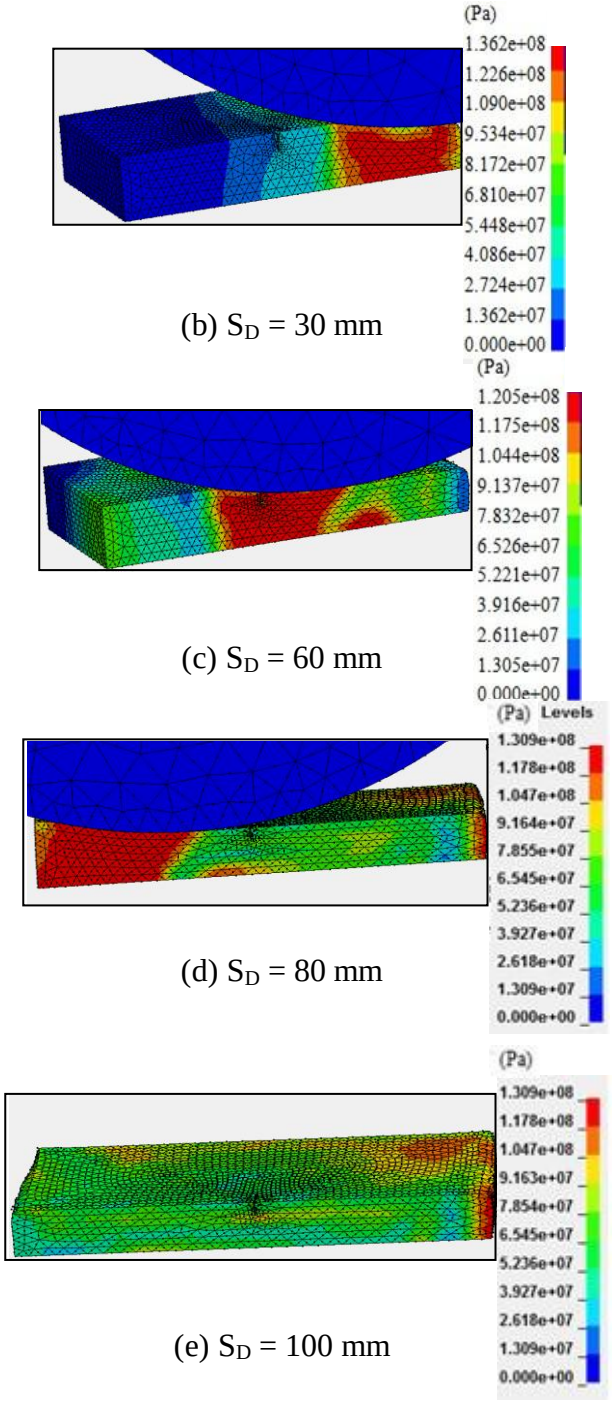

Figure 4.33 Distribution of von Mises stress for the V-shaped transverse crack

4.4.4 Plastic strain distribution

The plastic strain distributions for the V-shaped crack during hot rolling process are shown in Figure 4.34. The maximum distribution of plastic strain is similar compared with that of effective stress distribution. In both conditions, the

deformation zone in which the roll and workpiece interacts with each other has more plastic strain than areas outside the deformation zone.

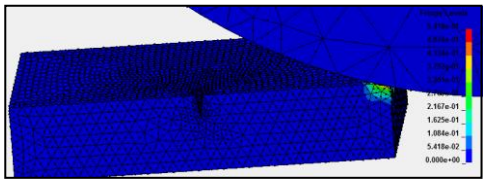

(a) S_D = 10 mm

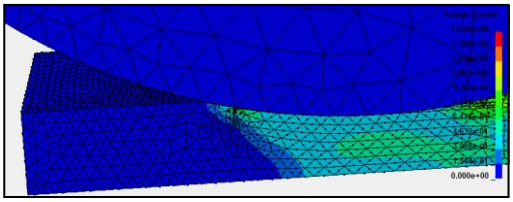

(b) S_D = 60 mm

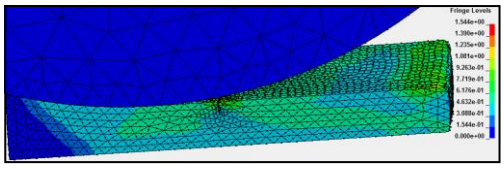

(c) S_D = 85 mm

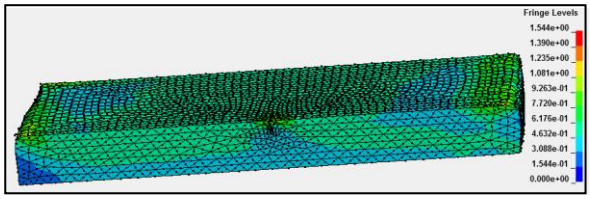

(d) S_D = 100 mm

Figure 4.34 Plastic strain distributions

4.4.5 Effect of mesh density

As discussed before, the two different element types and meshes are used to simulate the V-shaped crack evolution. It can be seen that the elements with ten nodes shown in Figure 4.35 are more accurate than elements with eight nodes shown in Figure 4.29.

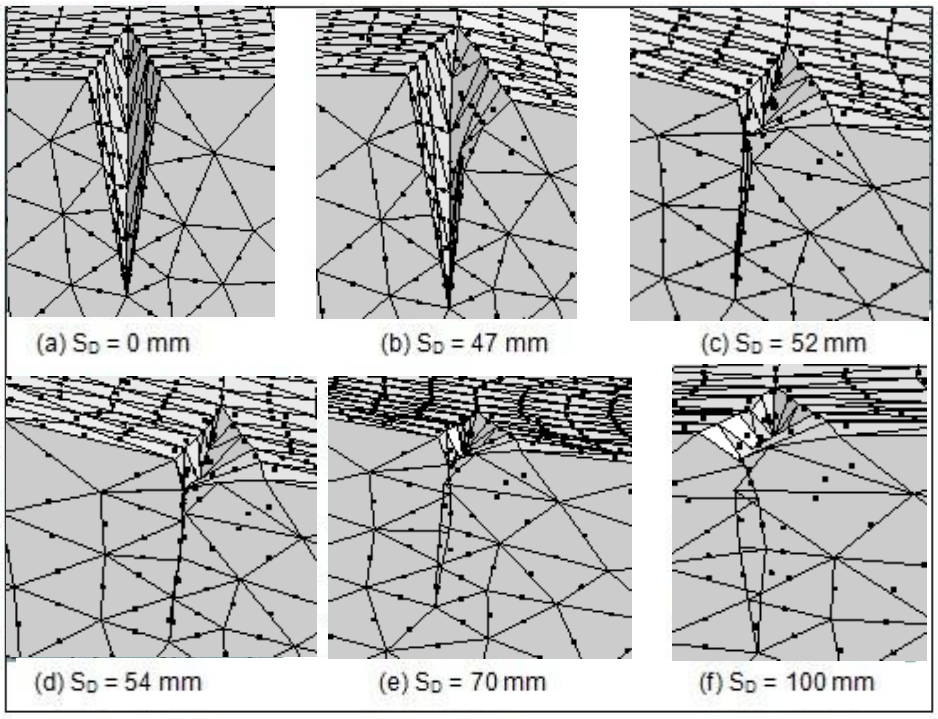

Figure 4.35 V-shaped transverse crack with element type of ten-node

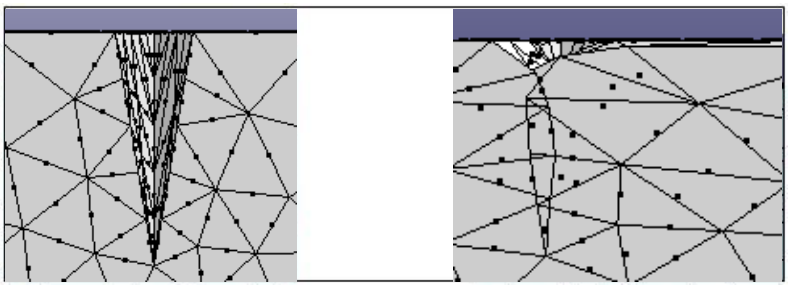

(a) Before rolling (b) After rolling

Figure 4.36 Evolution of V-shaped transverse crack along crack depth direction

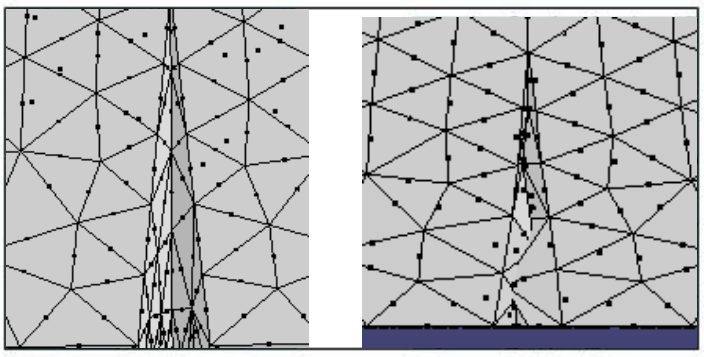

(a) Before rolling (b) After rolling

Figure 4.37 Evolution of V-shaped transverse crack along crack length direction

Figures 4.36 and 4.37 show the V-shaped transverse crack evolution from two viewpoints. The results obtained with elements of ten-node and elements of eight-node have a coherent final crack shape. Figure 4.36 shows the same results as Figure 4.31, and Figure 4.37 has the same results as shown in Figure 4.30. These comparisons indicate that the finite element method can obtain reasonable simulation results which could act as the reference together with the experimental approach.

4.4.6 Pressure distribution

It can be seen from Figure 4.38 that during the steady rolling state, the pressure is about 500 MPa and when the slab is rolled out of the roll gap, the value range around 400 MPa. However, during the whole process, the negative value appears which means that the tension exists when the slab is rolled.

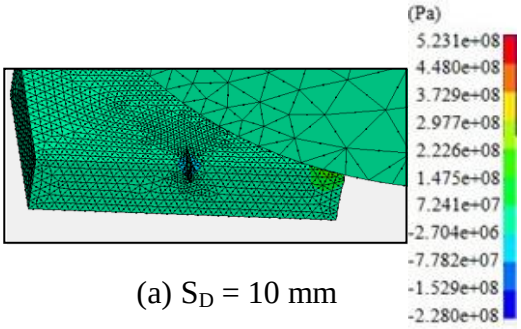

(a) S_D = 10 mm

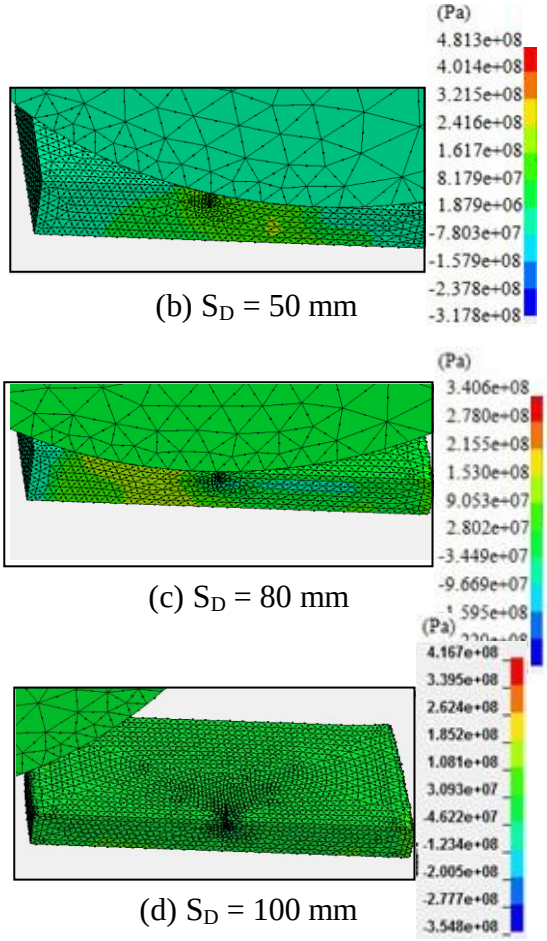

Figure 4.38 Pressure distributions (Pa)

The maximum tension is about 350 MPa and the minimum tension is approximately 200 MPa. The tensile stresses are undesirable because they tend to cause microcracks if the slab is not of good quality. The tensile stresses generally work along the rolling direction and the slab width direction. The compressive stress works in the slab thickness direction.

4.4.7 Distribution of maximum shear stress

The maximum shear stress is displayed in Figure 4.39. It can be seen that the maximum shear stress ranges during the whole rolling process from 75 to 7.5 MPa. The deformation zone experiences the most shear stress. The shear stress decreases

when the slab is rolled out from the contact region.

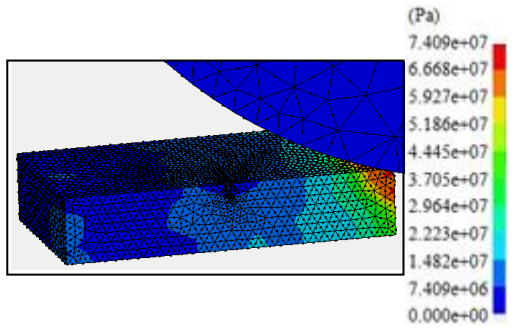

(a) S_D = 10 mm

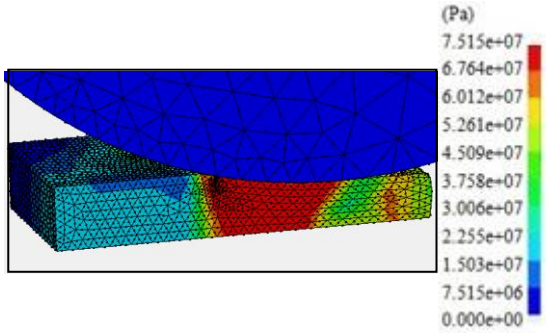

(b) S_D = 50 mm

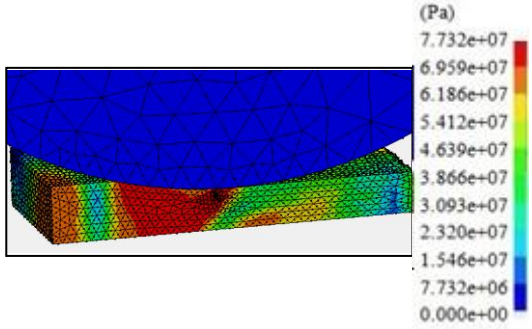

(c) S_D = 80 mm

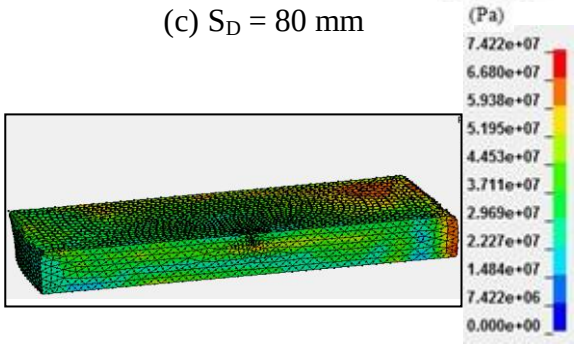

(d) S_D = 100 mm

Figure 4.39 Distributions of maximum shear stresses (Pa)

4.4.8 Distributions of effective strains

Figure 4.40 shows the distribution of the effective strains during the hot rolling process with a V-shaped transverse crack. It can be seen that the magnitude of the effective strain during the process ranges from 0.08 to 0.8. The regions around the V-shaped crack area experience the largest effective strain which is about 0.8. This means that there is a large deformation in this region.

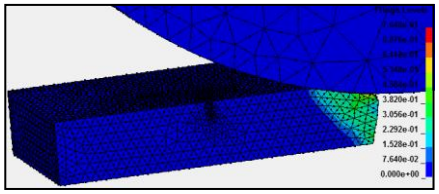

(a) S_D = 20 mm

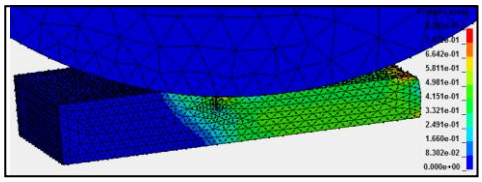

(b) S_D = 90 mm

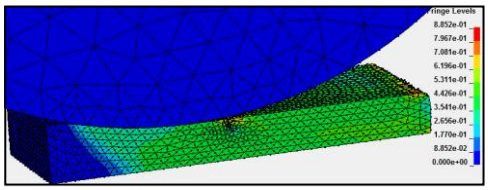

(c) S_D = 100 mm

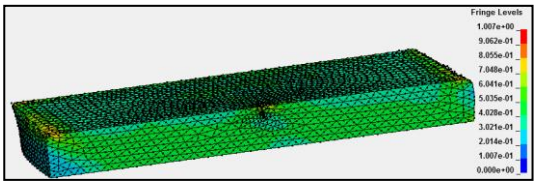

(d) S_D = 100 mm

Figure 4.40 Distributions of effective strain

4.4.9 Distribution of temperature

Figure 4.41 shows the temperature distributions at the slab centre and at the midpoint in the thickness of the slab. The two regions are denoted by the characters A and B, respectively. The locations of A and B are clearly shown in Figure 4.42. Both of the two regions are on the symmetrical planes, which means that there is no heat loss through convection and radiation to the environment

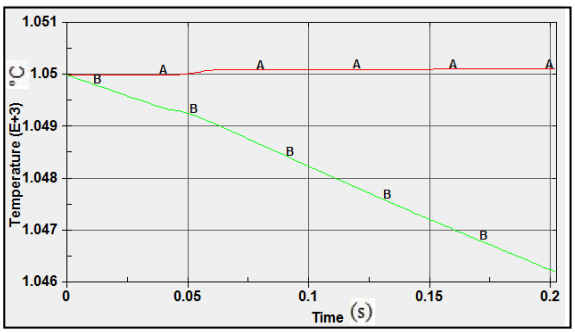

Figure 4.41 Temperature distributions along the symmetrical plane

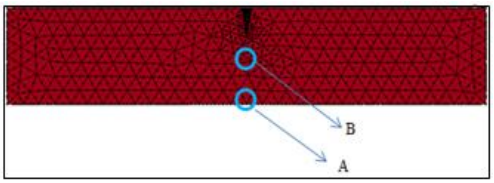

Figure 4.42 Location of selected areas A and B

It can be seen that the temperature of the slab centre increases to a certain extent with the final temperature being slightly higher than its initial value of 1050 ℃. This is because when the slab is rolled into the deformation region, the heat will be generated by the plastic deformation. This causes the temperature of the central region to rise.

By comparing the temperature of the central region with the temperature at the mid-point in the slab thickness, it can be seen that this value will dramatically drop from the beginning of the rolling process to the end. Although there is a heat generated from the deformation, it is not enough to compensate for the heat loss. Because it is located near the top surface of the slab, the heat will be largely influenced by the interface heat transfer between the slab and the work roll. The temperature at this region will drop from the initial value of 1050 ℃ to about 1046 ℃ through a rolling time of 0.2 s.

4.4.10 The influence of rolling conditions

Figure 4.43 shows the crack width behaviour during the rolling process. Two initial crack width conditions are taken into account. It can be seen that the trend for both of the two conditions is similar, and it increases to a peak value and then falls, and then it increases again. This is because when the crack is going towards the deformation zone, it experiences tensile stress and this makes the crack enlarge. When the slab is in the deformation zone, the compression makes the crack close to some extent. When the crack is rolled out of the deformation zone, the crack experiences tensile stress again, and the crack width increases to some extent.

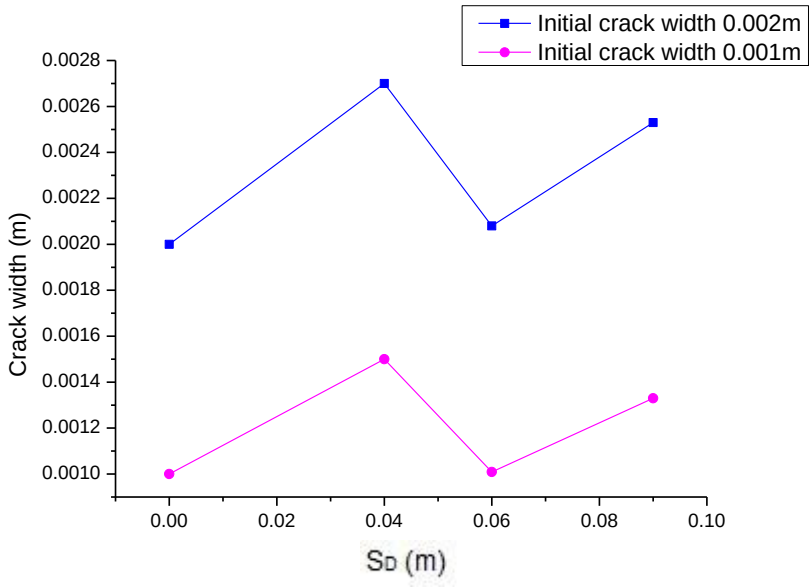

Figure 4.43 Crack width behaviour

The crack width behaviour under different initial crack length conditions is shown in Figure 4.44. It is clear that the crack will propagate significantly when the crack length is large. However, the effect is not significant when it increases to the first peak value, and the crack width in both of the two situations is around 0.0027 m.

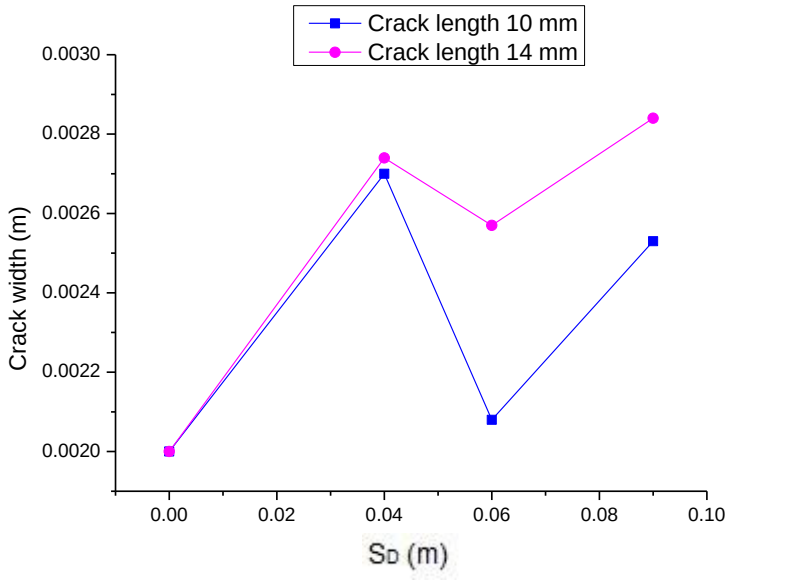

Figure 4.44 Crack length effect

The behaviours of crack depth under different crack depths are shown in Figure

4.45. The closure of the crack has little relationship with the size of crack depth, and it is clear to see that the cracks width are nearly the same at S_D = 0.09 m. By comparing Figure 4.45 with Figure 4.44, it can be concluded that the crack with a large crack length was hard to heal during the rolling process.

However, the crack depth does not influence the closure behaviour much as crack length does. This is because the strip experiences compression along the crack depth direction, and therefore, it is preferable for the crack to be self-healed. In the manufacturing industry, some measures should be taken to minimise crack propagation, especially for large crack length defects.

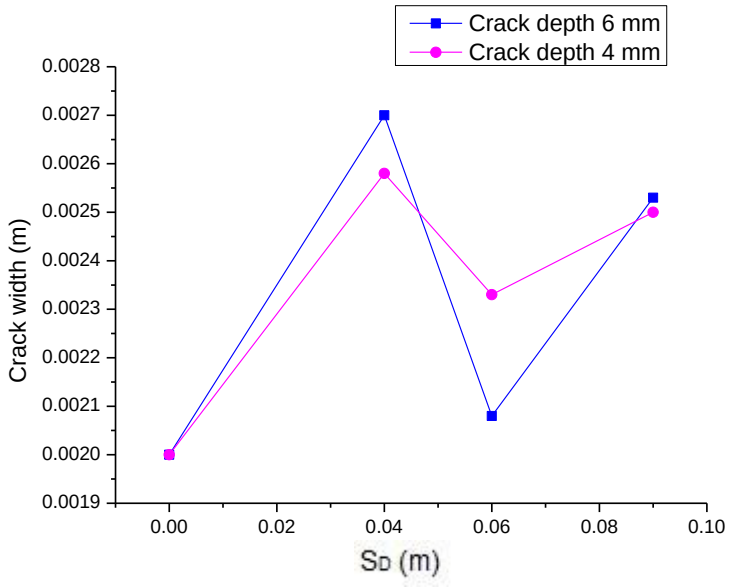

Figure 4.45 Crack depth effect

The effect of rolling reduction on crack width is shown in Figure 4.46. The rolling process with low reduction goes on more smoothly than the process with higher rolling reduction. The crack width with a rolling reduction of 20% increases gradually to approximately 2.5 mm at S_D = 0.09 m, which is nearly the same as the crack width increase when the rolling reduction of 30%. The effect of rolling reduction on crack closure behaviour is not significant.

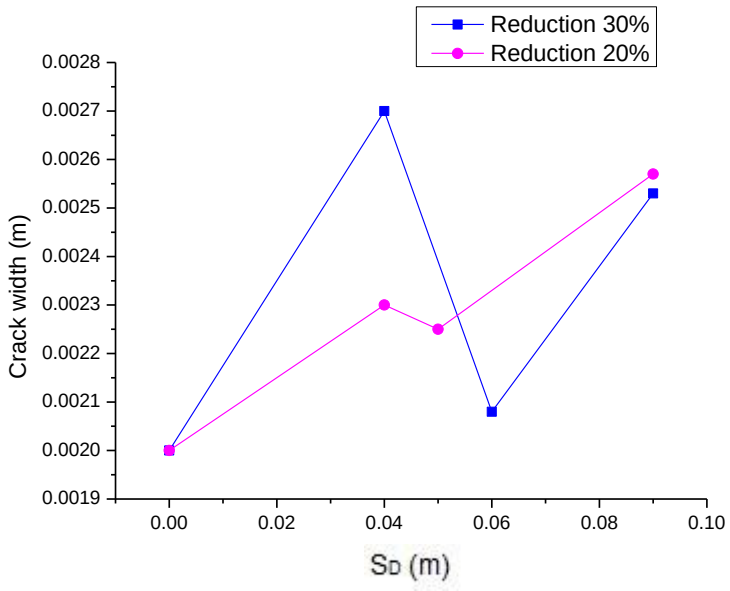

Figure 4.46 Reduction effect on crack width

Figure 4.47 shows the effect of work roll diameter on crack width. It can be seen that the crack width is smaller with an increase of work roll diameter. The final crack width changes from 2.53 to 2.19 mm when the roll diameter increases from 300 to 400 mm. This means that in order to minimise the defects on continuously casting slabs, a larger roll diameter should be employed, as the work roll diameter influences the crack closure behaviour significantly.

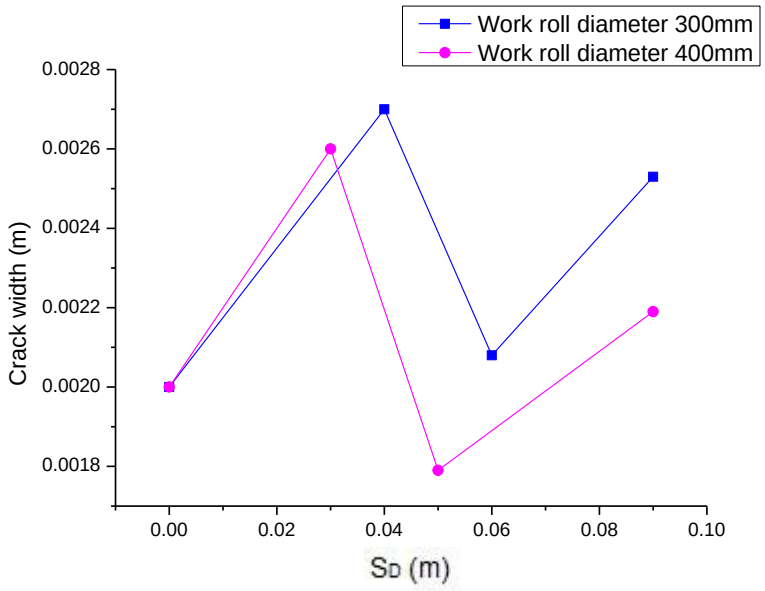

Figure 4.47 Effect of work roll diameter on crack width

4.5 Longitudinal crack behaviour during hot rolling process

Longitudinal surface cracks often exist on continuously cast slabs. Compared with transverse cracks, longitudinal cracks are usually much larger. The cracks are formed due to the non-homogenous cooling conditions during the solidification of the material. Many experiments have been carried out in order to find ways to minimise the defects. In this section, the longitudinal crack will be analysed in detail.

4.5.1 Behaviour of longitudinal cracks

The methods used for observation of longitudinal cracks are little different from those for observing transverse and edge cracks. It is necessary to know the inner crack shape evolution. Therefore, the section plane has been introduced here to observe the behaviour of the inner crack transfer mechanism.

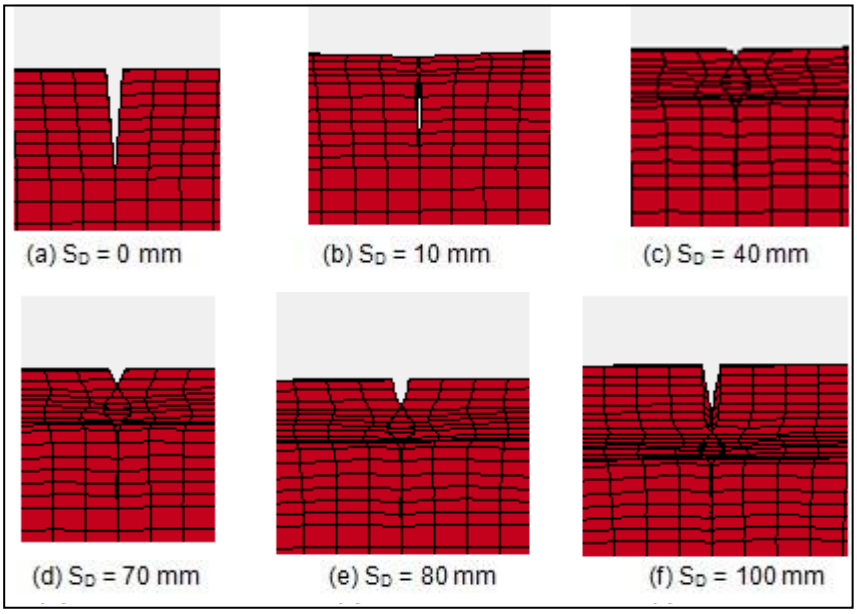

Figure 4.48 Longitudinal crack rolls into the work roll gap

Figure 4.48 shows that when a longitudinal crack is initially rolled into the work roll gap, the crack at the boundary will then be closed. When the strip is rolled, the deformation in the rear region will then be closed gradually. In order to obtain a good understanding of the process, a plane section was introduced to analyse this phenomenon. The section plane will transect the slab along the x direction.

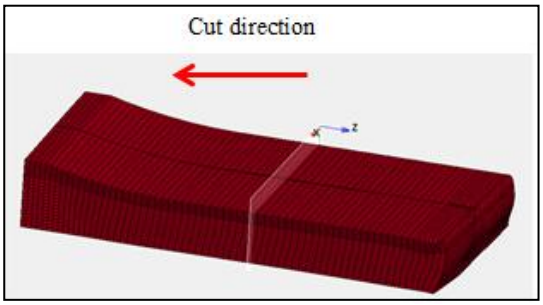

(a) Section plane in the strip

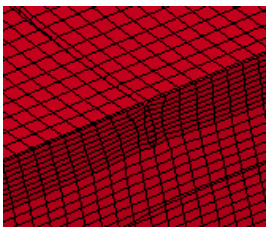

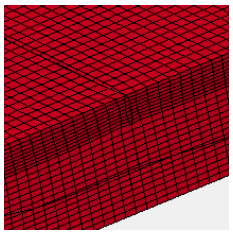

(b) Section plane at initial position (c) Section plane moves forward 10 mm

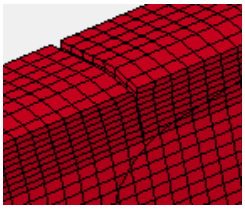

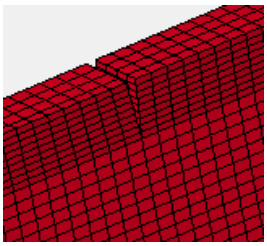

(d) Section plane moves forward 30 mm (e) Section plane moves forward 40 mm

Figure 4.49 The section planes in the slab showing the state of deformation zone

Figure 4.49(a) shows the section plane which will move forward gradually to cut the slab in order to obtain a cross section shape of the deformation on the longitudinal crack. From 4.49(b), (c), (d) and (e), it can be seen that in the central area the crack will close during the rolling process. It can also be seen that the bottom of the longitudinal crack closes earlier than the top of the crack.

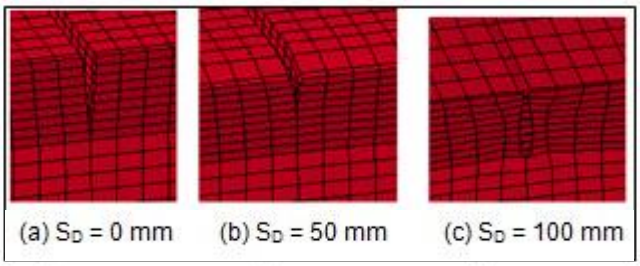

Figure 4.50 Longitudinal crack behaviour

From Figure 4.50, it can be seen that the longitudinal crack is slightly deformed when it enters the roll gap at S_D = 50 mm, and then the closure happens from the bottom towards the top as the rolling process continues. Therefore, it is necessary to examine the uniformity of the longitudinal crack evolution along the rolling direction.

Through the observation from Figure 4.50, it could be concluded that the crack closes well along the rolling direction. However, the crack near the top surface of the slab does not close as well as the inner part. This generates the fold layers on the slab surface, and may cause oxidation around the non-uniform distributed folded layers.

4.5.2 Rolling force

In order to find the possible influential parameters that may affect the rolling

process, different rolling conditions in terms of rolling speed, friction coefficient and the initial temperature of the slab (Table 4.1) were chosen for the proposed longitudinal model that has been given in Chapter 3.

Table 4.1 Rolling conditions of longitudinal crack

Rolling conditions			
Rrolling speed	1 (m/s)	2.7 (m/s)	3.5 (m/s)
Friction coefficient	0.3	0.2	04
Initial temperature of the slab	950 ℃	1050 ℃	1150 ℃

Figure 4.51 shows the rolling force under the condition of different roll diameters, thickness reductions and rolling speeds. It can be seen that the rolling force increases dramatically with the use of a larger roll diameter. The rolling forces for the roll diameters of 300 and 400 mm are about 3.4×10^5 and 4×10^5 N/m, respectively. It can be seen from Figure 4.51(b) that the rolling force increases with an increase of rolling reduction. The rolling forces for the reduction of 25 and 35 % are approximate 3.3×10^5 and 4.3×10^5 N/m, respectively. Compared with these two parameters (reduction and roll diameter), the rolling speed does not influence the rolling force significantly. Rolling force is about 3.4×10^5 N/m for both of the rolling speeds of 2.7 and 3.5 m/s.

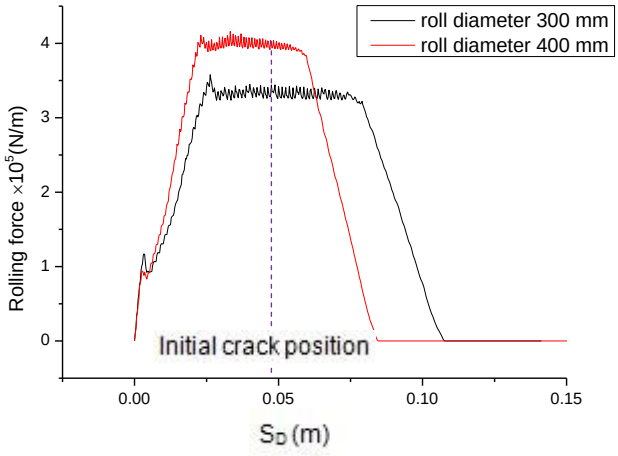

(a)

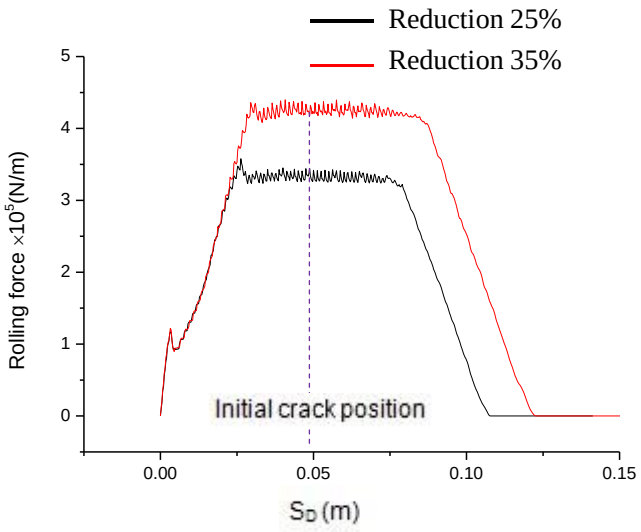

(b)

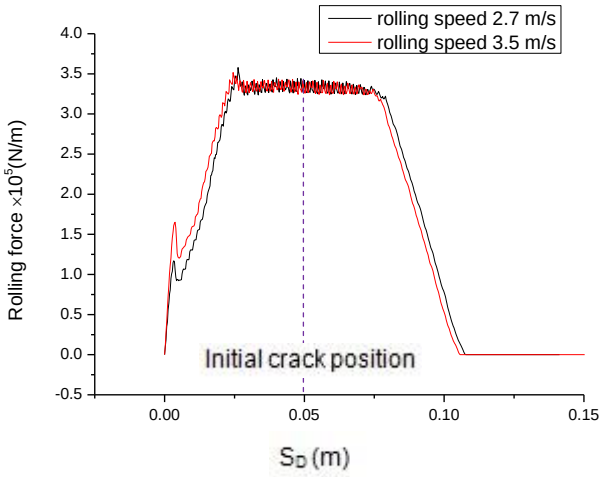

(c)

Figure 4.51 Rolling forces of the longitudinal crack

4.5.3 Effect of location on longitudinal crack behaviour

As discussed in Chapter 2, there is no research found about the effect of the location of longitudinal cracks on the crack behaviour. Therefore, in this section, different distances from the symmetrical plane of the strip have been simulated.

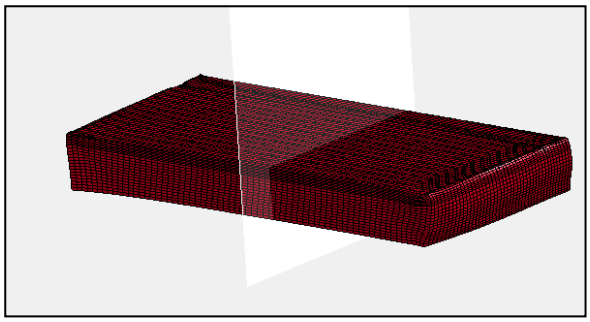

(a) Initial position of section plane

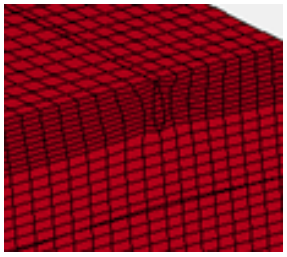

(b) Section plane moves forward 10 mm

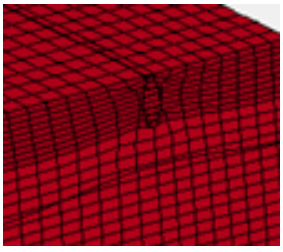

(c) Section plane moves forward 30 mm

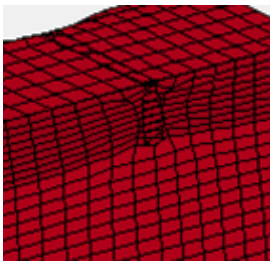

(d) Section plane moves forward 40 mm

Figure 4.52 Longitudinal crack evolution (d = 10 mm)

Figure 4.52 shows the behaviour of longitudinal crack for various section planes along the rolling direction. It can be seen that the crack closes when the distance to the slab symmetrical plane decreases from 30 to 10 mm. By comparing Figure 4.52 with Figure 4.50, it can be seen that the crack has more deformation for the distance value of 10 mm.

It can be concluded that it is more preferable for the longitudinal crack to be located near the symmetrical centre. This is in the position near the centre there is more pressure on the two contact surfaces, which makes them close much better than at 30 mm.

4.5.4 Von Mises stress distribution

The von Mises stress distribution is shown in Figure 4.53 at different times during the hot rolling process. The maximum von Mises stress is about 137 MPa. It can be seen that when the contact between the slab and the work roll occurs, the deformation in this region will suddenly increase the strain rate. According to the constitutive equation, the effective stress will consequently rise.

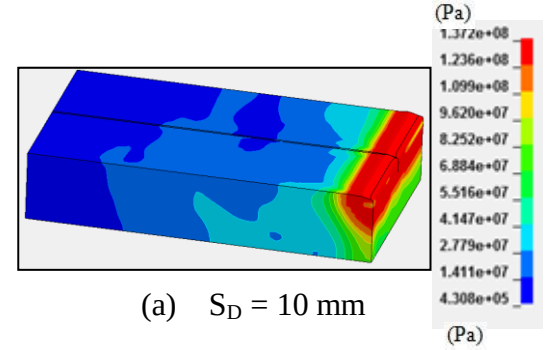

(a) S_D = 10 mm

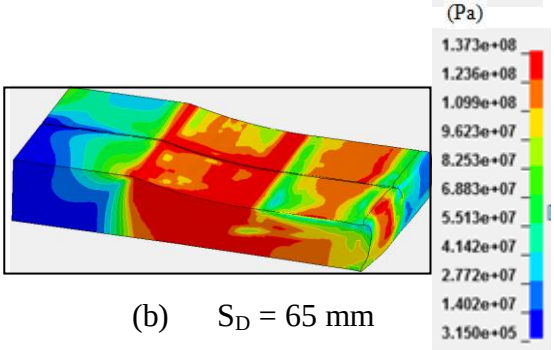

(b) S_D = 65 mm

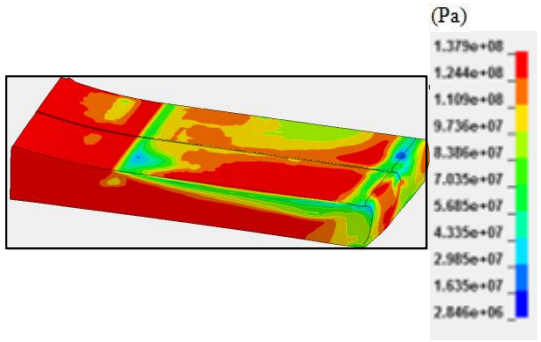

(c) S_D = 80 mm

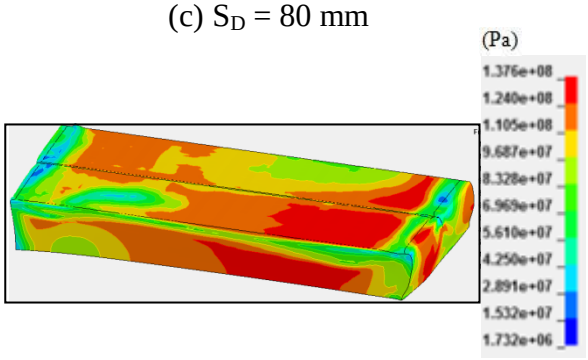

(d) S_D = 100 mm

Figure 4.53 Distributions of von Mises stress (Pa)

4.5.5 Plastic strain distribution

It can be seen from Figure 4.54 that the largest plastic strain takes place at the crack edge regions. The plastic strains for the crack edge areas range from 0.6 to 0.9, which indicates that the largest deformation happens in these areas. This can be explained by the evolution of the longitudinal crack. The crack along the rolling direction will be gradually closed with the slab entering into the contact region.

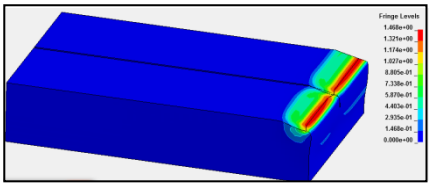

(a) S_D = 10 mm

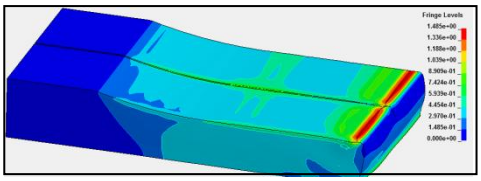

(b) S_D = 65 mm

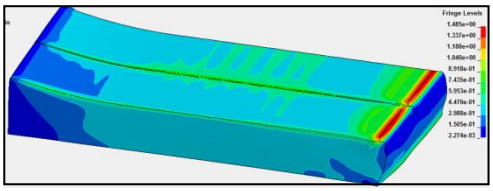

(c) S_D = 85 mm

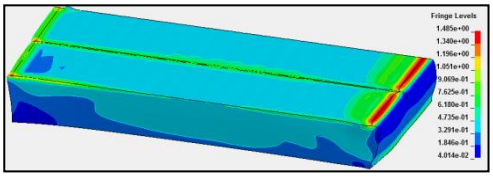

(d) S_D = 100 mm

Figure 4.54 Distributions of plastic strains

4.5.6 Pressure distribution

From Figure 4.55, it can be seen that when the slab enters into the contact region, it experiences pressure, and when the slab is rolled out of that region it experiences tension. The maximum pressure for the deformation zone is about 330 MPa. The tension is about 80 MPa. It can therefore be concluded that the pressure plays a more dominant roll through the whole process than tension.

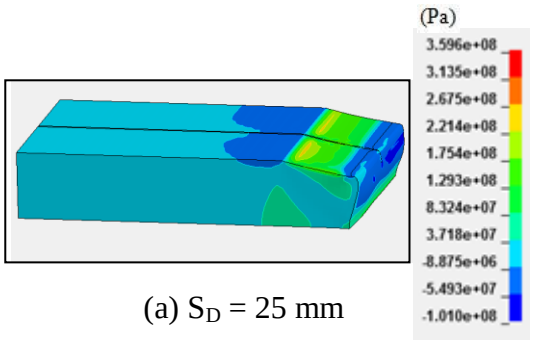

(a) S_D = 25 mm

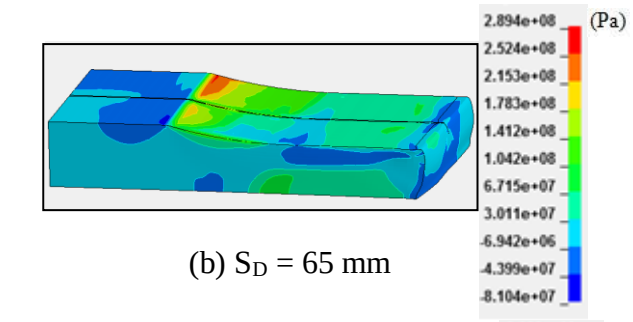

(b) S_D = 65 mm

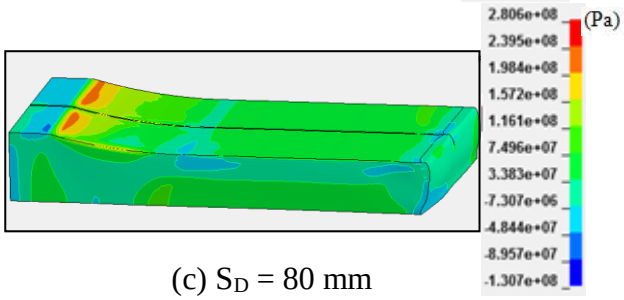

(c) S_D = 80 mm

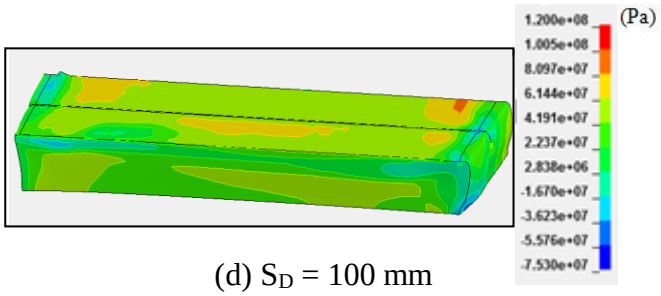

(d) S_D = 100 mm

Figure 4.55 Pressure distributions of the longitudinal crack (Pa)

4.5.7 Distributions of temperature

From the temperature distributions shown in Figure 4.56, it can be seen that the temperature will gradually drop from the initial 1050 to 1041 ℃ in the period of 0.1425 s. The heat loss though heat transfer at the contact interface is a large part by comparing heat convection and radiation. The detailed information about this will be discussed in the later section.

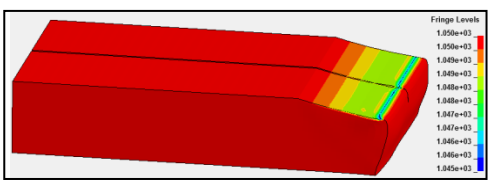

(a) t = 0.015 s

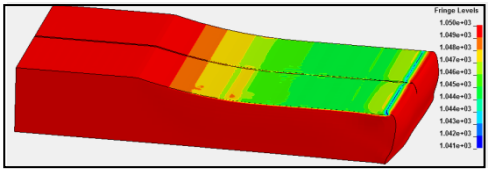

(b) t = 0.04875 s

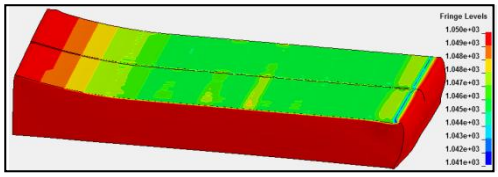

(c) t = 0.0755 s

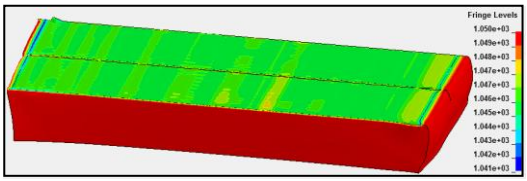

(d) t = 0.14125 s

Figure 4.56 Temperature distributions of the longitudinal crack (℃)

Figure 4.57 shows the temperature distribution around the crack. Figures 4.57(a), (b), (c), (d) and (e) show how the temperature range changes with the evolution of the shape of the crack. For the bottom contact region which has gained much more heat from the inner part of the slab, the temperature is much higher than on the outer surface area. By contrast, the outer crack region experiences more heat loss and, therefore, the temperature is lower than that in the inner region.

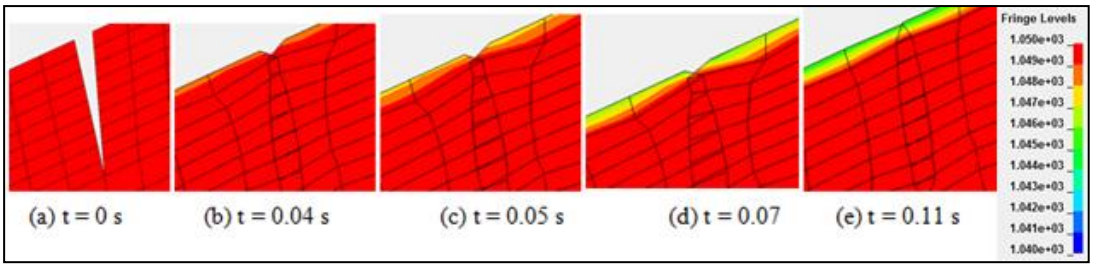

Figure 4.57 Cross-section temperature distributions of longitudinal crack (℃)

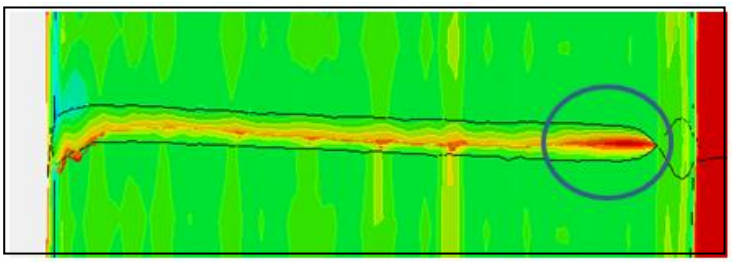

Figure 4.58 Temperature distributions along the longitudinal crack shape

It is clear from Figure 4.58 that the central region of a longitudinal crack is hotter than the edges of the crack. The temperature distribution is generally uniform along the rolling direction. It should be noted that the region which has been circled experiences more heat than the other parts. This is because the time for the circled area being rolled out of the contact region is more than that of the newly rolled part. This indicates there is more time for it to gain the heat again from the inner slab centre through the material conductivity mechanism.

4.5.8 Effect of convection and radiation through the environment

In this section, the convection and radiation to the environment will be discussed. From Chapter 2, we know that most of the researchers have neglected these aspects and only take into account the heat transfer when carrying out thermo-mechanical coupled FEM analysis. Consequently, detailed information about the effects of

convection and radiation has not been obtained. Therefore, it is necessary to implement models to investigate the relative information about this topic.

Figure 4.59 shows the temperature distributions around the strip corner. The reason for choosing this area is that the corner experiences much more time of the getting contact with the ambient air than the other regions. It is clear that the corner temperatures drop significantly with time due to the convection and radiation.

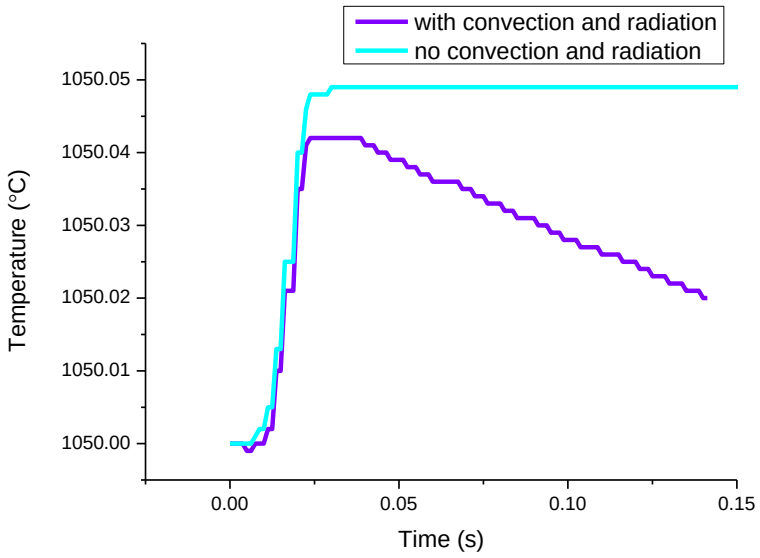

Figure 4.59 Effects of convection and radiation on slab corner

In contrast, the corner with no convection and radiation keeps the same level over time. Although the difference is only 0.05 ℃, it cannot be neglected as the time is so short for this simulation. In the real manufacturing, this effect is an important issue. The oxidation is easily caused, and it will affect the product quality.

4.5.9 Effect of contact heat transfer

Figure 4.60 shows the contact heat transfer at the top surface at the symmetrical plane with different contact heat transfer coefficients. It can be seen that the contact heat has a large influence on the final temperature. The difference of temperature for the two given parameters is about 40 ℃. Therefore, it should be carefully

considered about the contact condition for manufacturing industry to obtain a proper heat transfer conditions to ensure the product quality.

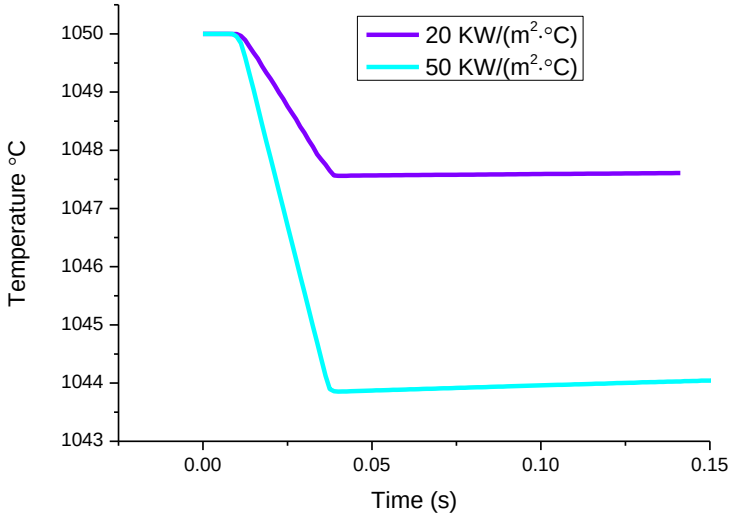

Figure 4.60 Effect of contact heat transfer

4.5.10 Effect of deformation heat

In order to determine the magnitude of heat generated from deformation, Figure 4.61 has been used to show its effect. The model only considers the effect of deformation on temperature. The model proposed here only takes into account the heat converted from the plastic deformation. It can be seen that the initial temperature of 1050 ℃ increases to 1050.49 ℃ for a given period of time.

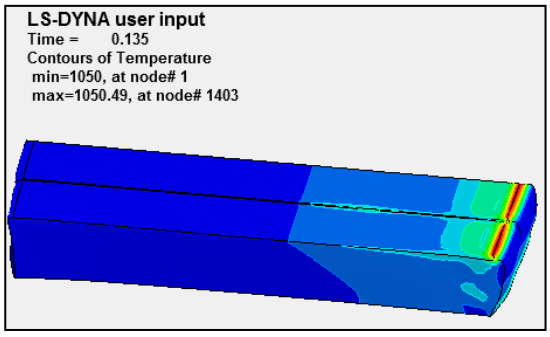

Figure 4.61 Heat generated from deformation

4.5.11 Heat loss by convection and radiation

The model proposed only considers convection and radiation in order to find their influence. Figure 4.62 shows the line contours of temperature. It was found that the initial temperature of 1050 ℃ dropped to 1049.73 ℃ under the conditions of convection and radiation.

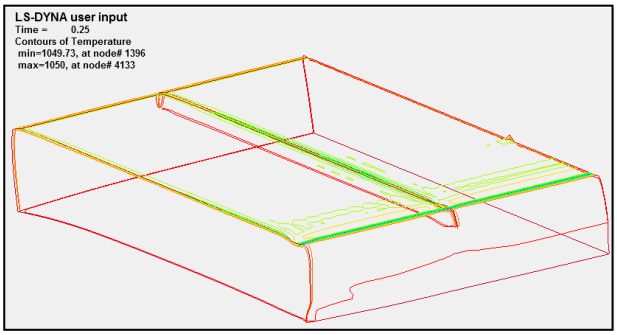

Figure 4.62 Line contours of temperature

Chapter 5

Conclusions and Recommendations

5.1 Conclusions

Through the simulations of the hot rolling of stainless steel 304 using the commercial FEM program ANSYS/LS-DYNA, an analysis of surface crack evolution has been conducted. It was found that edge cracks were propagated and that they were hard to heal after hot rolling. For transverse and longitudinal cracks they are indicated that these defects may heal after rolling operations. For longitudinal cracks, their location is important for the healing process. When they are near the slab centre, it is much easier for them to be self-healed.

It is found from this study that transverse cracks will influence rolling force to some extent. When the work roll experiences the crack region, the rolling force drops a little, and then the rolling force increases to resume its steady state. The stress and the folded layers may be found at the longitudinal cracks. For transverse cracks, the crack width is less when the cracks are located in the symmetrical area than when they are on the outer surface areas.

The mesh density and element type have an influence on the final crack evolution. When an element with ten nodes is used, a more accurate simulation result can be obtained than when an element with eight nodes is used. The simulation results from both elements have a good agreement with each other. However, it is evident that when using the ten-node elements, the computational time increases dramatically.

By introducing thermal parameters, the temperature fields during the hot rolling of stainless steel were obtained. The relative influences of effective stress, plastic strain, pressure and maximum shear stress are also discussed. The distributions of large plastic strain indicate the possibility of the large deformation. Before the strip enters the plastic deformation zone, the pressure occurs which normally means the compressive stress is dominant at this state. After the slab is rolled out of the deformation zone, the main influential factor is the tensile stress. This may cause further crack propagation and have a great influence on the surface quality of the final product.

By investigating thermal effects, it has been found that the heat transfer at the interface plays an important role in determining the strip temperature distribution. The effects of convection and radiation through the ambient air are not as significant as those of interface heat transfer. However, the effects of convection and radiation become large when the strip is exposed to air for a relatively long period of time. The heat generated from the plastic deformation is also an influential factor that increases the temperature at the deformation zone.

5.2 Recommendations

The results obtained from the finite element method can serve not only as a guide to predict crack propagation, but also to clarify the plastic deformation and heat transfer behaviour of hot rolling of stainless steels. The results provide an instructive basis for further investigation of this topic which can be focused on the evolution of microstructures.

In order to obtain more accurate data on surface defects during the hot rolling process, oxidation should be introduced as well as the lubrication and some other factors such as grinding methods which may be used in practical industrial productions.

The coupled thermo-mechanical investigations should also be carried out by employing new numerical models to find out a more suitable method to obtain the accurate results, and to minimise the computational time.

Investigations should also be implemented to understand the microstructures of the material used in the simulation.

More materials should be used in experiments to analyse more simulation parameters. As the database of materials is so limited it is sometimes difficult to compare the properties of certain kinds of materials.

References

[1] A.R. Shahani, S. Setayeshi, S.A. Nodamaie, M.A. Asadi and S. Rezaie, *Prediction of influence parameters on the hot rolling process using finite element method and neural network*, Journal of Materials Processing Technology, Vol. 209 (2009), 1920-1935

[2] J.K. Brimacombe, *The challenge of quality in continuous casting processes*, Metallurgical and Materials Transactions, Vol. 30B (1999), 553-566

[3] J. Zimmerman, W. Wlosinski and Z.R. Lindemann, *Thermo-mechanical and diffusion modeling in the process of ceramic-metal friction welding*, Journal of Materials Processing Thecnology, Vol. 209 (2009), 1644-1653

[4] E. Ubici, *Identification and counter measures to resolve hot strip mill chatter*, Steel Technology, Vol. 5 (2001), 3

[5] J.L. Sun, Y. Peng, H.M. Liu and G.B. Jiang, *Vibration of moving strip with distributed stress in rolling process*, Journal of Iron and Steel Research, International, Vol. 17(2010), 24-30

[6] X. Yang, C.N. Tong, G.F. Yue and J.J. Meng, *Coupling dynamic model of chatter for cold rolling*, Journal of Iron and Steel Research, International, Vol. 17 (2010), 30-34

[7] M.A. Younes, M. Shahtout and M.N. Damir, *A parameters design approach to improve product quality and equipment performance in hot rolling*, Journal of Materials Processing Technology, Vol. 171 (2006), 83-92

[8] G.G. Lee, B.G. Thomas, S.H. Kim, H.J. Shim, S.K. Baek, C.H. Choi, D.S. Kim and S.J. Yu, *Microstructure near corners of continuous-cast steel slabs showing three-dimensional frozen meniscus and hooks*, Acta Materialia, Vol. 55 (2007), 6705-6712

[9] A.K. Bhattacharya, S. Debjani, A. Roychowdhury and J. Das, *Optimization of continuous casting mould oscillation parameters in steel manufacturing*

process using genetic algorithms, IEEE Congress on Evolutionary Computation, (2007), 3998-4004

[10] J. Sengupta, H.J. Shin and B.G. Kim, *Micrograph evidence of meniscus solidification and sub-surface microstructure evolution in continuous-cast ultra-low carbon steels*, Acta Materialia, Vol. 54 (2006), 1165-1173

[11] E. Ervasti, U. Stahlberg, *Behavior of longitudinal surface cracks in the hot rolling of steel slabs*, Journal of Materials Processing Technology, Vol. 94 (1999), 141-150

[12] R. Misicko, T. Kvackaj, M. Vlado, L. Gulova, M. Luptak and J. Bidulska, *Defects simulation of rolling strip*, Materials Engineering, Vol. 16 (2009), 7-12

[13] P. Zahumensky, M.J. Merwin, I. Kohutek, *Evolution of artificial defects from slab to rolled products*, Acta Metallurgica Slovaca, Vol. 11 (2005), 189-196

[14] F. Novy, M. Cincala, P. Kopas and O. Bokuvka, *Mechanisms of high-strength structural materials fatigue failure in ultra-wide life region*, Material Science Engineering, Vol. 462A (2007), 189-192

[15] A. Kainz, S. Llie, E. Parteder and K. Zeman, *From slab corner cracks to edge-defects in hot rolled strip – experimental and numerical investigations*, Steel Research Int, Vol. 79 (2008), 861-867

[16] E. Ervasti and U. Stahlberg, *Transversal cracks and their behavior in the hot rolling of steel slabs*, Journal of Materials Processing Technology, Vol. 101 (2000), 312-321

[17] Y. Maehara, K. Yasumoto, H. Tomono, T. Nagamichi and Y. Ohmori, *Surface cracking mechanism of continuously cast low carbon low alloy steel slabs*, Material Science Technology, Vol. 6 (1990) 793-806

[18] H. Shibata, Y. Arai, M. Suzuki and T. Emi, Metall. Trans, Vol. 31B (2000), 981-991

[19] M. Herrera-Trejo, J.J. Ruiz, M.C. Roman and H. Solis, *Star cracks in continuously cast peritectic steel slabs*, Ironmaking and Steelmaking, Vol. 37 (2010), 452-457

[20] T. Kajitani, M. Wakoh, N. Tokumitsu, S. Ogibayashi and S. Mizoguchi, *Influence of temperature and strain of surface crack due to residual copper in carbon steel*, Process Steelmaking Conference, Vol. 79 (1996), 621-626

[21] P.K. Tripathy, S. Das, M.K. Jha, J.B. Singh, A.M. Kumar and A.K. Das, *Migration of slab defects during hot rolling*, Ironmaking and Steelmaking, Vol. 33 (2006), 477-483

[22] S. Das, PhD Dissertation, The effect of boundary conditions and material data representation on the simulation of deformation during hot rolling, The University of Sheffield, Sheffield, UK, 2002

[23] R. Balcombe, M.T. Fowell, A.V. Olver, S. Ioannides and D. Dini, *A coupled approach for rolling contact fatigue cracks in the hydrodynamic lubrication regime: The importance of fluid/solid interactions*, Wear, Vol. 271 (2011), 720-733

[24] M. Sraml, J. Flasker and I. Potrc, *Numerical procedure for predicting the rolling contact fatigue crack initiation*, International Journal of Fatigue, Vol. 25 (2003), 585-595

[25] K. Ogura and Y. Miyoshi, *Threshold behavior of small fatigue crack at notch root in type 304 stainless steel*, Engineering Fracture Mechanics, Vol. 25 (1986), 31-46

[26] T. Goshima, *Thermomechanical effects on crack propagation in rolling contact fatigue failure*, Journal of Thermal Stresses, Vol. 26 (2003), 615-639

[27] W.R. Tyfour and J.H. Beynon, *The effect of rolling direction reversal on fatigue crack morphology and propagation*, Tribology International, Vol. 27 (1994), 273-282

[28] S. Bogdanski and M. Trajer, *A dimensionless multi-size finite element model of a rolling contact fatigue crack*, Wear, Vol. 258 (2005), 1265-1272

[29] J.B. Delbos, G. Kermouche, J. Rech, H. Hamdi and H. Zahouani, *Numerical modeling of fatigue crack's initiation in rolling cotact of stainless steels*, Journal of Materials Processing Technology, Vol. 164-165 (2005), 1185-1191

[30] H. Suzuki, S. Nishimura, J. Imamura and Y. Nakamura, Testsu-to-hagane, Vol. 67 (1981), 1180

[31] Y. Maehara, K. Yasumoto and Y. Ohmoni, High Temp. Tech. Vol. 4 (1986), 13

[32] B. Hwang, H.S. Lee, G.K. Yang and S. Lee, *Analysis and prevention of side cracking phenomenon occurring during hot rolling of thick low-carbon steel plates*, Material Science and Engineering, Vol. A 402 (2005), 177-187

[33] S. Castagne, PhD Thesis, Finite element mesoscopic analysis of damage in microalloyed continuous casting steels at high temperature, University of New South Wales, 2007

[34] H.B. Xie, PhD Thesis, The research on the edge crack of cold rolled thin strip, University of Wollongong, 2011

[35] C.C. Tasan, J.P.M. Hoefnagels, T. Hornchlj, *Experimental analysis of strain path dependent ductile damage mechanics and forming limits*, Mechanics of Materials, Vol. 41:11 (2009), 1264-1276

[36] C. Sommitsch, P. Polt, F. Ruf and S. Mitsche, *On the modeling of the interaction of materials softening and ductile damage during hot working of alloy 80A*, Journal of Materials Processing Technology, Vol. 177:1-3 (2006), 282-286

[37] N. Hfaiedh, K. Saanouni, M. Francois and A. Roos, *Self-consistent intragranular ductile damage modeling in large plasticity for FCC polycrystalline materials*, Procedia Engineering, Vol. 1:1 (2009), 229-232

[38] D.F. Zhang, Q.W. Dai, L. Fang and X.X. Xu, *Prediction of edge cracks and plastic-damage analysis of Mg alloy sheet in rolling*, Transactions of Nonferrous Metals Society of China, Vol. 21 (2011), 1112-1117

[39] M. Kiuchi, S.H. Hsiang, Plast Work, Vol. 22 (1981), 927-934

[40] S.A. Rajak, N.V. Reddy and J. Mater, Process Thchnol, Vol. 159 (2005), 409-417

[41] W. Deng, D.W. Zhao, X.M. Qin, L.X. Du, X.H. Gao and G.D. Wang, *Simulation of central crack closing behavior during ultra-heavy plate rolling*, Computational Materials Science, Vol. 47 (2009), 439-447

[42] D.W. Zhao, L.X. Du, X.H. Liu and G.D. Wang, Analysis of closing or developing a central burst during slab hot rolling, Iron Steel Press

[43] J.A. Eckel, P.C. Glaws and J.O. Wolfe, *Advances in the production and use of steel with improved internal cleanliness*, West Conshohocken, USA, American Society for Testing and Materials, 1999, 1-11

[44] T.B. Lund, K.P. Olund and J.K. Mahaney, *Advances in the production and use of steel with improved internal cleanliness*, West Conshohocken, USA, American Society for Testing and Materials, 1999, 32-48

[45] E. Fuchs and P. Jonsson, *High temperature materials and processes*, Vol. 19:5 (2000), 333-343

[46] C. Luo and U. Stahlberg, *Deformation of inclusions during hot rolling of steels*, Journal of Materials Processing Technology, Vol. 114 (2001), 87-97

[47] E. Ervasti and U. Stahlberg, *Void initiation close to a maco-inclusion during single pass reductions in the hot rolling of steel slabs: A numerical study*, Journal of Materials Processing Technology, Vol. 170 (2005), 142-150

[48] N. Kasai and M. Iguchi, *Fluid flow in continuous casting mold and behavior of non-metallic inclusions*, Iron and Steel Institute of Japan, 2002, 243-264

[49] L.F. Zhang, *Inclusion and bubble in steel – A review*, Journal of Iron and Steel Research International, Vol. 13:3 (2006), 1-8

[50] *Hot grinding saves time, energy, and slab surfaces*, Metal Producing Processing, Vol. 39:6 (2001), 22-23

[51] G.D. Quinn, L.K. Ives and S. Jahanmir, *On the nature of machining cracks in ground ceramics: Part II, Comparison to other silicon nitrides and damage maps*, Machine Science Technology, Vol. 9:2 (2005), 211-237

[52] T. Liu, A. Latella and L. Zhang, *Grinding of ceramics-strength, surface features and grinding conditions*, Key Engineering Matetial, Vol. 196 (2001), 53-60

[53] Y.S. Jung, Y. Gao, W. Nakao, K. Takahashi, K. Ando and S. Saito, *Crack-healing behavior and resultant high-temperature fatigue strength of machined Si3N4/SiC composite ceramic*, Fatigue Fracture Engineering, Vol. 31 (2008), 2-11

[54] Y.S. Jung, W. Nakao, K, Takahashi, K. Ando and S. Saito, *Crack healing of machining cracks introduced by wheel grinding and resultant high-temperature mechanical properties in a Si_3N_4/SiC Composite*, The American Ceramic Society, Vol. 92:1 (2009), 167-173

[55] S. Moir and J. Preston, *Surface defects-evolution and behaviour from cast slab to coated strip*, Journal of Materials Processing Technology, Vol. 125-126 (2002), 720-724

[56] H. Todoroki, T. Ishii, K. Mizuno and A. Hongo, *Effect of crystallization behaviour of mold flux on slab surface quality of a Ti-bearing Fe-Cr-Ni super alloy cast by means of continuous casting process*, Materials Science and Engineering, Vol. A 413-414 (2005), 121-128

[57] M. Zeze, A. Tanaka and R. Tsujino, *Formation mechanism of sliver-type surface defects with oxide scale on sheets and coils*, Testsu to Hagane, Vol. 87:2 (2001), 15-22

[58] S.W. Xiong, X.H. Liu, G.D. Wang and Q. Zhang, *A three-dimensional finite element simulation of the vertical-horizontal rolling process in the width*

reduction of slab, Journal of Materials Processing Technology, Vol. 101 (2000), 146-151

[59] F.L. Sui, L.Q. Chen, X.H. Liu and L.X. Xu, *Application of FEM to hot continuous rolling process for inconel 718 alloy round rod*, Journal of Iron and Steel Research International, Vol. 16:5 (2009), 43-49

[60] G.M. Zhang, H. Xiao and C.H. Wang, *Three-dimensional model for strip hot rolling*, Journal of Iron and Steel Research International, Vol. 13:1 (2006), 23-26

[61] L. Bouhala, A. Makradi, S. Belouettar, *Thermal and thermo-mechanical influence on crack propagation using an extended mesh free method*, Engineering Fracture Mechanics, Vol. 88 (2012), 35-48

[62] X. Duan and T. Sheppard, *Three dimensional thermal mechanical coupled simulation during hot rolling of aluminium alloy 3003*, International Journal of Mechanical Science, Vol. 44 (2002), 2155-2172

[63] S.M. Hwang, C.G. Sun, S.R. Ryoo and W.J. Kwak, *An integrated FE process model for precision analysis of thermo-mechanical behaviors of rolls and strip in hot strip rolling*, Computer Methods in Applied Mechanics and Engineering, Vol. 191 (2002), 4015-4033

[64] Z. Pater, J. Kazanecki and J. Bartnicki, *Three dimensional thermo-mechanical simulation of the tube forming process in Diescher's mill*, Journal of Materials Processing Technology, Vol.177 (2006), 167-170

[65] Z.C. Lin and T.G. Huang, *Hot rolling of an aluminium-copper sandwich flat strip with the three-dimensional finite element method*, Journal of Materials Processing Technology, Vol. 99 (2000), 154-168

[66] H. Yang, M. Wang, L.G. Guo and Z.C. Sun, *3D coupled thermo-mechanical FE modelling of blank size effects on the uniformity of strain and temperature distributions during hot rolling of titanium alloy large rings*, Computational Materials Science, Vol. 44 (2008), 611-621

[67] M. Bagheripoor and H. Bisadi, *Effects of rolling parameters on temperature distribution in the hot rolling of aluminium strips*, Applied Thermal Engineering, Vol. 31 (2011), 1556-1565

[68] P. Montmitonnet, *Hot and cold strip rolling processes*, Computer Methods in Applied Mechanics and Engineering, Vol. 195 (2006), 6604-6625

[69] P. Zahumensky and M. Merwin, *Evolution of artificial defects from slab to rolled products*, Journal of Material Processing Technology, Vol. 196 (2008), 266-278

[70] F.J. Belzunce, A. Ziadi and C. Rodriguez, *Structural integrity of hot strip mill rolling rolls*, Engineering Failure Analysis, Vol. 11 (2004), 789-797

[71] E. Mancini, M. Sasso, D, Amodio, R. Ferretti and F. Sanfilippo, *Surface defect generation and recovery in cold rolling of stainless steel strips*, Journal of Tribology, Vol. 133 (2011), 012202:1-012202:9

Appendix A Kinetic Energy

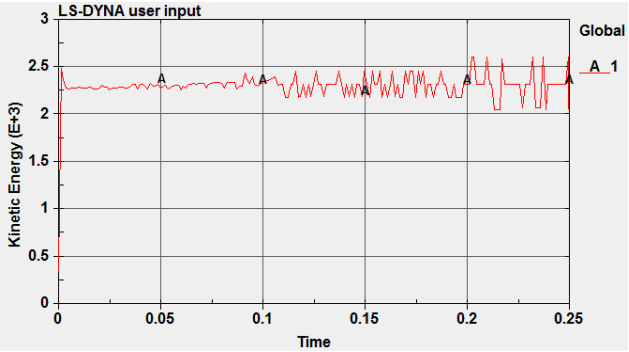

(Edge crack model 1)

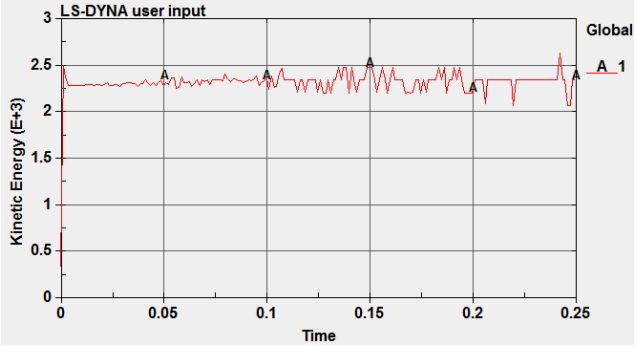

(Edge crack model 2)

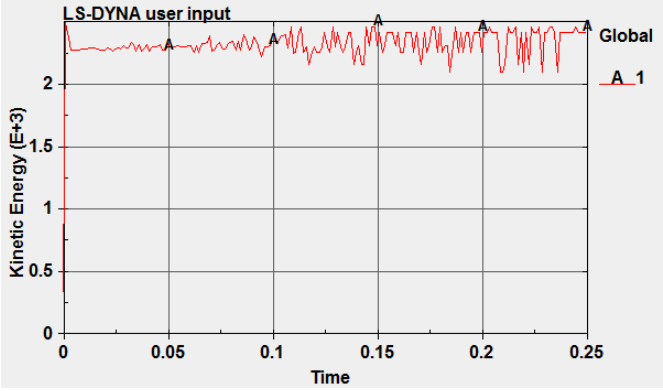

(Edge crack model 3)

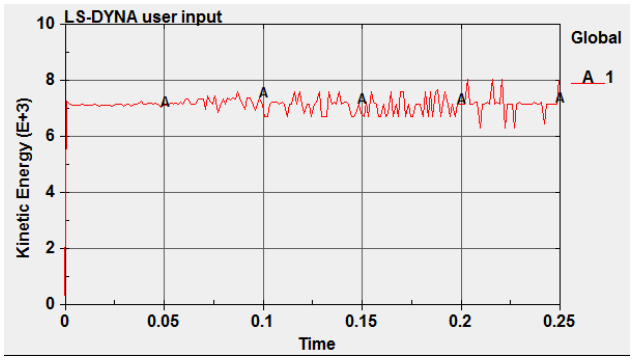

(Edge crack model 4)

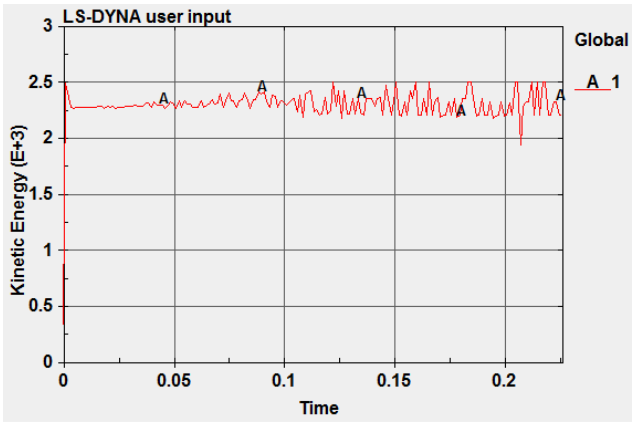

(

Edge crack model 5)

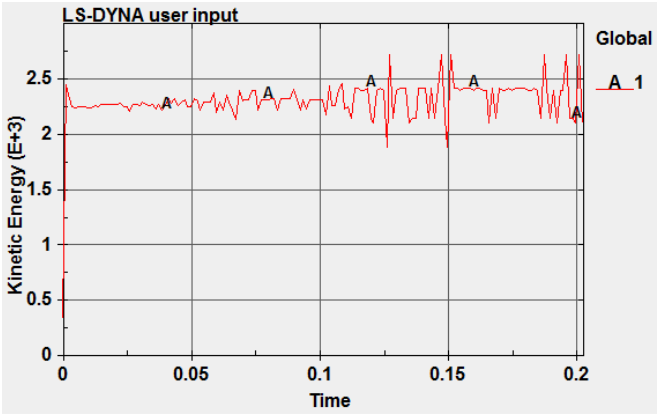

(V-shaped transverse crack model 1)

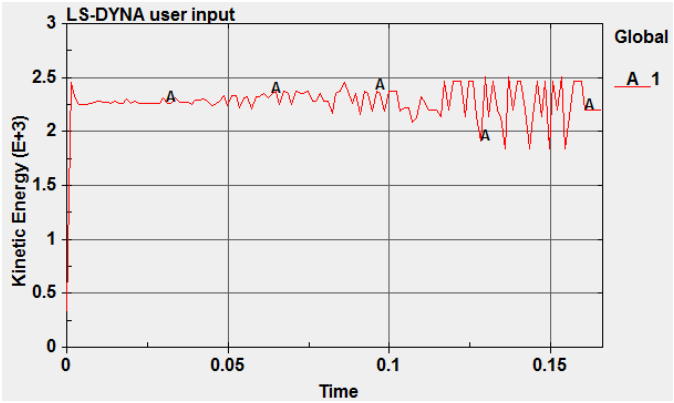

(V-shaped transvers crack model 2)

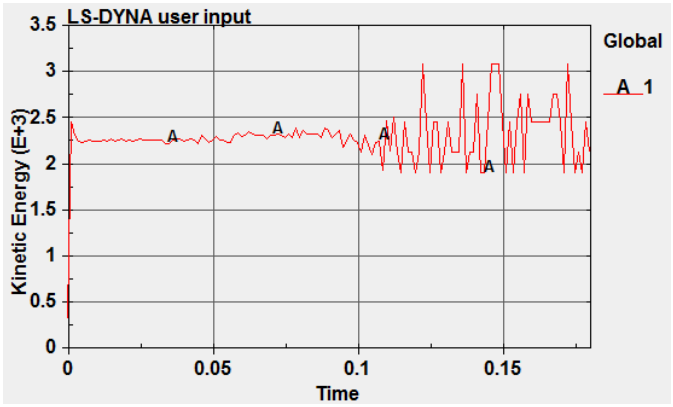

(V-shaped transverse crack model 3)

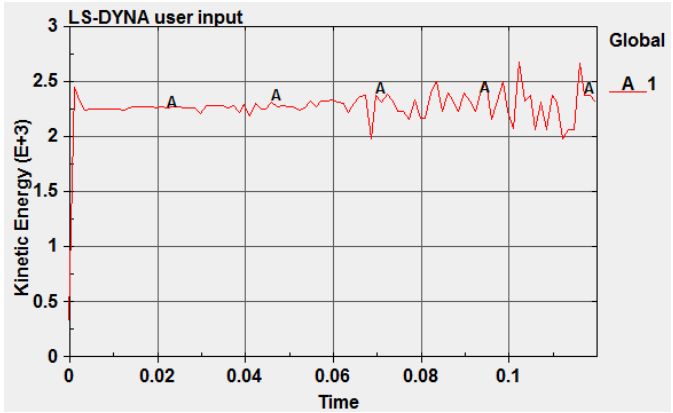

(V-shaped transverse crack model 4)

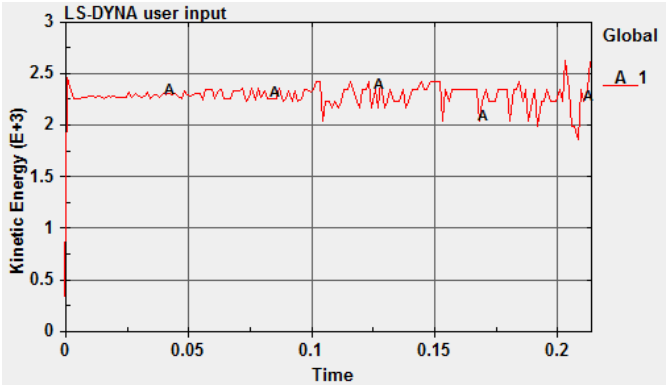

(V-shaped transverse crack 5)

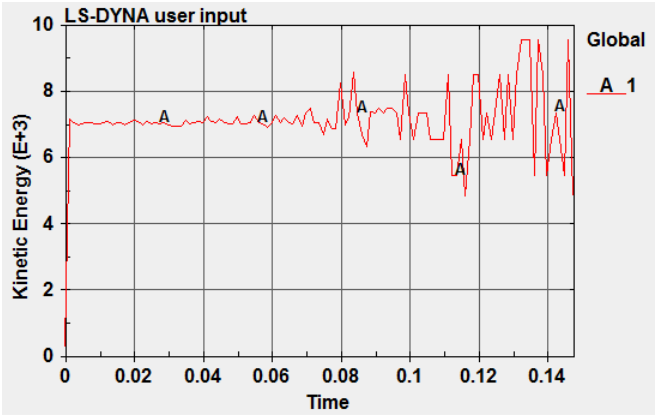

(V-shaped transverse crack model 6)

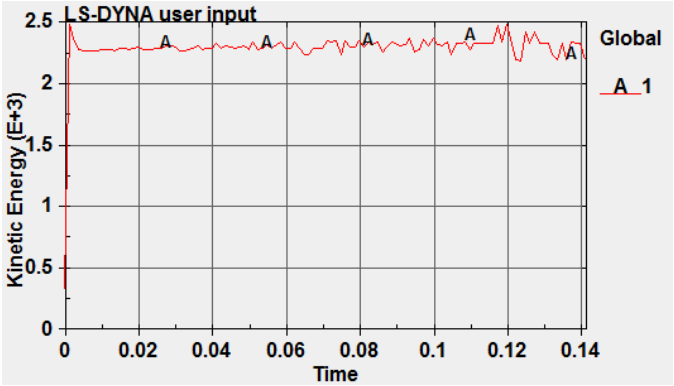

(Longitudinal crack model 1)

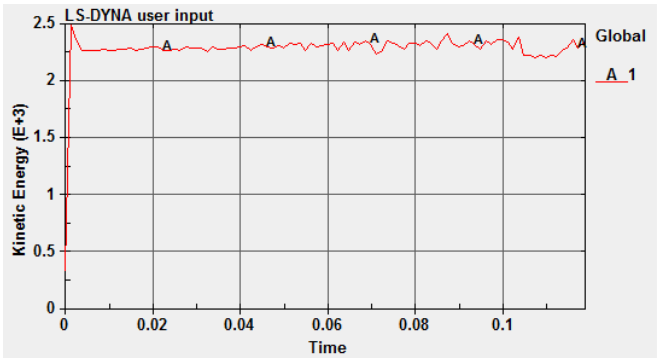

(Longitudinal crack model 2)

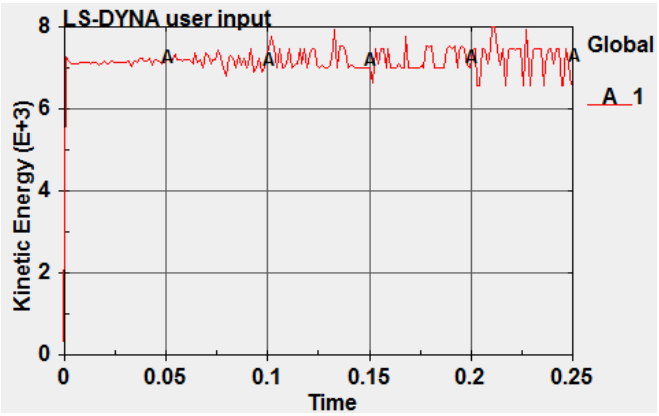

(Longitudinal crack model 3)

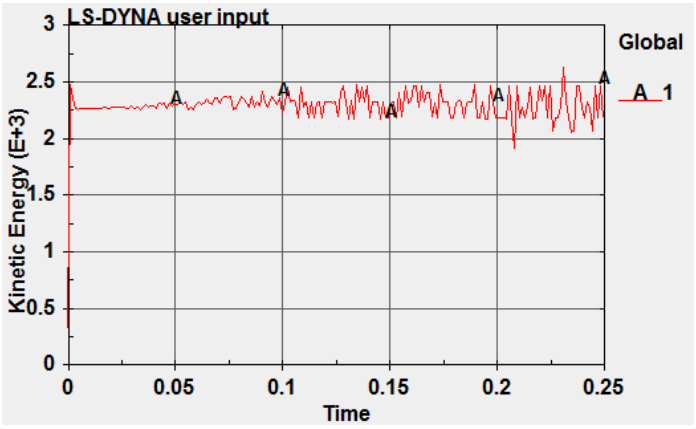

(Longitudinal crack model 4)

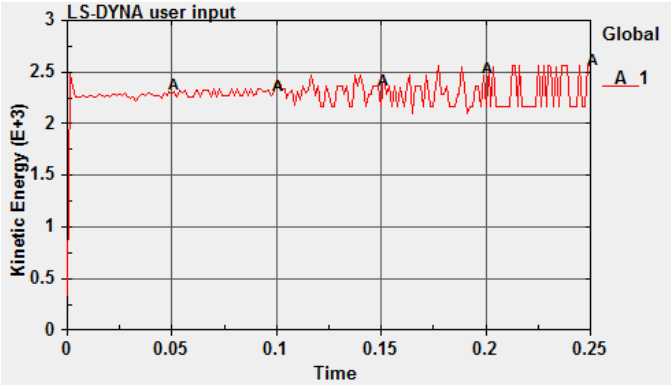

(Longitudinal crack model 5)

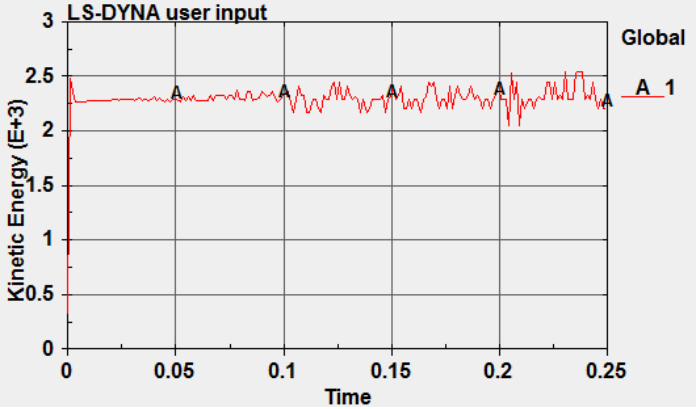

(Longitudinal crack model 6)

Appendix B Internal Energy

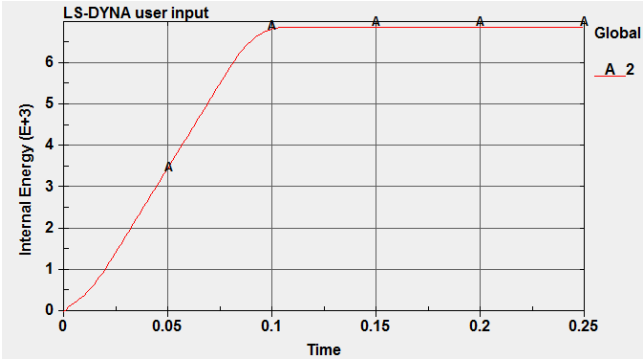

(Edge crack model 1)

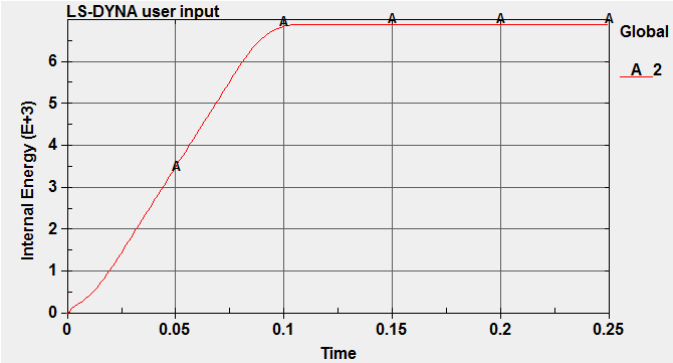

(Edge crack model 2)

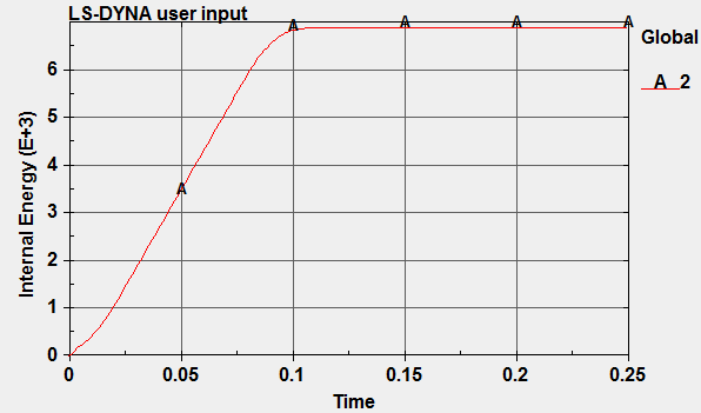

(Edge crack model 3)

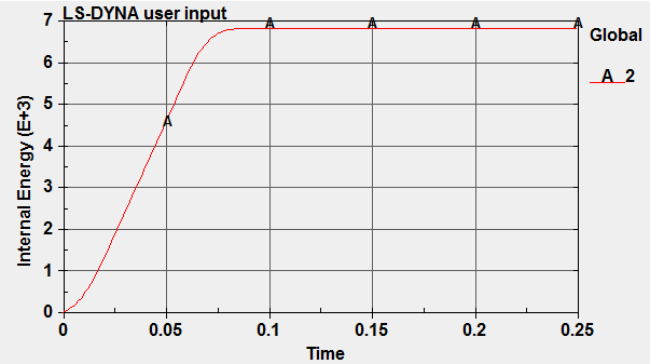

(Edge crack model 4)

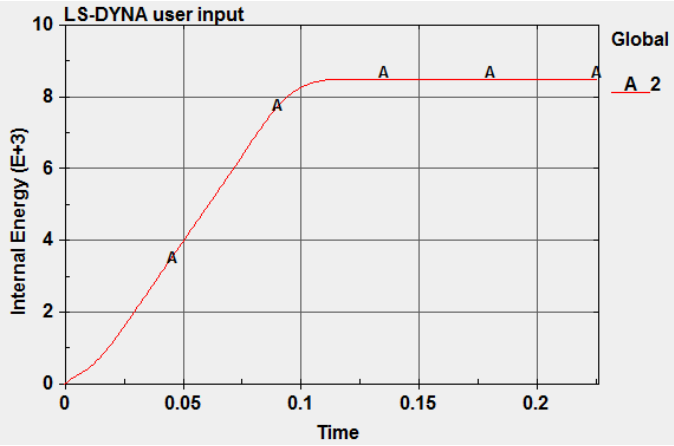

(Edge crack model 5)

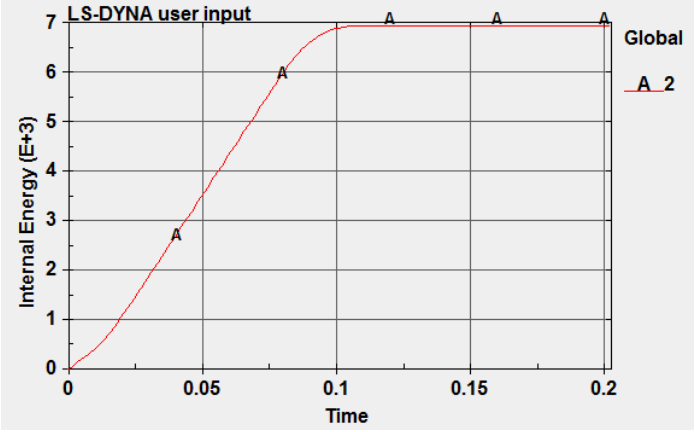

(V-shaped transverse crack model 1)

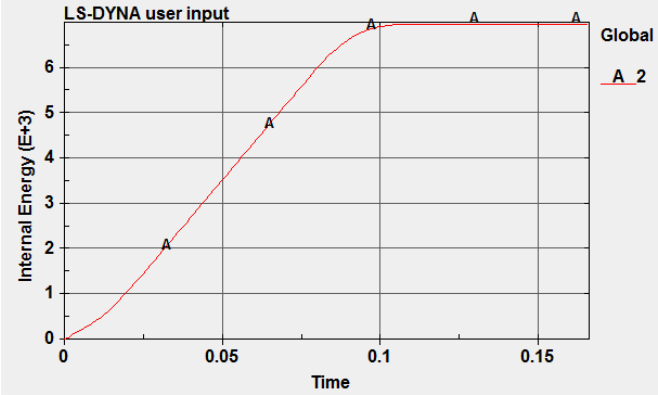

(V-shaped transverse crack model 2)

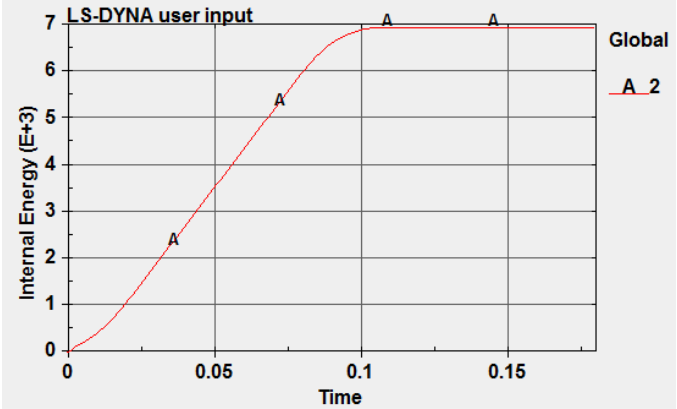

(V-shaped transverse crack model 3)

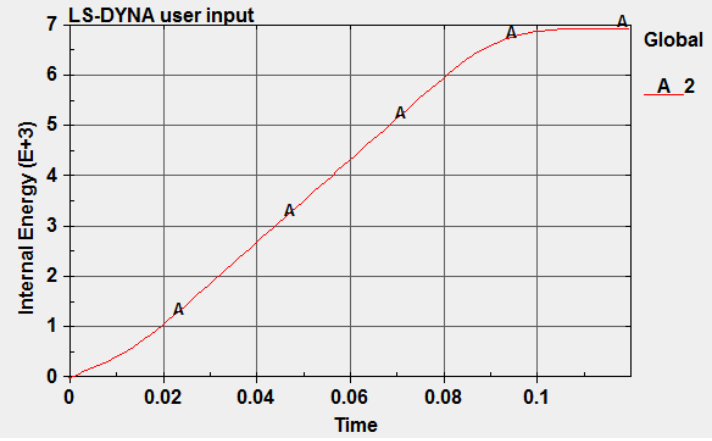

(V-shaped transverse crack model 4)

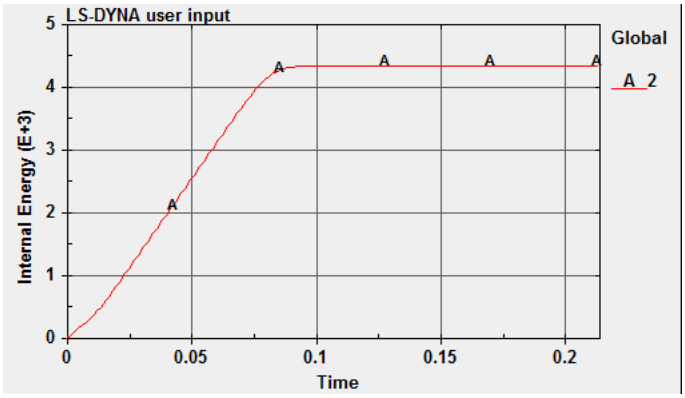

(V-shaped transverse crack model 5)

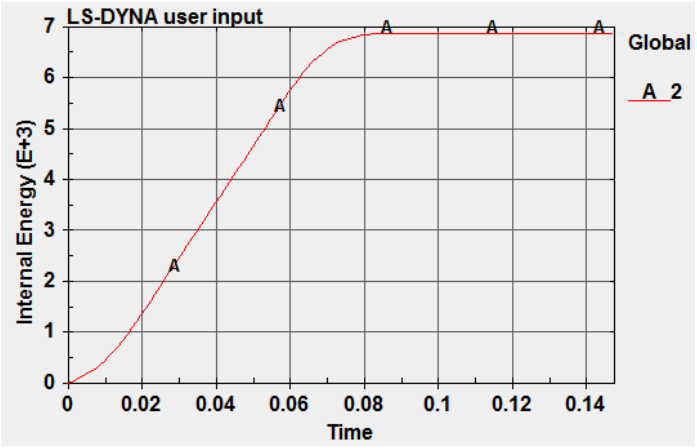

(V-shaped transverse crack model 6)

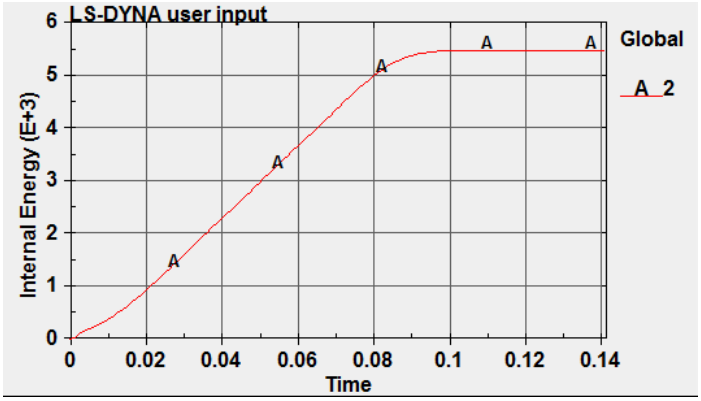

(Longitudinal crack model 1)

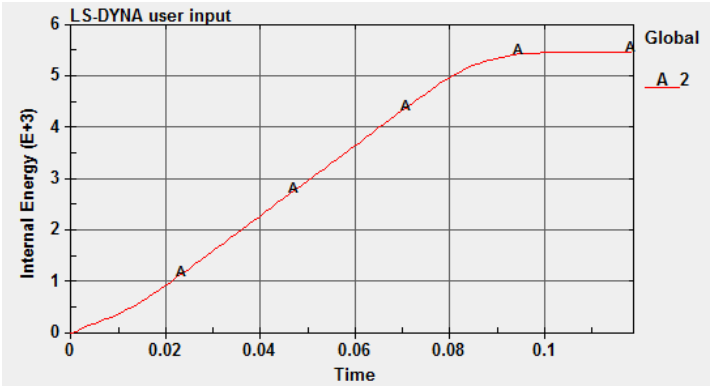

(Longitudinal crack model 2)

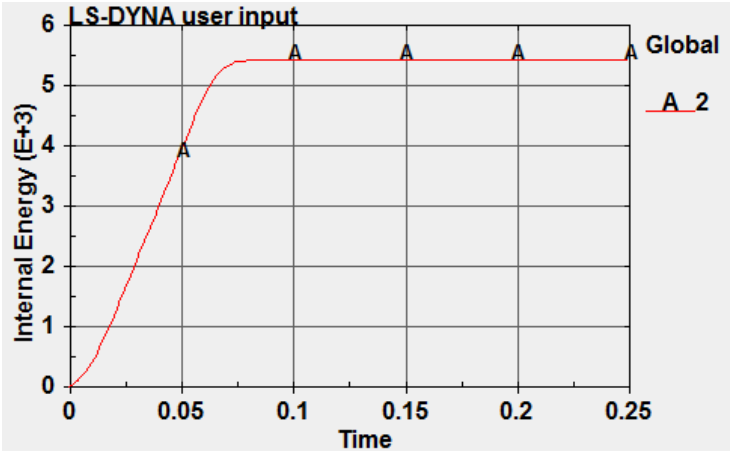

(Longitudinal crack model 3)

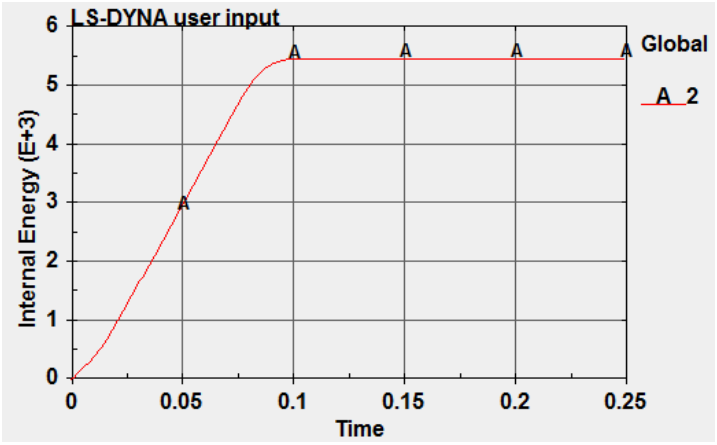

(Longitudinal crack model 4)

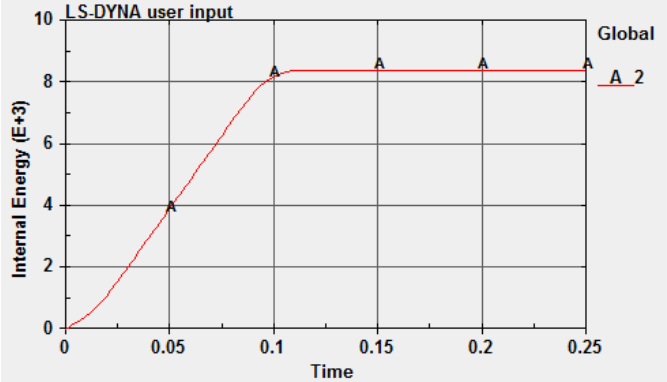

(Longitudinal crack model 5)

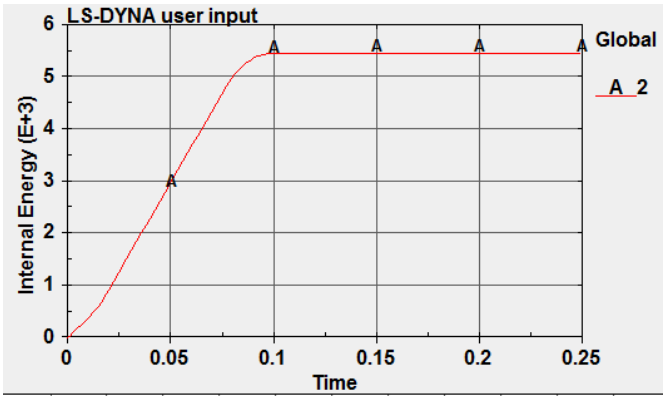

(Longitudinal crack model 6)

Appendix C Comparisons of Crack Behaviours

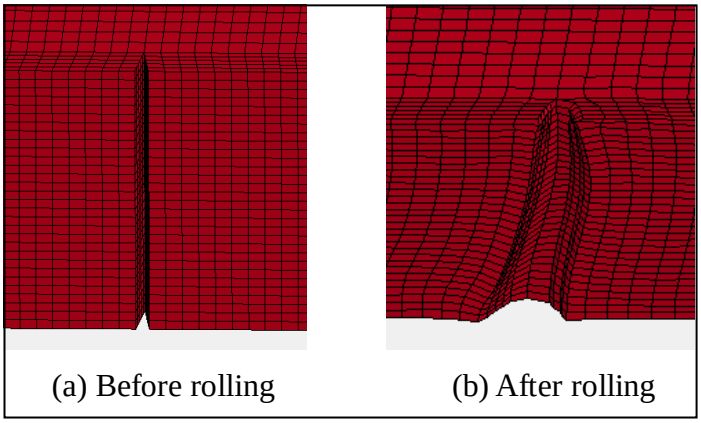

(Edge crack model 1)

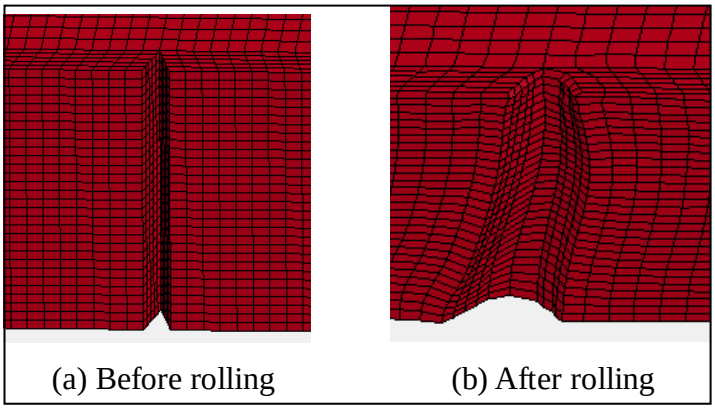

(Edge crack model 2)

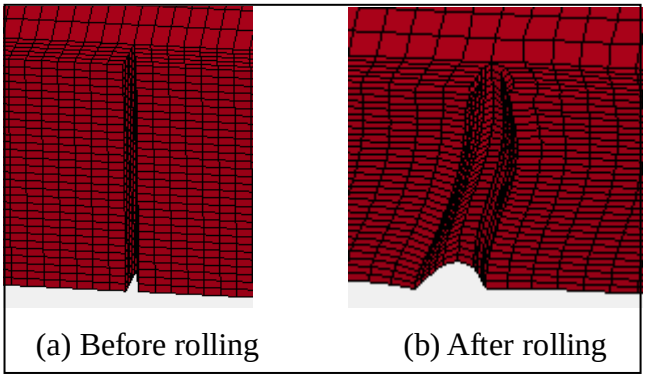

(Edge crack model 3)

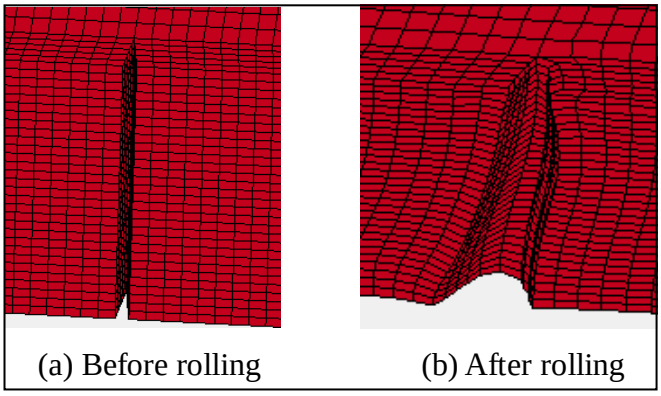

(Edge crack model 4)

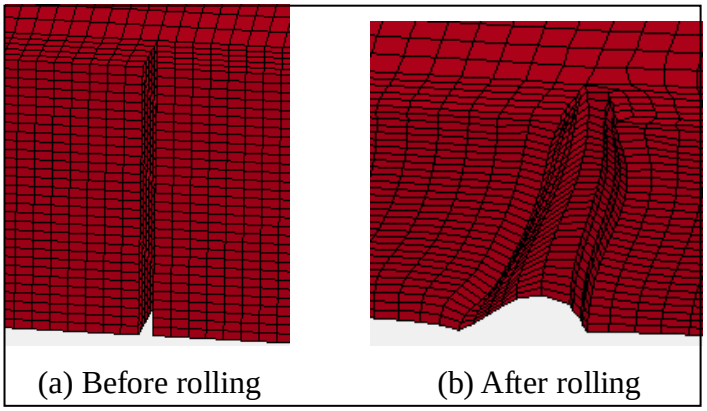

(Edge crack model 5)

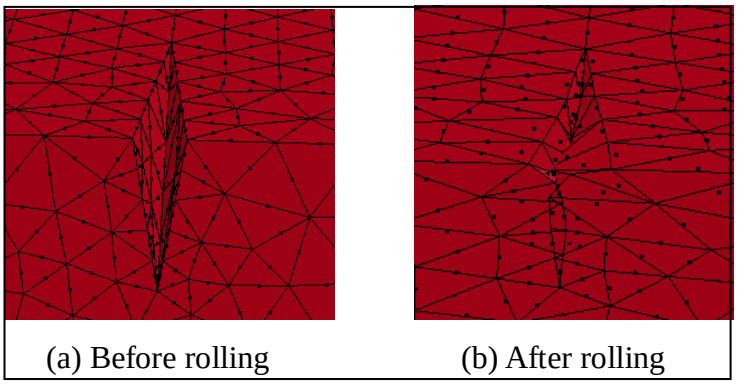

(V-shaped transverse crack model 1)

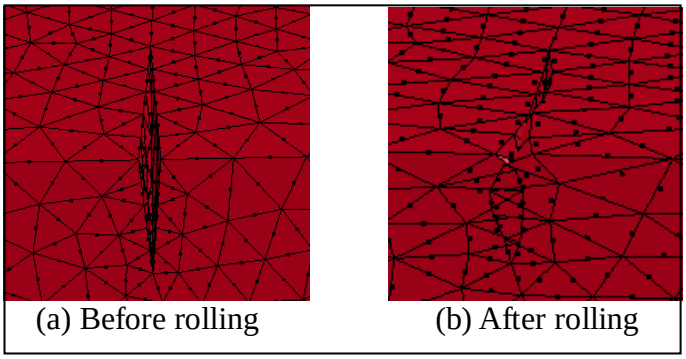

(V-shaped transverse crack model 2)

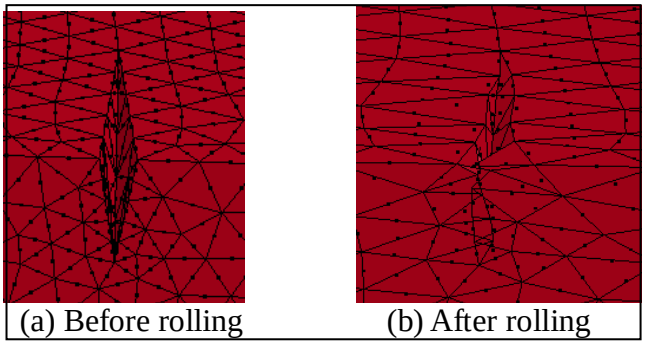

(V-shaped transverse crack model 3)

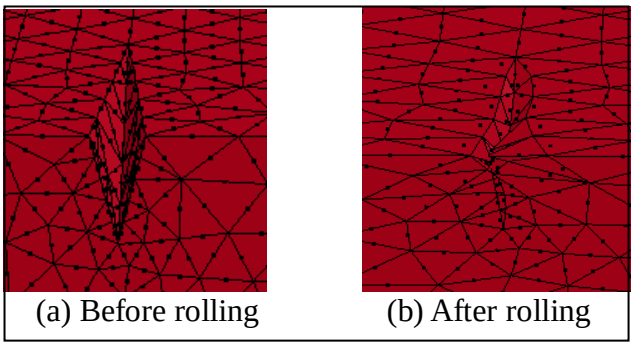

(V-shaped transverse crack model 4)

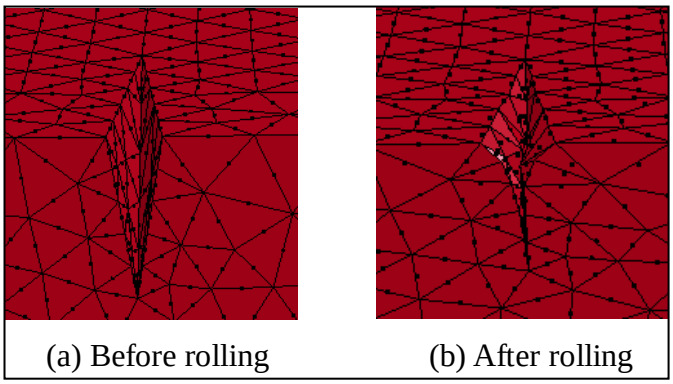

(V-shaped transverse crack model 5)

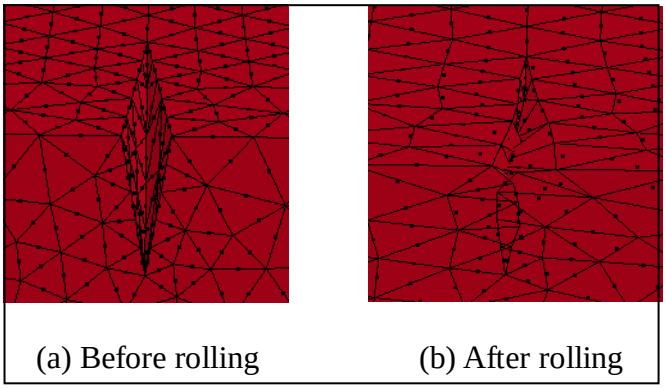

(V-shaped transverse crack model 6)